IDENTIFICATION AND LOCALIZATION OF DAMAGE: A FLEXIBILITY-BASED APPROACH

A Thesis Presented by

Burcu Gunes

to

The Department of Civil and Environmental Engineering

in partial fulfillment of the requirements
for the degree of

Doctor of Philosophy

in the field of

Civil Engineering

Northeastern University
Boston, Massachusetts

December, 2001

ABSTRACT

Changes in the flexibility matrices have been investigated by several researchers as a possible means of characterizing damage. However, no systematic approach has been offered to map these changes to responsible elements of the structure. The **D**amage **L**ocating **V**ector (DLV) approach presented in the thesis provides a systematic and theoretically based methodology for interrogating the changes in flexibility and localizing the damage. In this regard, a related issue addressed in this study is the development of an approach to assemble the flexibility matrices exclusively from the measured vibration data without computing the undamped modes, which often presents challenges in practice. Another source of difficulty with the available methods that use flexibility derives from the fact that they are restricted to cases where the input is known deterministically. A fundamental contribution made in this direction is the development of a procedure for extracting matrices that differ from the flexibility by a single undetermined multiplier for cases where the excitation derives from ambient sources and is not known in a deterministic sense. The last issue examined in this study is estimation of the degree of damage using the synthesized flexibility at the damaged state. The results of the application of the methodology to the ASCE-IASC benchmark structure indicate that the localization technique is robust in the presence of noise, modal truncation and modeling errors. Quantification of the damage, however, requires an accurate baseline model.

ACKNOWLEDGEMENTS

Working on my doctorate degree has been both an exciting and frustrating experience and I would like to thank all the people that made it a memorable experience. First of all, I would like to thank my advisor Prof. Bernal for his invaluable guidance throughout my Ph.D. study. He has been a great mentor and a constant inspiration to me, especially with regard to his unsurpassable research skills. His enthusiasm, dedication and creative ideas impelled me to keep going despite the many challenges that confronted me. I shall consider myself extremely lucky if I managed to gain a bit of his insight, intuition and his talent to express questions and ideas in a crystal clear manner. With his admirable generosity, he has always been there for me and anybody else that needed his help. Without his help and criticism, much of this work would not have been possible.

I gratefully acknowledge the financial support of Northeastern University through a teaching assistantship.

I would like to thank Dr. Yegian, Dr. Wadia-Fascetti, Dr. Sasani, Dr. Shafai and Dr. Adams for serving on my dissertation committee. I would like to express my heart-felt gratitude to Dr. Yegian for his guidance, encouragement and support throughout my graduate study at Northeastern. I wish to extend my thanks to Pat Michaud for her assistance, her dedication to improve the quality of life in the department and most importantly for her friendship. Special thanks go to Vahe Ghahraman for all his help and supervision with the structures lab and the teaching responsibilities.

I would also like to thank Nalan and Ahmet Yakut for being such wonderful friends anyone could possibly have.

Special recognition is owed to my parents for whom I am very fortunate and eternally grateful. They have been a constant source of love, affection and encouragement throughout my life. Finally I would like to express my profound gratitude to my beloved husband who has brought so much happiness to my life. Without his love, patience, advice and constant encouragement, I would not be able to endure such a long journey. This thesis is dedicated to him and to our unborn baby girl.

TABLE OF CONTENTS

LIST OF FIGURES

LIST OF TABLES

NOTATION

A	*state matrix in discrete time*
B	*input influence matrix in discrete time*
A_c	*state matrix in continuous time*
B_c	*input influence matrix in continuous time*
C	*output influence matrix*
D	*direct transmission matrix*
E_U	*material stiffness matrix at the undamaged state*
E_U	*material stiffness matrix at the damaged state*
DF	*change in flexibility*
d_g	*normalization constants*
DLV	*damage locating vector*
f	*natural frequency (Hz)*
F_U	*flexibility matrix (undamaged state)*
F_D	*flexibility matrix (damaged state)*
H	*Hankel matrix*
I	*identity matrix*
K	*stiffness matrix*
L	*load vectors*
m	*number of outputs*
M	*mass matrix*
n	*order of the system*
N	*number of modes*
N	*null space*
nsi	*normalized stress index*
P	*observability matrix*
Q	*controllability matrix*
r	*number of inputs*
R	*stress influence matrix*
$\Re$	*real part*
RMS	*root mean square*

S	*singular values*
T	*transformation matrix*
u	*input vector*
WSI	*weighted stress index*
x	*state vector*
y	output vector
Y	*Markov parameters*
ε_U	*strain field (undamaged state)*
ε_D	*strain field (damaged state)*
ϕ	*eigenvectors*
κ	*condition number*
λ	*Eigenvalues*
υ	*displacement*
$\dot{\upsilon}$	*velocity*
$\ddot{\upsilon}$	*acceleration*
ω	*circular frequency (rad)*
Ω	*observer gain matrix*
Ω_U	undamaged region
Ω_D	damaged region
ξ	*damping ratio*
Ψ_m	*modes at the output sensor locations (displacement partition)*
Ψ_{nc}	*modes at the non-collocated input sensors (displacement partition)*
ζ	*damping matrix*

CHAPTER 1

Introduction

Structural systems are susceptible to damage during their service lives due to many factors such as earthquakes, winds, and operating loads. Undetected damage can accumulate and eventually compromise the system's integrity. It is important, therefore, to device techniques that will ensure that damage is detected when it occurs even if it is not directly visible. Unfortunately, most of the damage characterization methods currently available are mostly local evaluation tools. They include either visual or local experimental methods such as acoustic or ultrasonic methods, magnetic field methods, radiograph, eddy-current methods and thermal field methods (Doherty, 1987). All of these experimental techniques require that the location of damage be known apriori and that the portion of the structure being inspected be accessible. Subjected to these limitations, these methods can detect damage on or near the surface of the structure.

One approach that can operate without knowledge on the vicinity of damage and can give a general idea on the existence and the location of damage is by inspection of vibration signals. Based on a vibration-based technique, an automated health monitoring system envisioned to lead to a more effective infrastructure and disaster management is depicted in Figure 1.1. If a building is instrumented and continuously monitored, then it is possible to analyze the data recorded after a major hazardous event and assess the damage as changes introduced to the system. The output of such an automated damage assessment program will be useful to public safety officials and building owners in their decision on what action should be taken, if any in the aftermath of a severe loading event.

Especially in recent years, considerable research efforts have been directed towards the use of vibration test data for damage diagnostics. Despite the vast amount of information produced by

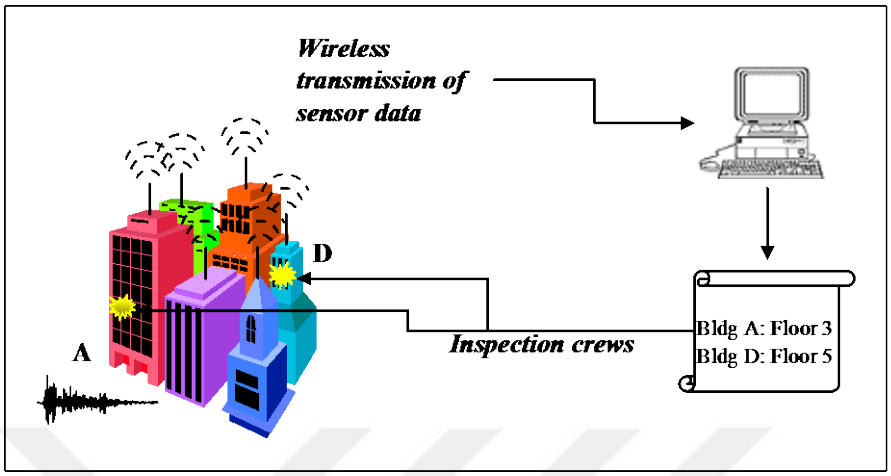

Figure 1.1 An automated structural health monitoring system

these efforts however, a global technique that can be applied with confidence to complex structures has not yet materialized. This chapter provides a brief overview of the available literature on global methods that have been proposed to infer damage from changes in vibration characteristics of structures. The objectives and the scope of this study is then followed by the organization of the work presented in this thesis.

1.1 Vibration-Based Damage Identification

The fundamental idea behind vibration-based damage detection methods is that changes in vibration characteristics (modal properties) can provide information regarding damage. These methods consider the fact that the vibration characteristics of the structure are functions of the mechanical properties (stiffness, mass and damping) and any changes in these properties will reflect as changes in vibration signatures; specifically the natural frequencies, associated mode shapes and modal damping.

The most commonly used feature in vibration based damage detection is the resonant frequencies. Frequency shifts have been widely investigated as a potential damage indicator and a significant amount of literature is available on this subject (Cawley and Adams, 1979; Kenley and Dodds, 1980; Osegueda et al., 1992; Fox 1992; Penney, et al., 1993; Friswell et al., 1994; Silva and Gomes, 1994; Meneghetti and Maggiore, 1994; Salawu, 1997). It is widely recognized that

natural frequencies can generally be measured with good accuracy and have much less statistical variation from random errors than mode shapes. Identification of damage using frequency changes, however, have significant practical limitations in applications to structures (Farrar et al., 1997; Doebling et al., 1997). The most fundamental challenge is related to the fact that damage is a local phenomenon and it may not significantly affect the lower frequencies, which are the ones that are typically measured during vibration tests. This low sensitivity of the frequency shifts to damage requires either very precise measurements in a controlled environment or large levels of damage. Furthermore, frequency shifts generally can only provide information on the presence of damage in a structure, not on the location. Damage at two different locations, for example, may lead to the same amount of frequency change. At higher modal frequencies however, an exception to this limitation occurs. Since these modes are associated with local responses, one may be able to use them to obtain spatial information about structural changes. Nevertheless, the problem with these local modes is that they can be difficult to identify in practice. Multiple frequency shifts can also provide localization information in some cases because changes in the structure at different locations will cause different combinations of changes in the modal frequencies. As pointed out by several authors, however, there is often an insufficient number of frequencies with significant shifts to determine the location of the damage uniquely (Doebling et al., 1998).

Another modal characteristic that has been explored aggressively as a feature to characterize damage is the mode shape information (West, 1984; Fox, 1992; Kim et al., 1992; Ko et al., 1994). Damage detection techniques that uses mode shapes generally analyze changes between the measured vectors before and after the damage. The changes in mode shapes may provide spatial information regarding damage when frequencies alone may not. In contrast to the modal frequencies, however, mode shape estimates have much higher error levels. In many cases, the error in the identification due to factors such as noise may overwhelm the changes due to damage (Conturisi et. al., 1997). Furthermore, most of the methods that utilize the mode shapes require the measurement of complete mode shapes. This is impractical and almost impossible for a large flexible structure with respect to the degrees-of-freedom corresponding to the finite-element model. The common practice to circumvent this problem is to expand the measured mode shapes to the degrees-of-freedom of the finite-element model. Unfortunately, this process inevitably introduces errors in the expanded mode shapes and increases the difficulty in damage detection (Law et al., 1998). These difficulties are compounded when the structure under test exhibits complex mode shapes and the finite element model used for the expansion produces normal

modes. Pairing of the modes between the pre- and post-damage is an additional factor that makes the application of these techniques difficult. The selection of the modes used in the analysis is also found to have a significant effect on the success of the localization. It has been shown that particular mode pairs can indicate damage but when all mode pairs are used, the indication of damage can be masked by modes that are not sensitive to the damage (Salawu et al., 1994; Ko et al.,1994).

An alternative to using displacement mode shapes is to use the second derivative, or curvature of the mode shapes which is more sensitive to changes in the system than the mode shapes themselves for flexural systems (Pandey et al., 1991; Stubbs et al., 1992,1996). Mode shape curvature can be computed by numerically differentiating the displacement mode shape vector twice. They can be applied to beam and plate–like structures for which changes in curvature can be related to changes in the strain energy. However, numerical calculation of curvature from mode shape results presents a challenge for practical application of this method since one needs a lot of sensors to get an accurate curvature from the displacements. The study by Chance et al. (1994) shows that using measured strains to obtain curvature directly may be a more practical alternative.

Another class of damage identification methods uses the comparison of dynamically measured flexibility matrices assembled from the available modes before and after the damage (Aktan et al., 1994; Pandey et al., 1994, 1995; Peterson et al., 1995). These techniques avoid the problem of one-to-one pairing of the mode shapes between the two states of the system. However, mapping of the changes in the flexibility matrices to specific elements of the structure presents a challenge for a systematic application of these methods. The typical approach has been to examine the diagonal of the change in flexibility and assert that the damage is 'likely to be located' near the sensor where the largest change has taken place. This type of heuristic approach is very much system dependent and has obvious difficulties with multiple damage scenarios. Another source of difficulty with the methods that use flexibility is the fact that they are restricted to cases where the input is known deterministically. The approach to be presented in detail later in this thesis is a flexibility-based technique that offers solutions to these issues. In particular, it provides a systematic approach for interrogating the changes in flexibility and extends the applicability of these techniques to the case of stochastic input.

Model updating techniques provide a wide range of methods that have been tried for damage identification purposes. These methods are based on the modification of the structural parameters such as mass, stiffness and damping to reproduce the measured dynamic data as closely as possible. Comparison of the updated matrices to the original correlated matrices provides an indication of the damage and can be used to identify both the location and the extent of damage. Optimal matrix update methods (Smith et al., 1991; Zimmerman et al., 1992, and Kaouk, 1993), sensitivity based update methods (Hemez, 1993; Ricles, 1991; Sanayei et al., 1991), and eigenstructure assignment method (Lim 1994, 1995; Lim and Kashangaki, 1994) are among the several update algorithms that have been applied in formulating the constrained optimization problem based on the equations of motion and the measured data. The main difficulty with these methods is choosing the right parameters to update. These parameters are commonly selected from those with the lowest assurance values. However, updating the most uncertain elements that have a significant effect on the objective function that is being optimized, may not necessarily lead to correct characterization of the damage.

Examination of the damage identification methods presented thus far reveals that most of the existing techniques are conceived for particular types of structures and few can operate with multiple damage scenarios and with an arbitrary number of sensors. In many cases a technique that works well in theory is very difficult to apply to a real structure due to the fact that the results are sensitive to one or more assumptions which in practice are not entirely satisfied. Most importantly, in many of the available techniques the localization strategy based on postulating an index that is ‘reasonable to expect', is correlated with the spatial location of the damage. Because of their heuristic base, these methods are difficult to analyze in a fundamental sense. An excellent review of the literature on the damage characterization problem up to 1996 can be found in Doebling et. al. (1996).

1.2 The IASC-ASCE Benchmark Structure

It is generally accepted by the research community that to advance in the field of structural health monitoring (SHM) full-scale international benchmark problems that define realistic conditions are needed. Efforts to address this need were initiated at the 1996 International Workshop on Structural Control (Chen, 1996). In particular, three SHM task groups were formed, one for

Europe, one for Asia and one for the US. The US task group eventually solidified in 1999 under the joint auspices of the International Association of Structural Control (IASC) and the Dynamics Committee of the American Society of Civil Engineers (ASCE) decided to focus their first efforts on preparing a well-defined benchmark problem to provide a common platform for consistent evaluation of the numerous SHM techniques proposed by several researchers. Keeping in mind that credible SHM technology must be shown to work with real data, a benchmark problem for which a physical model was available was selected (Black and Ventura, 1998). A series of cases for analytical simulations were developed and presented to the participants (Johnson et. al, 2000). The objective was to explore the damage identification problem with techniques selected by the participants but with the focus placed on a common structure and a set of clearly defined assumptions. To understand the advantages and disadvantages of the various methods, several aspects of the problem such as having full or partial sensor information, the effect of noise in measurement signals, modeling errors were incorporated into the simulation cases. The flexibility-based methodology developed in this thesis is applied to this benchmark problem as a part of this effort.

1.3 Objectives and Contributions of this Thesis

This thesis is developed within the framework of the mission of the ASCE-SHM Task group. The objectives of the work therefore, were not initially defined completely, but evolved within the context of this mission. Our fundamental objective is to develop a damage identification method that minimizes the problems deriving from the limitations in the imperfect nature of the measured data, inevitable errors in the mathematical model as well as the assumptions inherent in the technique itself. Upon investigation of several techniques (which are not included in this document) such as the use of Hilbert transform and instantaneous frequency approaches (Bernal and Gunes, 2000), the flexibility-based methodology developed in this thesis is found to be the one that best satisfies the constraints imposed regarding the ability to operate with imprecise data, arbitrary number of sensors and partial modes.

The two fundamental contributions of this thesis are:

1. The development of an approach to extract system matrices (including the flexibility) for the deterministic input cases and the matrices that are proportional to the system matrices in the particular case of stochastic input using the identified complex modes.
2. The development of an approach to map changes in flexibility to damage location. The methodology is rigorous and eliminates the need for heuristic approaches that have been used thus far (Bernal, 2002).

In addition, it is also an objective of this thesis to contribute to the combined effort in evaluating the current capability of the SHM methods. For this purpose, damage localization approach developed in this thesis is applied to the IASC-ASCE benchmark problem.

1.4 Organization of the Thesis

The first step in damage identification problem is the extraction of the modal characteristics from the measured data. In this thesis a state-space formulation which leads to system realization based identification is used. In chapter 2 the mathematical framework of the realization theory is presented. The basic concepts of system realization, the theory of controllability and observability and the computational steps of the eigensystem realization algorithm (ERA) are discussed in the chapter.

The second step in the damage identification approach explored here is the extraction of flexibility matrices from the realization results. The necessary theory to do this is presented in chapter 3. This chapter also contains a discussion on the extraction of the mass and the damping matrices of the second order formulation. The formulations are presented both for the deterministic and stochastic input cases.

The general methodology to map the change in flexibility to the damage in the structure is discussed in chapter 4. The method presented is designated as the **D**amage **L**ocating **V**ector (DLV) approach. As will be shown, although the DLVs can be computed exclusively from the measured data, a reference model is needed for computing the stress fields under these load vectors to locate damage. The technique, however, does not require a detailed finite element model and knowledge about the system is restricted to that needed for a static analysis in the

undamaged state, namely, the undamaged topology and, if the structure is indeterminate, the relative stiffness characteristics.

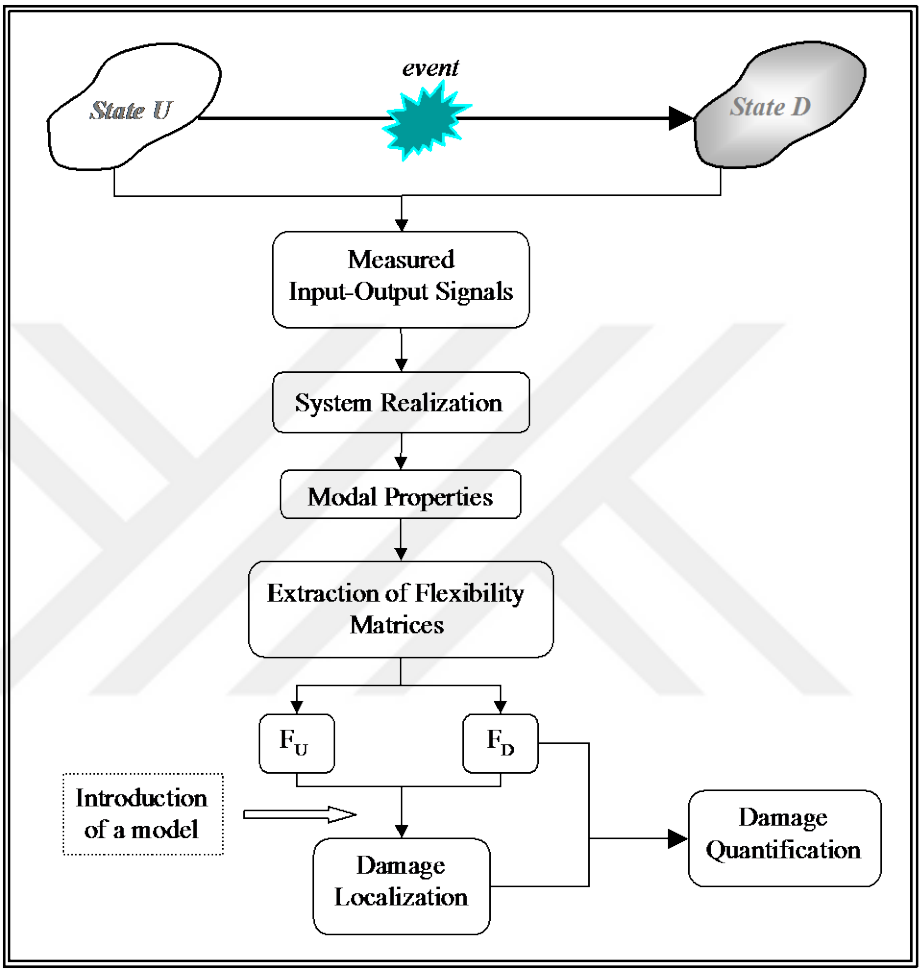

Figure 1.2 The flexibility-based approach

Chapter 5 concludes the methodology and considers the issue of damage quantification and severity estimation. In this regard it is worth noting that accurate damage localization may prove to be all the information that is needed from a health monitoring system in many applications. In this chapter the use of the information in the flexibility for the quantification of the damage is pursued. As will be shown, this step is much more sensitive to errors in the mathematical model than the localization stage. The steps of the flexibility-based methodology discussed in chapters 1-5 are depicted in Figure 1.2.

Chapter 6 details the first phase of the IASC-ASCE benchmark problem and shows how the methodology previously developed applies to this structure. Finally, chapter 7 contains a summary of main findings of this dissertation, together with some guidelines for future research in the field.

The dissertation includes three appendices: Appendix A contains the MATLAB® programs generated for this research project, appendix B tabulates the analytically computed values of the natural frequencies and the story stiffnesses for the benchmark structure and appendix C presents some preliminary work on reducing error due to modal truncation when flexibility matrices are inverted.

CHAPTER 2

System Realization and Modal Identification

2.1 Introduction

The process of constructing state-space representations from experimental data is called system realization. There are many system identification algorithms that produce state-space realizations from measured data (Longman et. al., 1991, Juang et. al., 1993). Most of these time-domain system identification methods are based on the impulse response functions also known as the Markov parameters. Among the various methods, the **E**igensystem **R**ealization **A**lgorithm (ERA) is widely used in the identification of structural dynamic systems (Juang, 1994). This chapter provides the mathematical framework and the basic concepts of realization including the theory of controllability and observability. The computational steps of ERA and its implementation using an observer Kalman filter are also discussed in the chapter.

2.2 Solution of State-Space Equations

Every linear time-invariant system can be described by the input-output description

$$\hat{Y}(s) = \hat{G}(s)\hat{U}(s) \tag{2.1}$$

where s is the Laplace operator, $\hat{G}(s)$ is the transfer matrix, and $\hat{U}(s)$ and $\hat{Y}(s)$ are the inputs and outputs in Laplace domain.

If the system is lumped as well, it can also be represented in state-space differential form as

$$\dot{x} = A_c\ x + B_c\ u \tag{2.2a}$$

$$y = C\ x + D\ u \tag{2.2b}$$

where the quadruplet {A_c, B_c, C and D} are the matrices of realization relating inputs u to outputs y through a state vector x. A_c is an $n \times n$ state matrix, where n is the order of the system, B_c is an $n \times r$ input influence matrix where r is the number of inputs, C is an $m \times n$ output influence matrix for the state vector x where m is the number of outputs and D is an $m \times r$ direct transmission matrix.

For a given dynamical system which is excited by the initial state $x(0)$ and the input $u(t)$ if the system matrices are known, the problem of finding the response hinges on the exponential function of A_c. The development of an explicit expression for the response can be done as follows:

Premultiplying both sides of eq.2.2a by $e^{-A_c t}$ yields

$$e^{-A_c t}\dot{x}(t) - e^{-A_c t}A_c x(t) = e^{-A_c t}B_c u(t) \tag{2.3}$$

which implies

$$\frac{d}{dt}(e^{-A_c t}x(t)) = e^{-A_c t}B_c u(t) \tag{2.4}$$

Integrating the above expression from 0 to t, one obtains

$$e^{-A_c t}x(\tau)\Big|_{\tau=0}^{t} = \int_0^t e^{-A_c \tau}B_c\ u(\tau)\,d\tau \tag{2.5}$$

Thus the solution to eq.2.2a is given by

$$x(t) = e^{A_c t} x(0) + \int_0^t e^{A_c (t-\tau)} B_c \, u(\tau) \, d\tau \tag{2.6}$$

Substituting eq.2.6 into eq.2.2b yields the solution of eq.2.2b as

$$y(t) = Ce^{A_c t} x(0) + C\int_0^t e^{A_c (t-\tau)} B_c \, u(\tau) \, d\tau + D\,u(t) \tag{2.7}$$

The above equations constitute the solutions for the continuous time state-space model of a dynamical system represented by eq.2.2. If this set of equations is to be computed on a digital computer they must be discretized. Any linear dynamical system having discretized inputs can be represented by a discrete-time state-space model which will be derived below.

The evaluation of $x(t)$ at equally spaced intervals of time t can be obtained by a discrete-time representation of eq.2.6. Let the equally spaced times given by 0, dt, $2dt$…,$(k+1)\,dt$, where dt is a constant interval. Assuming that the input is constant between sample times and substituting $t=(k+1)dt$ yields

$$x[(k+1)dt] = x_{k+1} = e^{A_c (k+1)dt} x(0) + \int_0^{(k+1)dt} e^{A_c [(k+1)dt-\tau]} B_c \, u(\tau) \, d\tau \tag{2.8}$$

$$x_{k+1} = e^{A_c dt}[e^{A_c kdt} x(0) + \int_0^{kdt} e^{A_c (kdt-\tau)} B_c u(\tau) d\tau] + \int_{kdt}^{(k+1)dt} e^{A_c (kdt+dt-\tau)} B_c u(\tau) \tag{2.9}$$

Substituting eq.2.6 and introducing the new variable $\alpha=kdt+dt-\tau$, one gets

$$x_{k+1} = e^{A_c dt} x_k + (\int_0^{dt} e^{A_c \alpha} d\alpha) \, B_c \, u_k \tag{2.10}$$

Thus, for an input that changes value only at discrete time instants eq.2.2a and 2.2b become

$$x_{k+1} = A\,x_k + B\ \ u_k \tag{2.11a}$$

$$y_k = C_d\ x_k + D_d\ u_k \tag{2.11b}$$

with

$$A = e^{A_c dt}$$
$$B = (\int_0^{dt} e^{A\tau} d\tau)\, B_c \tag{2.12}$$
$$C_d = C \quad , \quad D_d = D$$

This is a discrete-time state-space equation. Note that there is no approximation involved in this derivation beyond the step-wise treatment of the load and eq.2.11a yields the exact solution at $t = k\,dt$ if the input is piecewise constant.

The discrete-time matrix *B* may be computed using the Taylor series expansion of $e^{A_c t}$:

$$B = (\int_0^{dt} e^{A_c \tau} d\tau)\, B_c = \left(\int_0^{dt} (I + A_c \tau + A_c^2 \frac{\tau^2}{2!} + \cdots)\, d\tau \right) B_c \tag{2.13}$$

$$B = dt\, I + \frac{dt^2}{2!} A_c + \frac{dt^3}{3!} A_c{}^2 + \cdots \tag{2.14}$$

If *A* is non-singular, then the series can be written as

$$B = A_c{}^{-1} (dt A_c + \frac{dt^2}{2!} A_c{}^2 + \frac{dt^3}{3!} A_c{}^3 + \cdots + I - I)\, B_c \tag{2.15}$$

Recognizing the series expansion of e^{At} in the above equation, we have

$$B = A_c{}^{-1} (e^{A_c t} - I) B_c \tag{2.16a}$$

or,

$$B = A_c{}^{-1} (A - I) B_c \tag{2.16b}$$

Thus, the constant matrices {A_c, B_c, *C*, *D*} or {*A*, *B*, *C*, *D*} with appropriate dimensions represent the internal operation of the linear system, and can be used to determine the system's response to any given input that has a spatial distribution defined by the input influence matrix, *B*.

The ability to construct a discrete-time state space model hinges on whether or not all the system states of interest can be excited (controlled) and/or observed. In order to answer this question one

needs to understand the theories of controllability and observability. These concepts are briefly introduced in the next sections.

2.3 Controllability

A state x_p of a system at a given time step p is said to be controllable if there is a sequence of input values that can be used to attain this state starting from any arbitrary condition. If all the states are controllable, the system is said to be *completely controllable* or simply, *controllable* (Juang, 1994). Since the derivation of controllability and observability theories for the continuous-time case is similar to the discrete case, we will show only the discrete case in this thesis.

From the solution to the discrete representation (eq.2.11), one can see that

$$\begin{aligned} x_1 &= Ax_0 + Bu_0 \\ x_2 &= A^2x_0 + ABu_0 + Bu_1 \\ x_3 &= A^3x_0 + A^2Bu_0 + ABu_1 + Bu_2 \\ &\vdots \end{aligned} \tag{2.17}$$

or, in general the solution at time step p is

$$x_p = A^p x_0 + \sum_{i=0}^{p} A^{i-1} B\, u_{p-i} \tag{2.18}$$

Writing eq.2.18 in a compact matrix form, one gets

$$x_p = A^p x_0 + [B \quad AB \quad A^2B \quad \cdots \quad A^{p-1}B] \begin{bmatrix} u_{p-1} \\ u_{p-2} \\ \vdots \\ u_0 \end{bmatrix} \tag{2.19}$$

From eq.2.19, it is evident that an arbitrary x_p can be reached only if $(x_p - A^p x_0)$ lies in the column space of $[B \;\; AB \;\; A^2B \;\cdots\; A^{p-1}B]$, and, since $(x_p - A^p x_0)$ is arbitrary one concludes that controllability at step *p* is equivalent to requiring that the matrix $[B \;\; AB \;\; A^2B \;\cdots\; A^{p-1}B]$ be full rank.

Thus, a linear finite dimensional discrete-time system of order *n* is controllable at step *p* if the [*n*×*pr*] block matrix Q_p is of rank *n*, where

$$Q_p = [B \;\; AB \;\; A^2B \;\cdots\; A^{p-1}B] \tag{2.20}$$

The block matrix Q_p in eq.2.20 is the controllability matrix. By the Cayley-Hamilton theorem, if $A \in \Re^{n\times n}$, then A^{n+j} for $j \geq 0$, can be expressed as a linear combination of $\left[I \;\; A \;\; A^2 \;\cdots\; A^{n-1}\right]$ (Kailath, T., 1980). It follows then than that the number of independent columns in eq.2.20 will not increase if $p \geq n$. Therefore,

$$rank[B \;\; AB \;\cdots\; A^{n-1}B] = n \tag{2.21}$$

is a necessary and sufficient condition for controllability of system given by eq.2.11.

2.4 Observability

A state $x(p)$ is said to be observable at time step *p* if it can be determined completely from knowledge of the past of the input and the output ($0 < k \leq p$). If all the states are observable, then the system is said to be *completely observable* or simply, *observable* (Juang, 1994).

By inspection of eq.2.18, it is evident that the state x_p is fully determined by the input and the initial condition x_0. The question of observability is therefore the same as asking if the initial condition is unique for a given input-output history from time step 0 to *p*.
Substituting eq.2.19 into eq.2.11b, one gets

$$y_p = CA^p x_0 + C[B \quad AB \quad A^2B \quad \cdots \quad A^{p-1}B]\begin{bmatrix} u_{p-1} \\ u_{p-2} \\ \vdots \\ u_0 \end{bmatrix} + Du_p \tag{2.22}$$

This leads to

$$y_p - C[B \;\; AB \;\; A^2B \;\cdots\; A^{p-1}B]\begin{bmatrix} u_{p-1} \\ u_{p-2} \\ \vdots \\ u_0 \end{bmatrix} - Du_p = CA^p x_0 \tag{2.23}$$

or

$$z_p = CA^p x_0 \tag{2.24}$$

Expanding this for all the states, one can write

$$Z_p = \begin{bmatrix} z_0 \\ z_1 \\ \vdots \\ z_{p-1} \end{bmatrix} = \begin{bmatrix} C \\ CA \\ \vdots \\ CA^{p-1} \end{bmatrix} x_0 \tag{2.25}$$

Thus one can conclude that x_0 is unique if the block matrix P_p defined as

$$P_p = \begin{bmatrix} C \\ CA \\ \vdots \\ CA^{p-1} \end{bmatrix} \tag{2.26}$$

is of rank n, where P_p is the observability matrix of size ($pm \times n$). Again by the Cayley-Hamilton theorem if P_p is of rank n for some p, then P_n is also rank n. This means

$$rank[C^T \quad A^TC^T \quad \cdots \quad (A^T)^{n-1}C^T] = n \tag{2.27}$$

is a necessary and sufficient condition for observability of the system.

2.5 Basic Concepts of Realization and Eigensystem Realization Algorithm

Computation of the quadruplet [*A, B, C, D*] from measured data for a given set of inputs and outputs is called a realization. In other words it is the identification of a system by constructing a state-space representation from experimental data. Any system has an infinite number of realizations that will predict identical response for any particular input. Minimum realization means a model with the smallest state-space dimensions among all realizable systems that have the same input-output realizations. The matrices that define the realization, even a minimal realization, are not unique. This can easily be shown by assuming that *x* is a minimum dimension state vector and defining a new state vector, *z*, such that

$$x = T\,z \tag{2.28}$$

where *T* is a non-singular matrix. Substituting eq.2.28 into eq.2.11 yields

$$z_{k+1} = T^{-1}AT\,z_k + T^{-1}Bu_k \tag{2.29a}$$

$$y_k = CT\,z_k + D\,u_k \tag{2.29b}$$

from where it is apparent that the effect of the input, u_k on the output, y_k is unchanged so the matrices [$T^{-1}AT$, $T^{-1}B$, *CT* and *D*] describe the same input-output relationship as the matrices [*A, B, C,* and *D*]. In addition, since the system matrices of any two realizations are related by a similarity transformation, the eigenvalues are preserved.

To develop the basics of system realization theory we begin by applying a unit value of load, *u* at *k*=0 for each one of the inputs in eqs. 2.11a and 2.11b; one gets;

$$\begin{array}{llll} x_1 = Ax_0 + Bu_0 & x_2 = Ax_1 & x_3 = Ax_2 & \cdots\cdots \\ y_0 = Cx_0 + Du_0 & y_1 = CAx_0 + CBu_0 & y_2 = CA^2x_0 + CABu_0 & \cdots\cdots \end{array} \tag{2.30}$$

Assuming the initial state $x_0 \equiv 0$, the outputs can be assembled into a pulse response matrix *Y* as follows:

$$\begin{gathered} Y_0 = D \quad Y_1 = CB \quad Y_2 = CAB \quad Y_3 = CA^2B\cdots \\ Y_k = CA^{k-1}B \end{gathered} \tag{2.31}$$

The constant matrices in the sequence are known as the *Markov parameters*. Each of the Markov parameters, Y_i, is an $m \times r$ matrix giving the output at the m coordinates at time step i when the input is a pulse on each of the excitation coordinates. Note that we have not discussed how one obtains the Markov parameters from experimental input and output data. Computation of these parameters based on measurements will be discussed in the next section.

After identification of the Markov parameters the first task is to form the generalized $\alpha m \times \beta r$ Hankel matrix

$$H_{k-1} = \begin{bmatrix} Y_k & Y_{k+1} & \cdots & Y_{k+\beta-1} \\ Y_{k+1} & Y_{k+2} & \cdots & Y_{k+\beta} \\ \vdots & \vdots & \vdots & \vdots \\ Y_{k+\alpha-1} & Y_{k+\alpha} & \cdots & Y_{k+\beta+\alpha-2} \end{bmatrix} \tag{2.32}$$

Recalling that $P_\alpha = \begin{bmatrix} C \\ CA \\ \vdots \\ CA^{\alpha-1} \end{bmatrix}$ and $Q_\beta = [B \quad AB \quad A^2B \quad \cdots \quad A^{\beta-1}B]$, one can write

$$P_\alpha A^{k-1} Q_\beta = \begin{bmatrix} CA^{k-1}B & CA^k B & \cdots \\ CA^k B & CA^{k+1}B & \cdots \\ \vdots & \vdots & \vdots \end{bmatrix} = H_{k-1} \tag{2.33}$$

Thus, the Hankel matrix of size $\alpha m \times \beta r$ is equal to the product of $\alpha m \times n$ block observability matrix, the system matrix A^{k-1} and $n \times \beta r$ block controllability matrix.

For k=1,eq.2.33 leads to

$$H_0 = P_\alpha Q_\beta \tag{2.34}$$

Expressing the Hankel matrix as a triple product using singular value decomposition, one gets

$$H_0 = R \Sigma S^T \tag{2.35}$$

Discarding the zero (or nearly zero) singular values leads to

$$H_0 \cong R_n \Sigma_n S_n^T \tag{2.36}$$

If there are *n* significant singular values then a balanced minimum realization can be obtained by expressing the above equation as

$$H_0 = (R_n \Sigma_n^{1/2})(\Sigma_n^{1/2} S_n^T) \tag{2.37}$$

The term 'balanced' is used due to the way the singular values are separated in eq.2.37. (i.e, a separation into $P_\alpha = R_n\Sigma$ and $Q_\beta = S_n^T$ would not be a balanced realization) (Juang, 1994).

Comparing eq.2.34 and eq.2.37, one can write

$$\begin{aligned} P_\alpha &= R_n \Sigma_n^{1/2} \\ Q_\beta &= \Sigma_n^{1/2} S_n^T \end{aligned} \tag{2.38}$$

Eq.2.20 and 2.26 indicate that the first *r* columns of Q_β are equal to *B* and the first *m* rows of P_α are equal to *C*. Also note that $D=Y_0$ as shown in eq.2.31. Hence, from the matrices of realization the only unknown left is the system matrix *A*. To get the system matrix *A* one can examine the Hankel matrix at $k = 2$:

$$H_1 = P_\alpha A Q_\beta = R_n \Sigma_n^{1/2} A \Sigma_n^{1/2} S_n^T \tag{2.39}$$

Given the orthogonality of R_n and S_n, eq.2.39 can be written as

$$A = \Sigma_n^{-1/2} R_n^T H_1 S_n \Sigma_n^{-1/2} \tag{2.40}$$

This completes the basic formulation of realization for the eigensystem realization algorithm. Defining O_q as the null matrix of order *q*, and I_j as the identity matrix of order *j* so that

$$E_m^T = [I_m \quad O_m \quad \cdots \quad O_m], \quad E_r^T = [I_r \quad O_r \quad \cdots \quad O_r] \tag{2.41}$$

The triplet

$$A = \Sigma_n^{-1/2} R_n^T H_1 S_n \Sigma_n^{-1/2}, \quad B = \Sigma_n^{1/2} S_n^T E_r, \quad C = E_m^T R_n \Sigma^{1/2} \tag{2.42}$$

is a balanced minimum realization of order *n*.

2.6 Observer/Kalman Filter Identification

Many of the system identification techniques including the eigensystem realization algorithm described in the previous section requires the impulse response time histories which are known as the system Markov parameters. The basic approach to get these parameters from measured data is to compute the frequency response functions (FRF) as the ratio of the Fourier transforms of the output to input and then use the inverse Fourier transform to compute the impulse response functions. With this approach problems arise due to the periodicity introduced by the sampling of the signals and the FRF may be quite inaccurate at frequencies where input signal is low in amplitude. An alternative to this approach is to use deconvolution and solve for the Markov parameters directly in the time-domain.

Consider the discrete time state-space formulation given by eqs. 2.11a and 2.11b. Solving for the output y_{l-1} in terms of the previous inputs yields

$$\begin{aligned}
x_1 &= Ax_0 + Bu_0 & y_0 &= Cx_0 + Du_0 \\
x_2 &= A^2 x_0 + ABu_0 + Bu_1 & y_1 &= CAx_0 + CBu_0 + Du_1 \\
&\vdots & &\vdots \\
x_{l-1} &= A^{l-1} x_0 + \sum_{i=1}^{l-1} A^{i-1} Bu_{l-1-i} & y_{l-1} &= CA^{l-1} x_0 + \sum_{i=1}^{l-1} CA^{i-1} Bu_{l-1-i} + Du_{l-1}
\end{aligned} \tag{2.43}$$

Defining

$$y = \begin{bmatrix} y_0 & y_1 & \cdots & y_{l-1} \end{bmatrix},\ X_0 = \begin{bmatrix} x_0 & 0 & \cdots & 0 \\ 0 & x_0 & \cdots & 0 \\ \vdots & \vdots & \ddots & \vdots \\ 0 & 0 & \cdots & x_0 \end{bmatrix},\ U = \begin{bmatrix} u_0 & u_1 & \cdots & u_{l-1} \\ 0 & u_0 & \cdots & u_{l-2} \\ & & \ddots & \vdots \\ & & & u_0 \end{bmatrix} \tag{2.44}$$

one can express eq.2.11b as

$$y = [C \quad CA \quad \cdots \quad CA^{l-1}]X_0 + [D \quad CB \quad CAB \quad \cdots \quad CA^{l-2}B]U \tag{2.45}$$

Recalling the Markov parameter matrix Y and the observability matrix, P_l, one has

$$y = P_l X_0 + Y U \tag{2.46}$$

where, $Y \in \Re^{m \times l\, r}, U \in \Re^{l\, r \times l}, y \in \Re^{m \times l}$

If one assumes that the initial state is zero, the above expression simplifies to

$$y = Y U \tag{2.47}$$

Note that the matrix U in eq.2.47 is square only in the case of single input (r=1). The solution for the matrix Y can be determined uniquely for r=1. This, is in contradiction with physical reality because it is known that for a linear system, Y must be unique for any r. To resolve this apparent paradox, consider partitioning eq.2.47 such that

$$y = \begin{bmatrix} Y_1 & Y_2 \end{bmatrix} \begin{bmatrix} U_1 \\ U_2 \end{bmatrix} \tag{2.48}$$

For an asymptotically stable system, i.e. $A^k \approx 0$ for $k \geq p$, one can assume with little error that $Y_2 \approx 0$ if one chooses a sufficiently large p for the above partition. Then eq.2.47 can be approximated by

$$Y_1 = y U_1^{\mathrm{t}} \tag{2.49}$[1]

where $U_1 \in \Re^{r(p+1) \times l}, Y_1 \in \Re^{m \times r(p+1)}, y \in \Re^{m \times l}$ and the number of Markov parameters is p+1. In this case, one can solve for Y for an arbitrary number of inputs.

[1] t indicates pseudo-inverse operation

A drawback of this direct approach (eq.2.49), however, is that the p value must be very large for lightly damped systems to attain $A^k \approx 0$ for $k \geq p$, and this requires a very large input matrix to be inverted.

A solution to the slow decay problem of the system Markov parameter is to use an asymptotically stable observer to form a stable model for the system to be identified (Phan et. al., 1992). Introduction of an observer allows the data to be compressed by fictitiously adding damping and improves the system identification results.

Consider again eqs. 2.11a and 2.11b, and add and subtract the term Ωy_k to the right-hand side of the state equation as follows:

$$x_{k+1} = Ax_k + Bu_k + \Omega y_k - \Omega y_k \tag{2.50a}$$

$$y_k = Cx_k + Du_k \tag{2.50b}$$

where Ω is the observer gain matrix.

One can substitute the output expression, eq.2.50b into eq.2.50a and obtain

$$x_{k+1} = (A + \Omega C)x_k + [B + \Omega D \quad -\Omega]\begin{Bmatrix} u_k \\ y_k \end{Bmatrix} \tag{2.51}$$

or;

$$x_{k+1} = \overline{A}\, x_k + \overline{B}\, v_k \tag{2.52a}$$

where

$$\begin{aligned} \overline{A} &= A + \Omega C \\ \overline{B} &= [B + \Omega D, -\Omega] \\ v(k) &= \begin{bmatrix} u(k) \\ y(k) \end{bmatrix} \end{aligned} \tag{2.52b}$$

As can be seen, eq.2.52 has the exact same form as the standard one, except that the input has to be expanded by y_k and the matrices A and B have been changed to $\overline{A}$ and $\overline{B}$. Because the form of the previous equations is the "same" as the standard case, one can solve just as before for the

Markov parameters of the modified system (observer Markov parameters, $\overline{Y}$) using the same approach as eq.2.49 (Juang, 1994):

$$y = \overline{Y} V \tag{2.53a}$$

where

$$\overline{Y} = [D \quad C\overline{B} \quad C\overline{A}\overline{B} \quad \cdots \quad C\overline{A}^{p-1}\overline{B}] \tag{2.53b}$$

Note that if we solve for this modified Markov parameters, we have no explicit decision in what the observer gain matrix Ω is, but we are attempting to obtain a realization that contains as input a vector containing the true input and the output. One intuitively expects that this modified system has the shortest Markov parameters since we wish to predict the output using the input and the previous outputs.

Substituting eq.2.52b into eq.2.53b, one gets

$$\begin{aligned} \overline{Y}_0 &= D \\ \overline{Y}_k &= C\overline{A}^{k-1}\overline{B} \\ \overline{Y}_k &= [C(A+\Omega C)^{k-1}(B+\Omega D) \quad -C(A+\Omega C)^{k-1}\Omega] \end{aligned} \tag{2.54}$$

Defining the first term in $\overline{Y}_k$ as $\overline{Y}_k^{(1)}$ and the second term as $\overline{Y}_k^{(2)}$, the relationship between the observer Markov parameters and the system Markov parameters can be obtained as

$$Y_k = \overline{Y}_k^{(1)} - \sum_{i=1}^{k} \overline{Y}_i^{(2)} Y_{k-i} \qquad \text{for } k = 1, \ldots, p \tag{2.55}$$

2.7 Stochastic Identification

In this section we will summarize the essential steps in the identification of a stochastic systems. The stochastic identification problem consists of extracting the stochastic system matrices given output data only. For a more detailed description of the technique the reader is referred to Van Overschee and Moor (1996).

The unknown stochastic system is represented by

$$x_{k+1} = A x_k + w_k \tag{2.56a}$$

$$y_k = C x_k + v_k \tag{2.56b}$$

where w_k and v_k are white noise vectors. The objective of the realization is to establish the matrices A and C and the covariance of the process that generates the w_k and v_k sequences. It is assumed that the stochastic process is stationary, and the state is uncorreleated with both process noise and the output noise, i.e;

$$E(x_k v_k^T) = 0 \, , E(x_k w_k^T) = 0 \, , E(x_{k+1} x_{k+1}^T) = \Sigma \tag{2.57a,b,c}$$

Substitution of eq.2.57c into eq.2.56a yields

$$E\ [(Ax_k + w_k)(Ax_k + w_k)^T] = \Sigma \tag{2.58}$$

$$E(Ax_k w_k^T) + E(Ax_k x_k^T A^T) + E(w_k w_k^T) + E(w_k x_k^T A^T) = \Sigma \tag{2.59}$$

and substitution of eq.2.57b and eq.2.57c into eq.2.59 leads to

$$\Sigma = A \Sigma A^T + Q \tag{2.60}$$

where $Q = E(w_k w_k^T)$

Defining the output covariance matrix Λ_i for a shift i as

$$\Lambda_i = E(y_{k+i} y_k^T) \tag{2.61}$$

and substituting eq.2.56b into eq.2.61, one gets

$$\Lambda_i = E[(C x_{k+i} + v_{k+i})(C x_{k+i} + v_{k+i})^T] \tag{2.62}$$

$$\Lambda_i = E(C x_{k+i} v_k^T) + E(C x_{k+i} x_k^T C^T) + E(v_{k+i} v_k^T) + E(v_{k+i} x_k^T C^T) \tag{2.63}$$

Simplifying the above expression by substituting $E(v_{k+i}v_k^T) = 0$ (except for i=0) and $E(x_k v_k^T) = 0$, one obtains

$$\Lambda_i = E(C x_{k+i} x_k^T C^T) \tag{2.64}$$

Now, examining eq.2.56a one can conclude that

$$x_{k+i} = A^i x_k + A^{i-1} w_k + A^{i-2} w_{k+1} + \cdots + w_{k+i-1} \tag{2.65}$$

Post-multiplying by x_n^T, all the terms (except for the first one) cancel and the following expressions are obtained for the output covariance matrices:

$$\Lambda_i = C A^i \Sigma C^T \tag{2.66a}$$

$$\Lambda_0 = C \Sigma C^T + R \tag{2.66b}$$

where $R = E(v_k v_k^T)$.

Defining;

$$\begin{aligned} \bar{G} &= E(x_{k+1} y_k^T) \\ &= E\,[(Ax_k + w_k)\ \ (Cx_k + v_k)^T] \\ &= E\,[Ax_k v_k^T + Ax_k x_k^T C^T + w_k v_k^T + w_k x_k^T C^T] \end{aligned}$$

$$\bar{G} = A\Sigma C^T + S \tag{2.67}$$

where; $E(w_k v_k^T) = S$, one can write

$$A^{-1}\bar{G} = \Sigma C^T + A^{-1} S \tag{2.68}$$

Substituting eq.2.68 into eq.2.66a yields

$$\begin{aligned} \Lambda_i &= CA^i (A^{-1}\bar{G} - A^{-1}S) \\ \Lambda_i &= CA^{i-1}\bar{G} - CA^{i-1}S \end{aligned} \tag{2.69}$$

Assuming the process and the output noise are uncorrelated, one has

$$\Lambda_i = CA^{i-1}\bar{G} \tag{2.70}$$

So, by analogy with eq.2.31 of the deterministic case, the output covariance can be treated as Markov parameters of a system defined by *A,* $\bar{G}$, *C,* and Λ_0. By taking the output covariances and forming the Hankel matrix, one can identify, using ERA for example, the system matrices *A,* $\bar{G}$ and *C*. Once these matrices are available, one gets

$$R = \Lambda_0 - C \quad A^{-1}\bar{G} \tag{2.71}$$

Assuming *S*=0, one can obtain *Q* from eqs.2.60 and 2.66b.

2.8 Concluding Remarks

System realization based identification is the first step of the damage identification problem. The purpose of system realization is to construct a state-space model from measured data. Among the many models realized that have the same input-output relations, the one that possesses the minimum order is particularly important. Among the various techniques that can obtain a minimum order realization, the technique called as the ERA is found to be suitable for the purpose of modal parameter identification.

CHAPTER 3

Extraction of System Matrices from State-Space Realizations

3.1 Introduction

Extraction of properties associated with the second-order dynamics from the state-space modeling of the measured input/output data has been the focus of research in recent years especially in damage localization applications. The problem of extracting these matrices from a realization has been traditionally regarded as being equivalent to that of identifying mass normalized modes and frequencies (Yang and Yeh, 1990; Alvin and Park, 1994). This, however, is a difficult problem because one can only extract the damped modal properties from measured data. Computation of the undamped modes and frequencies from the complex modes, although can be done when the system damping is exactly proportional, presents challenges in the general case of an arbitrary viscous damping distribution. Much research has focused on how to transform a truncated complex modal basis to the corresponding real one. (Ibrahim, 1983; Zhang and Lallemant 1987; Ibrahim and Fullekrug, 1990; Balmes, 1997). It appears, however, that an exact solution may not be feasible since the truncated complex and the real modes may not span the same space (Ibrahim and Sestieri, 1995).

The objective of this chapter is to present an approach for extracting the system matrices, or more precisely, their inverses, M^{-1}, ζ^{-1} and K^{-1} from experimentally obtained state-space realizations without computing the undamped modes. In most cases one must be content with getting a modal approximation to these matrices because only a truncated modal space is available. From a practical perspective it is the truncated problem that is of most interest. The method presented in this chapter uses the orthogonality properties of the identified eigenvectors in formulating these matrices in terms of the complex modes of the system. The formulations are presented both for the deterministic and stochastic input cases (Bernal and Gunes, 2002). Although a simplified

approach can be derived for systems that are classically damped, in this chapter we discuss the formulation for the case of general viscous damping.

The chapter is organized as follows: The first section reviews the transformations that are needed to extract the complex modes of the system in standard displacement-velocity form from the matrices of realization. The derivation of the expressions for the system matrices of the second-order differential equations of motion is presented in the next section. The chapter concludes with a numerical example illustrating the application of the procedures developed for the deterministic and stochastic input cases.

3.2 Transformation to Displacement-Velocity Basis

After obtaining a discrete-time state-space realization (as discussed in the previous chapter) the first task is to transform the realization results into displacement-velocity (D-V) basis. Consider any two realizations that define the same input/output map given by

$$\dot{x} = A_c\, x + B_c\, u \tag{3.1a}$$

$$y = C\, x + D\, u \tag{3.1b}$$

and

$$\dot{z} = A_z\, z + B_z\, u \tag{3.2a}$$

$$y = C_z z + D\, u \tag{3.2b}$$

As shown in the previous chapter, since

$$x = T\, z \tag{3.3}$$

one has;

$$A_c = T^{-1} A_z T \tag{3.4a}$$

$$B_c = T^{-1} B_z \tag{3.4b}$$

$$C = C_z T \tag{3.4c}$$

Expressing the matrices A_c and A_z in terms of their eigenvalues and eigenvectors, eq.3.4a can be written as

$$\Phi \Lambda \Phi^{-1} = T^{-1} \varphi \Lambda \varphi^{-1} T \tag{3.5}$$

where Λ is a diagonal matrix containing the eigenvalues (which is unaffected by the basis selection), Φ and φ are matrices whose columns are the eigenvectors of A_c and A_z respectively. From eq.3.5, one concludes that

$$T = \varphi \Phi^{-1} \tag{3.6}$$

Substituting eq.3.6 into eq.3.4c gives;

$$C \Phi = C_z \varphi \tag{3.7}$$

The equation of motion for a linear dynamic system is given by

$$M \ddot{\upsilon} + \zeta \dot{\upsilon} + K \upsilon = b_2 u(t) \tag{3.8}$$

where M, ζ, and K are the mass, damping and stiffness matrices, $u(t)$ is the forcing function, $\upsilon, \dot{\upsilon}$ and $\ddot{\upsilon}$ are the displacement, velocity and acceleration responses, respectively, and b_2 is the spatial distribution of the loading.

The response of the system, as a matrix output equation, can be written as

$$y = C_a \ddot{\upsilon} + C_v \dot{\upsilon} + C_d \upsilon \tag{3.9}$$

Solving for $\ddot{\upsilon}$ from eq.3.8 and substituting into eq.3.9 yields

$$y = C_a M^{-1} [b_2 u(t) - \zeta \dot{\upsilon} - K \upsilon] + C_v \dot{\upsilon} + C_d \upsilon \tag{3.10}$$

Comparison of eq.3.10 with eq.3.2b leads to the expression for the output influence matrix, C_z and the direct transmission matrix, D as

$$C_z = [C_d - C_a M^{-1} K \qquad C_v - C_a M^{-1} \zeta] \tag{3.11a}$$

$$D = C_a M^{-1} b_2 \tag{3.11b}$$

where C_d, C_v, and C_a are matrices connecting the output vector y to the physical coordinates.

Requiring that the state-space formulation in standard displacement-velocity form be the one associated with eq.3.2, the generalized eigenvalue problem can be written as:

$$\begin{bmatrix} 0 & I \\ -M^{-1}K & -M^{-1}\zeta \end{bmatrix} \begin{bmatrix} \Psi \\ \Psi \Lambda \end{bmatrix} = \begin{bmatrix} \Psi \\ \Psi \Lambda \end{bmatrix} [\Lambda] \tag{3.12}$$

where Ψ stands for the displacement partition of the eigenvector matrix.

Combining eq.3.7 with the second partition of eq.3.12 and then with eq.3.11 for displacement, velocity and acceleration measurements one at a time, one can show that

$$\Psi = C \, \Phi \, \Lambda^{-p} \tag{3.13}$$

$$\varphi = \begin{bmatrix} C \Phi [\Lambda^{-p}] \\ C \Phi [\Lambda^{-p+1}] \end{bmatrix} \tag{3.14}$$

where p = 0, 1 or 2 for displacement, velocity or acceleration sensing respectively. Eq.3.14 allows the computation of the D-V eigenvectors from those of an arbitrary realization (Bernal and Gunes, 2000). Note that from the eigenvalues of the system matrix in continuous time, Λ, one can extract the 'undamped' frequencies and the damping ratios. Since the complex eigenvalues (in complex conjugate pairs) are given by

$$\Lambda_i = -\xi_i \omega_i \pm i \, \omega_i \sqrt{(1 - \xi^2)} \tag{3.15}$$

Expressing eq.3.15 as

$$\Lambda_i = \alpha_i \pm i\beta_i \tag{3.16}$$

yields

$$\omega_i = \sqrt{\alpha_i^2 + \beta_i^2} \tag{3.17a}$$

$$\xi_i = \frac{-\alpha_i}{\sqrt{\alpha_i^2 + \beta_i^2}} \tag{3.17b}$$

where ω_i and ξ_i are typically noted as the undamped frequency and the damping ratio. However it should be noted that this value from eq.3.17 is equal to the true undamped frequency only in the case of classical damping and for the general case it is just an approximation of the true undamped value.

3.3 System Matrices in terms of the Complex Eigenvalue Solution

While the modes of the undamped system associated with eq.3.8 can be used to diagonalize the mass and the stiffness matrices, these modes diagonalize the damping matrix only in the special case referred to as classical or proportional damping. To determine a set of eigenvectors that uncouples the equations of motion in the general case, it is convenient to transform the original homogenous problem into the Hamilton canonical form, namely,

$$E\,\dot{y} = G\,y \tag{3.18}$$

where;

$$E = \begin{bmatrix} \zeta & M \\ M & 0 \end{bmatrix}, \qquad G = \begin{bmatrix} -K & 0 \\ 0 & M \end{bmatrix}, \qquad y = \begin{bmatrix} x \\ \dot{x} \end{bmatrix} \tag{3.19a,b,c}$$

The transformation to the first order form shown in eq.3.18 is not unique but it is one for which the matrices are symmetrical so that the eigenvectors prove to be orthogonal to the matrices *E* and *G*.

Consider eq.3.18, assuming a solution of the form

$$y = \phi\, e^{\lambda t} \tag{3.20}$$

and substituting this solution into eq.3.18 leads to the eigenvalue problem given by

$$E\,\phi\,\lambda = G\,\phi \tag{3.21}$$

Since the matrices *E* and *G* are real, the solution to eq.3.21 yields either real eigenvalues or eigenvalues in complex conjugate pairs. All the solutions can be conveniently organized in two matrices Φ_E and Λ_E, namely

$$\Phi_E = \begin{bmatrix} \Psi & \Psi^* \\ \Psi\Lambda & \Psi^*\Lambda^* \end{bmatrix}, \qquad \Lambda_E = \begin{bmatrix} \Lambda & \\ & \Lambda^* \end{bmatrix} \tag{3.22a, b}$$

where

$$\begin{bmatrix} \Psi \\ \Psi\Lambda \end{bmatrix} = \Phi = \begin{bmatrix} \phi_1 & \phi_2 & \cdots \end{bmatrix}, \quad \text{and} \quad \Lambda = \begin{bmatrix} \lambda_1 & & \\ & \lambda_2 & \\ & & \ddots \end{bmatrix} \tag{3.23a, b}$$

and the superscript * means complex conjugate.

The orthogonality property of the eigenvectors with respect to the matrices *E* and *G* provides the basis for developing equations for the system matrices. To illustrate the orthogonality relationships, consider two arbitrary eigenvectors ϕ_1 and ϕ_2 with the associated eigenvalues λ_1 and λ_2. From eq.3.21 one can write

$$E\,\phi_1\,\lambda_1 = G\,\phi_1 \tag{3.24a}$$

$$E\,\phi_2\,\lambda_2 = G\,\phi_2 \tag{3.24b}$$

Pre-multiplying eq.3.24a by ϕ_2^T and eq.3.24b by ϕ_1^T, one gets

$$\phi_2^T E \phi_1 \lambda_1 = \phi_2^T G \phi_1 \tag{3.25a}$$

$$\phi_1^T E \phi_2 \lambda_2 = \phi_1^T G \phi_2 \tag{3.25b}$$

Transposing eq.3.25a, recalling that *G* and *E* are Hermitian and subtracting eq.3.25b from eq.3.25 a leads to

$$\phi_1^T E \phi_2 (\lambda_1 - \lambda_2) = 0 \tag{3.26}$$

Therefore, provided that $\lambda_1 \neq \lambda_2$ one concludes that

$$\phi_1^T E \phi_2 = 0 \tag{3.27}$$

Although the orthogonality property has been demonstrated for the case of distinct eigenvalues, for repeated eigenvalues it is always possible to find an orthogonal set of eigenvectors if a complete set of independent eigenvectors exists. It is important to note that because the eigenvectors are not unique when the eigenvalues are repeated one must be careful to chose a set that satisfies the orthogonality relations. Finally, if an eigenvalue is repeated *m* times and there is not a set of *m* independent eigenvectors then it is not possible to satisfy eq.3.27 and one must operate with the general Jordan form. In the following treatment, we assume that eq.3.27 is satisfied.

It follows also from eqs. 3.25b and 3.27 that

$$\phi_1^T G \phi_2 = 0 \tag{3.28}$$

It is evident that from eqs.3.27 and 3.28 and the definitions in eqs.3.22 and 3.23, one can write

$$\Phi_E^T E \Phi_E = \begin{bmatrix} d_e & \\ & d_e^* \end{bmatrix}^{-1} \tag{3.29}$$

$$\Phi_E^T G \Phi_E = \begin{bmatrix} d_g & \\ & d_g^* \end{bmatrix}^{-1} \tag{3.30}$$

From eqs.3.29 and 3.30, it follows that

$$E^{-1} = \Phi_E \begin{bmatrix} d_e & \\ & d_e^* \end{bmatrix} \Phi_E^T \tag{3.31}$$

$$G^{-1} = \Phi_E \begin{bmatrix} d_g & \\ & d_g^* \end{bmatrix} \Phi_E^T \tag{3.32}$$

The inverse of the matrices E and G can also be obtained explicitly in terms of the system matrices. From eqs.3.19a and 3.19b, one gets

$$E^{-1} = \begin{bmatrix} 0 & M^{-1} \\ M^{-1} & -M^{-1}\zeta M^{-1} \end{bmatrix} \tag{3.33}$$

$$G^{-1} = \begin{bmatrix} -K^{-1} & 0 \\ 0 & M^{-1} \end{bmatrix} \tag{3.34}$$

Substituting the expression for Φ_E given by eq.3.22a into eq.3.31 and 3.32 and equating the results with eq.3.33, one gets the following equalities:

$$M^{-1} = 2\Re\,(\Psi\,\Lambda\, d_g \Lambda^T \Psi^T) \tag{3.35}$$

$$M^{-1} = 2\Re\,(\Psi d_e\ \Lambda^T \Psi^T) \tag{3.36}$$

$$K^{-1} = -2\Re\,(\Psi\, d_g\ \Psi^T) \tag{3.37}$$

$$M^{-1}\zeta M^{-1} = -2\Re\ \ (\Psi\ \ \Lambda\ \ d_e \Lambda^T \Psi^T) \tag{3.38}$$

$$\Re\ (\Psi\,\Lambda\, d_g\ \Psi^T) = 0 \tag{3.39}$$

$$\Re\ (\Psi\, d_e\ \Psi^T) = 0 \tag{3.40}$$

By examining eq.3.35 and eq.3.36, we get

$$\Lambda\, d_g\ = d_e \tag{3.41}$$

It follows from eq.3.41 then that eqs. 3.35-3.40 are reduced to;

$$M^{-1} = 2\Re(\Psi\Lambda^2 d_g \Psi^T) \tag{3.42}$$

$$K^{-1} = -2\Re(\Psi\, d_g\, \Psi^T) \tag{3.43}$$

$$M^{-1}\zeta M^{-1} = -2\Re(\Psi\,\Lambda^3\, d_g\, \Psi^T) \tag{3.44}$$

$$\Re(\Psi\,\Lambda\, d_g\, \Psi^T) = 0 \tag{3.45}$$

Note that eqs.3.42 and 3.43 lead to the partitions of the inverse of the mass and the flexibility matrices at the measured coordinates. Leaving aside the errors due to round-off or measurement noise, the errors in these expressions derive from modal truncation. If one has all the modes, then these matrices are exact and they can be inverted to yield condensed mass and stiffness matrices at the measured coordinates. If the modal basis is truncated however, then eqs.3.42 and 3.43 provide modal contributions to the partitions of the inverse of the mass and flexibility matrices. Note that even when the modal basis is sharply truncated, accurate estimates of the flexibility matrix can be obtained since it is dominated by the lower modes. This, however, does not mean that its inverse (if exists) can also be obtained with the same accuracy. Indeed, a classical result from matrix theory states that

$$\frac{\left\|(S+\Delta S)^{-1} - S^{-1}\right\|}{\left\|S^{-1}\right\|} \le \kappa(S)\frac{\left\|\Delta S\right\|}{\left\|S\right\|} \tag{3.46}$$

where S is an arbitrary matrix for which det $S \neq 0$, ΔS is an infinitesimal error on S, and $\kappa(S)$ is a measure of relative errors in the inverse of S when the latter is perturbed by an arbitrary, infinitesimally small matrix. Hence, according to eq.3.46, error in S can be amplified as much as its condition number during inversion. In order to circumvent this inversion problem, an alternative means of computing the inverse has been explored using the Cayley-Hamilton theorem and the results of this initial examination are presented in Appendix C.

All one can say about the damping matrix appears to be limited to eq.3.44 in the general case of viscous damping with partial sensors and truncated modal basis. If the modal basis is complete, and one has full sensor information, then the damping matrix can be isolated from eq. 3.44 as;

$$\zeta = -M \quad [2\Re \ (\Psi \Lambda^3 d_g \Psi^T)] \ M \tag{3.47}$$

In addition, if the number of sensors is limited but their arrangement is such that the unmeasured partition of the mass matrix is uncoupled from the measured partition, then one can still use eq.3.47 to obtain the partition of the damping matrix associated with the measured coordinates. If the damping is classical, however, then the inverse of the damping matrix can be calculated from

$$\zeta^{-1} = -M^{-1} \quad [2\Re \ (\Psi \Lambda^3 d_g \Psi^T)]^{-1} M^{-1} \tag{3.48}$$

since the middle term in brackets in eq.3.48, which needs to be inverted, is diagonal. The inverse of the damping matrix in this case includes the contributions from the modes that are measured.

The key issue that is left for discussion is how to obtain the normalization constants, d_g. As will be shown in the next section, one can calculate d_g only in the case where the measured data includes both input and output time histories and there is at least one collocated sensor-actuator pair. For these conditions, the inverse of the system matrices for all the available coordinates, including input as well as the output can be computed. When the input is not measured or, even if the input is measured but there are not collocated sensors then one can not obtain the normalization d_g without providing additional information. However, provided that mass matrix can be assumed diagonal, it is still possible to obtain a normalization that is proportional to d_g so all the matrices are then to within one missing scalar.

3.4 Deterministic Input

In the previous section we have derived formulas for the system matrices or for their inverses in terms of the complex modes of the system. This section outlines the procedure to attain the required normalization.

Recall that the results of a realization, after transformation to continuous time, provide the input-output map of the form given in eq.3.1. Taking a Fourier transform of eqs.3.1a and 3.1b, solving for the state vector from eq.3.1a and substituting the result in eq.3.1b one gets

$$y(\omega) = [C[I \cdot i\omega - A_c]^{-1} B_c + D]u(\omega) \tag{3.49}$$

The Fourier transform of the output vector can be expressed in terms of that corresponding to the displacement vector, y_D as

$$y(\omega) = (i\omega)^p \, y_D(\omega) \tag{3.50}$$

where p = 0, 1 or 2 for displacement, velocity or acceleration sensing, respectively. Substituting eq.3.50 into eq.3.49 yields

$$y_D(\omega) = \frac{1}{(i\omega)^p}[C[I \cdot i\omega - A_c]^{-1} B_c + D]u(\omega) \tag{3.51}$$

Recognizing that the flexibility relates $y_D(\omega)$ to $u(\omega)$ at $\omega = 0$ leads to

$$K^{-1} = \lim_{\omega \to 0} \frac{1}{(i\omega)^p}[C[I \cdot i\omega - A_c]^{-1} B_c + D] \tag{3.52}$$

Except for the case where p=0, the above limit leads to the indeterminate expression 0/0. However, differentiating the numerator and denominator an appropriate number of times one gets

$$K_{m,r}^{-1} = -CA_c^{-(p+1)} B_c \tag{3.53}$$

where $K_{m,r}^{-1}$ is the partition of the flexibility matrix associated with the m output sensors (rows) and r inputs (columns). Eq.3.53 therefore, provides a partition of eq.3.37 and by equating them one can solve for the missing diagonal. The procedure is illustrated next.

The partition of the flexibility matrix for the m output sensors and c collocated inputs can be written as

$$K_{m,c}^{-1} = -CA_c^{-(p+1)} B_{cc} \tag{3.54}$$

where B_{cc} are the columns of B_c associated with collocated sensors.

We can express eq.3.49 in terms of modal contributions, namely;

$$A_c = \Phi_E \Lambda_E \Phi_E^{-1} \tag{3.55}$$

where Φ_E and Λ_E are those defined by eqs.3.22 and 3.23.

Substituting eq.3.55 into 3.54, yields

$$K_{m,c}^{-1} = -C \Phi_E \Lambda_E^{-(p+1)} \Phi_E^{-1} B_{cc} \tag{3.56}$$

or;

$$K_{m,c}^{-1} = -2\Re \left(C\Phi\Lambda^{-(p+1)}\Phi^{-T} B_{cc}\right) \tag{3.57}$$

Since the displacement partition of the modes at the *m* output sensors can be obtained using

$$\Psi_m = C \Phi \Lambda^{-p} \tag{3.58}$$

substituting eq.3.58 into eq.3.57, one obtains

$$K_{m,c}^{-1} = -2\Re \left(\Psi_m \ \Lambda^{-1} \Phi^{-T} B_{cc}\right) \tag{3.59}$$

Equating eq.3.59 to the partition of the flexibility matrix at the collocated coordinates given by eq.3.37 leads to

$$d_g \ \Psi_{mc}^T = -\Lambda^{-1}\Phi^{-T} B_{cc} \tag{3.60}$$

where Ψ_{mc} are the rows of Ψ_m associated with the collocated sensors.

For a single collocated sensor, the rows in eq.3.60 give scalar equations that can be solved for each one of the entries in d_g. Redundant information, however, is available when there are

multiple collocated sensors, given that one can obtain estimates of each term in d_g from each collocated coordinate. For perfect data the estimates are identical but, needless to say, this is never the case in practice. While one can always proceed with a least square solution, a simpler, and perhaps preferable approach is to take the entries in d_g as the values corresponding to the largest value in the associated left side rows. The rationale being that the smallest error under noisy conditions is likely to be at the coordinate with the largest modal amplitude.

The modal amplitudes at the non co-located coordinates Ψ_{nc} (if any) for each mode j can then be computed from

$$C\Phi_{E,j}\,\Lambda_j^{-(p+1)}\,\Phi_{E,j}^{-T}\,B_{c,nc} = \Psi_{m,j}\,\Psi_{nc,j}^{T}\,dg_j \tag{3.61}$$

where $\Phi_{E,j}$ is the jth column of Φ_E and $\Phi_{E,j}^{-T}$ is the jth row of $\Phi_{E,j}^{-1}$.

Eq.3.61 provides as many estimates of $\Psi_{nc,j}$ as there are output coordinates. Based on the same rationale discussed previously, the result associated with the largest denominator is a reasonable choice.

Padding the mode shapes obtained in eq.3.58 with the amplitudes of Ψ_{nc} obtained from eq.3.61 yields

$$\Psi = \begin{bmatrix} \Psi_m \\ \Psi_{nc} \end{bmatrix} \tag{3.62}$$

The system matrices can then be computed using eqs.3.42, 3.43 and 3.47.

Illustration of the Deterministic Input Approach

The basic steps of the approach are illustrated using the simple system shown in Figure 3.1. The system is excited at coordinate 3 and output sensors that can measure acceleration are provided at coordinates 1, 2 and 3. Modal truncation and error in the identification are not contemplated in this example. Note that the damping is non-classical but the mass matrix is diagonal so that M_{12}=0 where the subscripts 1 and 2 denote the measured and unmeasured coordinates, respectively.

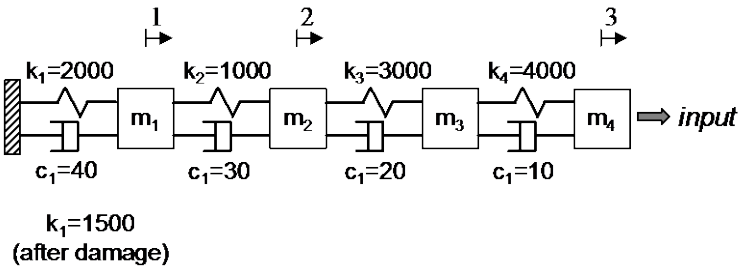

(m_1=20, m_2=24, m_3=28, m_4=32)

Figure 3.1 System considered

1. System matrices, *A*, *B* and *C* can be obtained analytically in this case as;

$$A = \begin{bmatrix} 0 & 0 & 0 & 0 & 1 & 0 & 0 & 0 \\ 0 & 0 & 0 & 0 & 0 & 1 & 0 & 0 \\ 0 & 0 & 0 & 0 & 0 & 0 & 1 & 0 \\ 0 & 0 & 0 & 0 & 0 & 0 & 0 & 1 \\ -150 & 50 & 0 & 0 & -3.5 & 1.5 & 0 & 0 \\ 41.67 & -166.7 & 125 & 0 & 1.25 & -2.08 & 0.83 & 0 \\ 0 & 107.14 & -250 & 142.86 & 0 & 0.71 & -1.07 & 0.36 \\ 0 & 0 & 125 & -125 & 0 & 0 & 0.31 & -0.31 \end{bmatrix}$$

$$B = \begin{bmatrix} 0 & 0 & 0 & 0 & 0 & 0 & 0 & 0.03 \end{bmatrix}^T$$

$$C = \begin{bmatrix} -150 & 50 & 0 & 0 & -3.5 & 1.5 & 0 & 0 \\ 41.67 & -166.67 & 125 & 0 & 1.25 & -2.08 & 0.83 & 0 \\ 0 & 0 & 125 & -125 & 0 & 0 & 0.31 & -0.31 \end{bmatrix}$$

2. From the eigenvalues and eigenvectors of *A*, one gets:

$$\Lambda = \begin{bmatrix} -0.08-2.60i & & & \\ & -0.65+10.79i & & \\ & & -1.75+13.47i & \\ & & & -1.00+19.49i \end{bmatrix}$$

$$\Phi=10^{-2}x\begin{bmatrix} -2.43+5.78i & -5.87-2.98i & -4.65+3.34i & -0.09-0.57i \\ -6.68+16.66i & -3.54-3.58i & 1.99-3.28i & 1.76+1.62i \\ -7.91+19.31i & 0.44-0.77i & 1.14-0.44i & -3.43-2.12i \\ -8.43+20.39i & 2.93+2.72i & -1.18+1.87i & 1.75+0.90i \\ -14.86-6.81i & 35.98-61.36i & -36.87-68.47i & 11.24-1.22i \\ -42.85-18.74i & 41-35.83i & 40.68+32.62i & -33.36+32.77i \\ -49.65-22.16i & 0.52+4.77i & 3.91+16.18i & 44.75-64.72i \\ -52.43-23.60i & -31.23+29.88i & -23.09-19.22i & -19.23+33.14i \end{bmatrix}$$

3. The arbitrarily scaled complex mode shapes Ψ_m at the sensor coordinates are obtained as:

$$\Psi_m = \begin{bmatrix} -0.024+0.058i & -0.059-0.030i & -0.047+0.033i & -0.001-0.006i \\ -0.067+0.167i & -0.035-0.036i & 0.020-0.033i & 0.018+0.016i \\ -0.084+0.204i & 0.029+0.027i & -0.012+0.019i & 0.018+0.009i \end{bmatrix}$$

4. From eq.3.60, the normalization constants d_g are:

$$d_g = \begin{bmatrix} -48.59-7.93i \\ 41.81-12.38i \\ 14.62+38.06i \\ 45.14+29.62i \\ -48.59+7.93i \\ 41.81+12.38i \\ 14.62-38.06i \\ 45.14-29.62i \end{bmatrix}$$

5. Since none of the coordinates have inputs only, Ψ_{nc}=[ ] and $\Psi=\Psi_{m.}$ Eqs.3.42, and 3.43 and 3.47 lead to:

$$M^{-1} = \begin{bmatrix} 0.05 & 0 & 0 \\ 0 & 0.0417 & 0 \\ 0 & 0 & 0.0312 \end{bmatrix}, \quad K^{-1} = \begin{bmatrix} 0.0005 & 0.0005 & 0.0005 \\ 0.0005 & 0.0015 & 0.0015 \\ 0.0005 & 0.0015 & 0.0021 \end{bmatrix}, \quad C = \begin{bmatrix} 70 & -30 & 0 \\ -30 & 50 & 0 \\ 0 & 0 & 10 \end{bmatrix}$$

which are exactly equal to the true values at sensor coordinates.

3.5 Stochastic Input

The inverse of the system matrices for the computed modes can not be assembled for output only systems without the introduction of some apriori knowledge because the matrix B_c in eq.3.53 is undefined. Hence, the basic idea implemented for the stochastic case is to use the known structure of the inverse of the mass matrix to provide the necessary constraints. In particular, one proceeds by assuming simply that M^{-1} is diagonal. It is evident, of course, that this approach essentially means that the off-diagonal part of M^{-1} is known to be zero. In this case because the equations are now all equal to zero one can compute the normalizing factors only up to q undetermined constants, where q is the nullity of the resulting coefficient matrix. The specifics used to arrive at the normalization constants in the case where M^{-1} is assumed diagonal are described next.

From the orthogonality relations of the complex eigensolution we have shown previously that

$$M^{-1} = \Re \sum_{j=1}^{N} \Psi_{m,j} \Psi_{m,j}^{T} \quad \Lambda_j^2 \quad d_{g,j} \tag{3.63}$$

where n=2N is the system order, d_g are complex constants and Ψ_m is given by eq.3.58.

Defining

$$H_R + H_I\, i = \Psi_{m,j}\, \Psi_{m,j}^{T}\, \Lambda_j^2 \tag{3.64}$$

eq.3.63 can be written in the domain of real numbers as

$$M^{-1} = \sum_{j=1}^{n} (H_{R,j}\, d_{gR,j} - H_{I,j}\, d_{gI,j}) \tag{3.65}$$

where d_{gR} and d_{gI} are the real and the imaginary components of the constant d_g .

Taking the upper (lower) triangular portion of M^{-1} (without the main diagonal) and placing it in vector form one can write

$$0 = \sum \hat{H}_{R,j}\, d_{gR,j} - \hat{H}_{I,j} d_{gI,j} \tag{3.66}$$

where $\hat{H}_j$ are vectors. Finally, defining the vector β as all the real components of d_g followed by all the imaginary components, namely

$$\beta = [d_{gR,1} \quad d_{gR,2} \quad \cdots \quad d_{gI,1} \quad d_{gI,2} \quad \cdots]^T \tag{3.67}$$

one gets;

$$\overline{H}\,\beta = 0 \tag{3.68}$$

where;

$$\overline{H} = [\hat{H}_{R,1}, \hat{H}_{R,2}, \ldots - \hat{H}_{I,1}, -\hat{H}_{I,2} \ldots] \tag{3.69}$$

It follows then that β (which contains the required normalizing constants ordered as per eq.3.69) is in the null space of the matrix $\overline{H}$. One can further restrict the subspace that contains β by taking advantage of the relationship given by

$$\Re \sum_{j=1}^{n} \Psi_{m,j} \Psi_{m,j}^T \Lambda_j\, d_{g,j} = 0 \tag{3.70}$$

Following the same approach used to arrive at eq.3.68, eq.3.70 can be expressed as

$$\overline{S}\,\beta = 0 \tag{3.71}$$

where the only difference is that the assembly of $\overline{S}$ includes the diagonal of the matrix in eq.3.70 .

Combining eq.3.69 and eq.3.71 one gets

$$\begin{bmatrix} \overline{H} \\ \overline{S} \end{bmatrix} \beta = Y\beta = 0 \tag{3.72}$$

which shows that β is in the null space of *Y*. If all the modes are available, *Y* is rank deficient by one and β can be computed to within a scalar*. Note that matrix $Y \in \Re^{m^2 \times 2N}$ where *m* is the number of sensors and *N* is the number of identified modes, needs to be a tall matrix. Splitting β back into the complex constants one obtains the d_g's in eq.3.67. The system matrices can then be obtained to within a scalar using eqs.3.42, 3.43 and 3.47. In practice, however, we seldom obtain 'all the modes' and the matrix *Y* in eq.3.72 is typically full rank. In these cases an approximate solution can be obtained by taking β as the singular vector associated with the smallest singular value of *Y*.

Illustration of the Stochastic Input Approach

The basic steps for the unmeasured input for the system shown in Figure 3.1 can be summarized as follows:

1. Once the complex modes are obtained as in the deterministic case, the next step is to obtain the normalization constants from eq.3.72. This requires that one assemble $\overline{H}$ and $\overline{S}$. The computations for the first mode are illustrated in the following. Assembling H_1 from eq.3.64 one gets;

$$H_1 = \begin{bmatrix} 0.017+0.020i & 0.051+0.057i & 0.062+0.071i \\ 0.051+0.057i & 0.149+0.161i & 0.180+0.199i \\ 0.062+0.071i & 0.180+0.199i & 0.219+0.247i \end{bmatrix}$$

2. The upper triangular part of the matrix (without the main diagonal) contains, in this case, 3 numbers. The real and the imaginary components of these numbers are used to form the vectors $\hat{H}_{R,1}$ and $\hat{H}_{I,1}$, namely;

$$\hat{H}_{R,1} = \begin{bmatrix} 0.051 \\ 0.062 \\ 0.180 \end{bmatrix} \quad \hat{H}_{I,1} = \begin{bmatrix} 0.057 \\ 0.071 \\ 0.199 \end{bmatrix}$$

* assuming that all the modes are coupled. If there are sets of uncoupled modes then the nullity of *Y* is typically larger.

where the order selected is arbitrary. Repeating these steps for all the modes one obtains the vectors needed to form $\overline{H}$. The result is;

$$\overline{H} = \begin{bmatrix} 0.051 & -0.072 & 0.073 & -0.034 & -0.057 & 0.381 & 0.399 & -0.041 \\ 0.062 & 0.071 & -0.047 & -0.018 & -0.071 & -0.299 & -0.229 & -0.040 \\ 0.180 & -0.021 & -0.031 & -0.044 & -0.199 & -0.234 & 0.154 & 0.174 \end{bmatrix}$$

where the columns of $\overline{H}$ corresponding to the first mode are highlighted.

3. The same approach is repeated to form $\overline{S}$. One gets;

$$S_1 = \begin{bmatrix} 0.008\text{-}0.007i & 0.021\text{-}0.020i & 0.026\text{-}0.025i \\ 0.021\text{-}0.020i & 0.060\text{-}0.059i & 0.074\text{-}0.072i \\ 0.026\text{-}0.025i & 0.074\text{-}0.072i & 0.092\text{-}0.087i \end{bmatrix}$$

Placing the results in vector form gives;

$$\hat{S}_{R,1} = \begin{bmatrix} 0.008 \\ 0.021 \\ 0.060 \\ 0.026 \\ 0.074 \\ 0.092 \end{bmatrix} \quad \hat{S}_{I,1} = \begin{bmatrix} -0.007 \\ -0.020 \\ -0.059 \\ -0.025 \\ -0.072 \\ -0.087 \end{bmatrix}$$

where we note that the main diagonal is also included since it is also zero according to eq.3.70. The matrix $\overline{S}$ is assembled by repeating the process for all the modes, the results is;

$$\overline{S} = \begin{bmatrix} 0.008 & -0.039 & 0.040 & -0.000 & 0.007 & -0.025 & -0.020 & 0.001 \\ 0.021 & -0.035 & -0.030 & 0.002 & 0.020 & -0.009 & 0.002 & -0.002 \\ 0.060 & -0.027 & 0.020 & -0.011 & 0.059 & 0.002 & 0.007 & -0.000 \\ 0.026 & 0.027 & 0.017 & 0.002 & 0.025 & 0.008 & -0.001 & -0.001 \\ 0.074 & 0.022 & -0.011 & -0.009 & 0.072 & -0.001 & -0.004 & -0.003 \\ 0.092 & -0.017 & 0.006 & -0.006 & 0.087 & -0.000 & 0.002 & -0.004 \end{bmatrix}$$

4. Combining $\overline{H}$ and $\overline{S}$ one obtains the matrix *Y*. From inspection of the singular values, *s*, it is evident that the nulity is one. The singular values s and the nullspace β are shown below.

$$s = \begin{bmatrix} 0.684 \\ 0.432 \\ 0.191 \\ 0.117 \\ 0.073 \\ 0.053 \\ 0.009 \\ 7.18E\text{-}17 \end{bmatrix} \qquad \beta = \begin{bmatrix} -0.3232 \\ 0.1191 \\ 0.0743 \\ 0.1491 \\ 0.3386 \\ -0.5149 \\ 0.5603 \\ -0.3999 \end{bmatrix}$$

From β one readily gets the complex constants, d_g from eq.3.67. The inverse of the mass, and stiffness matrices can then be calculated from eqs. 3.42, 3.43, and 3.47. One gets;

$$M^{-1} = \alpha \begin{bmatrix} 0.4068 & 0 & 0 \\ 0 & 0.3390 & 0 \\ 0 & 0 & 0.2542 \end{bmatrix}, \; K^{-1} = \alpha \begin{bmatrix} 0.0041 & 0.0041 & 0.0041 \\ 0.0041 & 0.0122 & 0.0122 \\ 0.0041 & 0.0122 & 0.0169 \end{bmatrix}, \; C = \alpha \begin{bmatrix} 8.6042 & -3.6875 & 0 \\ -3.6875 & 6.1458 & 0 \\ 0 & 0 & 1.2292 \end{bmatrix}$$

from where it can be seen that the difference is a simple scalar multiplier (α=0.1229).

3.6 Numerical Example with Identification Results

To illustrate the effects of measurement noise and modal truncation in the identified results consider a 10 DOF shear building that is subjected to some random white noise excitation at the first, eighth and the tenth floors. A total of five sensors recording the acceleration response are placed at every other floor starting with the second floor. The output noise is prescribed to have a root-mean-square (RMS) equal to 5% of the RMS of the response measured on the sensor located on the second floor. A non-proportional damping distribution is prescribed to the system as shown in Figure 3.2. Eq.3.73 displays the inverses of the exact system matrices at the sensor locations (including both input and output) for the structure under consideration. The ordering of the degrees-of-freedom is from the lowest to the highest floor.

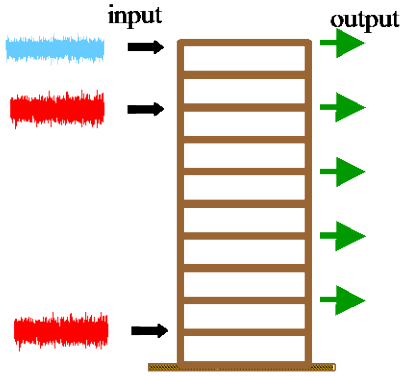

Floor	*m*	*c*	*k*
10	3	16	600
9	3	12	600
8	4	12	800
7	4	12	800
6	4	8	800
5	4	8	800
4	6	8	1000
3	6	8	1000
2	6	6	1000
1	8	6	2000

Figure 3.2 Structure utilized in numerical testing of the approach

$$K^{-1}=10^{-3}\begin{bmatrix} 0.50 & 0.50 & 0.50 & 0.50 & 0.50 & 0.50 \\ 0.50 & 2.50 & 2.50 & 2.50 & 2.50 & 2.50 \\ 0.50 & 2.50 & 4.50 & 4.50 & 4.50 & 4.50 \\ 0.50 & 2.50 & 4.50 & 7.00 & 7.00 & 7.00 \\ 0.50 & 2.50 & 4.50 & 7.00 & 9.50 & 9.50 \\ 0.50 & 2.50 & 4.50 & 7.00 & 9.50 & 12.83 \end{bmatrix} \quad M^{-1}=\begin{bmatrix} 0.13 & 0 & 0 & 0 & 0 & 0 \\ 0 & 0.17 & 0 & 0 & 0 & 0 \\ 0 & 0 & 0.17 & 0 & 0 & 0 \\ 0 & 0 & 0 & 0.25 & 0 & 0 \\ 0 & 0 & 0 & 0 & 0.25 & 0 \\ 0 & 0 & 0 & 0 & 0 & 0.33 \end{bmatrix} \tag{3.73}$$

Table 3.1 Comparison of the exact and identified frequencies

Mode no.	Exact f_u (Hz)	OKID $\bar{f}_u$ (Hz)	Sub-ID $\bar{f}_u$ (Hz)
1	0.35	0.35	0.36
2	0.93	0.93	0.93
3	1.59	1.59	1.60
4	2.18	2.19	2.24
5	2.68	2.71	2.75
6	2.96	2.93	2.85
7	3.41	3.51	
8	3.74	3.76	
9	4.01		
10	4.34		

where eigenvalues of $(A_c)= \lambda = 2\pi(\bar{f}_u \pm i\bar{f}_d)$

Modal identification is carried out by ERA-OKID and Sub-ID algorithms for the deterministic and stochastic input cases, respectively. Application of these algorithms yields 8 modes in the deterministic case and 6 modes in the stochastic case as presented in Table 3.1. Comparison of the identified results with the 'exact' ones shows slight deviations (within 1%) from the true

undamped values for the deterministic case pointing that the modal complexity is not severe. The results for the stochastic case are also in agreement, the maximum difference between the two is less than 4%.

The techniques outlined in sections 3.4 and 3.5 are coded using MATLAB® and the script '*micki.m*' is attached in Appendix A. The system matrices extracted using the approaches discussed in the previous sections are presented in Table 3.2 and Table 3.3 for the deterministic and stochastic cases, respectively. Note that, for the known input case, the extracted matrices are of size (6×6) since in addition to the five output sensors we have a non-collocated input; whereas for the stochastic case they are of size (5×5). To isolate the effect of modal truncation in the comparisons we make, the truncated versions of the matrices are also displayed in these tables. The results indicate that for the deterministic case, M^{-1} and K^{-1} are extracted with very good accuracy due to the fact that the method is exact and the discrepancies are due to the effects of noise. Since damping is non-classical and we have a truncated set of modes, ζ^{-1} obtained using using eq.3.48. will not have clear physical meaning. Therefore, in this example we did not attempt to obtain an estimate for the damping.

Table 3.2 Comparison of the system matrices at sensor locations for the deterministic case

	Exact with 8 Modes	Identified
$K^{-1}*10^{3}$	0.50 0.50 0.50 0.50 0.50 0.50 0.50 2.50 2.49 2.49 2.51 2.51 0.50 2.49 4.46 4.45 4.53 4.53 0.50 2.49 4.45 6.88 6.97 7.01 0.50 2.51 4.53 6.97 9.38 9.44 0.50 2.51 4.53 7.01 9.44 12.80	0.50 0.50 0.49 0.49 0.49 0.49 0.50 2.50 2.50 2.50 2.49 2.50 0.49 2.50 4.50 4.46 4.46 4.52 0.49 2.50 4.46 6.80 7.02 7.07 0.49 2.49 4.46 7.02 9.42 9.36 0.49 2.50 4.52 7.07 9.36 12.72
M^{-1}	0.12 0.00 0.00 0.00 0.00 0.00 0.00 0.16 -0.01 -0.01 0.01 0.01 0.00 -0.01 0.14 -0.04 0.02 0.02 0.00 -0.01 -0.04 0.16 -0.03 0.00 0.00 0.01 0.02 -0.03 0.17 -0.04 0.00 0.01 0.02 0.00 -0.04 0.31	0.13 0.00 0.00 0.00 0.00 0.00 0.00 0.17 0.00 0.00 -0.01 0.00 0.00 0.00 0.16 -0.04 -0.01 0.02 0.00 0.00 -0.04 0.12 0.01 0.03 0.00 -0.01 -0.01 0.01 0.17 -0.08 0.00 0.00 0.02 0.03 -0.08 0.30

Table 3.3 Comparison of the system matrices at sensor locations for the stochastic case

	Exact with 6 Modes	Identified
$K^{-1}*10^3$	$\begin{bmatrix} 2.41 & 2.46 & 2.54 & 2.47 & 2.53 \\ 2.46 & 4.41 & 4.49 & 4.52 & 4.47 \\ 2.54 & 4.49 & 6.83 & 6.99 & 7.03 \\ 2.47 & 4.52 & 6.99 & 9.35 & 9.47 \\ 2.53 & 4.47 & 7.03 & 9.47 & 12.70 \end{bmatrix}$	$\alpha \begin{bmatrix} 3.50 & 3.79 & 3.68 & 3.72 & 3.74 \\ 3.79 & 6.24 & 6.45 & 6.36 & 6.36 \\ 3.68 & 6.45 & 9.92 & 10.05 & 10.14 \\ 3.72 & 6.36 & 10.05 & 13.23 & 13.82 \\ 3.74 & 6.36 & 10.14 & 13.82 & 18.64 \end{bmatrix}$
M^{-1}	$\begin{bmatrix} 0.12 & -0.03 & 0.02 & -0.01 & 0.01 \\ -0.03 & 0.11 & -0.01 & 0.01 & -0.01 \\ 0.02 & -0.01 & 0.14 & -0.01 & 0.02 \\ -0.01 & 0.01 & -0.01 & 0.15 & -0.03 \\ 0.01 & -0.01 & 0.02 & -0.03 & 0.26 \end{bmatrix}$	$\alpha \begin{bmatrix} 0.14 & 0.00 & 0.00 & 0.00 & 0.00 \\ 0.00 & 0.14 & -0.01 & 0.00 & 0.00 \\ 0.00 & -0.01 & 0.20 & 0.00 & 0.00 \\ 0.00 & 0.00 & 0.00 & 0.18 & 0.00 \\ 0.00 & 0.00 & 0.00 & 0.00 & 0.34 \end{bmatrix}$

For stochastic input case the system matrices that differ from the true ones by a single undetermined multiplier are obtained by assuming that M^{-1} is diagonal. Note that the selected scaling normalizes the trace of M^{-1} to unity. Since we have an incomplete set of modes, the method outlined in the previous section becomes approximate (the off-diagonals of M^{-1} are not zero). The estimations, therefore, are not as accurate as the deterministic case. Fortunately however, comparison of the identified K^{-1} in Table 3.2 and Table 3.3 with the exact matrix given in eq.3.73 indicates that K^{-1} or the flexibility matrix, which will be used later in the damage localization stage, is estimated quite accurately in both cases since it is dominated mainly by the lower modes. Figure 3.3 illustrate the percent error in the identified flexibility coefficients for the deterministic and stochastic cases. The errors are computed as the deviation between the computed flexibility coefficient and the exact value, normalized by the largest value in the associated column of the exact matrix. In these figures, the value of the index corresponds to the location in the matrix that is obtained by counting from the main diagonal downward, from column to column, sequentially. The comparison in Figure 3.3(b) for the stochastic case is based on fixing the undetermined constant to be the mean of the ratio between the identified and the exact flexibility coefficients. By inspecting these results one can see that the mean error in the identified flexibility is less than 0.93% for the deterministic case and 2.2% for the stochastic case. The inverse of the mass is not identified as accurately due to the fact that the modal basis is incomplete and this matrix is not dominated by the lower modes.

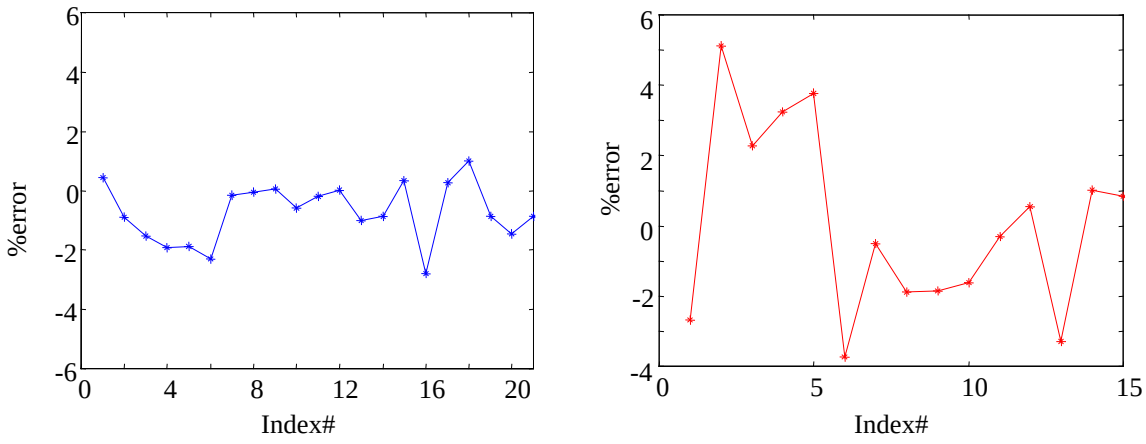

(a) (b)

Figure 3.3 Percent error in the coefficients of the identified flexibility matrix for (a) deterministic case, (b) stochastic case

3.7 Concluding Remarks

In this chapter an approach is presented for extracting the inverses of the system matrices from the matrices of realization. It was shown that in general the system matrices can not be extracted and one must be satisfied with the modal contributions to the partitions of the inverses. When the input is measured, the only requirement is that there must be at least one collocated sensor-actuator pair. The extension of the technique to cases where only output measurements are available requires additional information be introduced to the problem. In particular, by imposing a restriction on the structure of the mass matrix, the matrices that differ from the true ones by a scalar multiplier can be obtained. Although this approach is theoretically exact only when the modal basis is complete good approximations of the truncated flexibility can be obtained when the truncated space provides a reasonable approximation for M^{-1}. A general methodology that uses these flexibility matrices to locate damage is presented in the next chapter.

CHAPTER 4

Localization of Damage

4.1 Introduction

Changes in flexibility contain information regarding the location of the damage, but until recently mapping of these changes to the location of the physical damage in the structure had been done heuristically. In particular, the traditional approach was to examine the diagonal of change in flexibility and assert that damage was 'close' to the sensor where the largest change has been detected. This not only discards the off-diagonal information but is also system-dependent. As a part of the work done on the ASCE-IASC benchmark structure, the group at Northeastern University, led by D. Bernal, developed a rigorous approach for interrogating changes in flexibility with respect to the location of damage.

The technique, known as the damage locating vector (*DLV*) approach, identifies the elements of the structure that are damaged as belonging to the set of elements whose internal forces under the action of a certain set of load vectors are zero (Bernal, 2002). These vectors, designated here as *DLV*s, define a basis for the null space of the change in flexibility and can, therefore, be computed from the measured data without reference to a model of the structure. The localization of damage using the *DLV* technique is not, however, entirely model-free because the stress fields used to locate damage need to be computed with reference to a model. Nevertheless, sensitivity of the results to error in the mathematical model is typically small because only the undamaged topology and the values of the relative stiffness parameters enter into the computation of the stress fields. In this chapter, the technique is presented and the particulars of the application in the case of deterministic and stochastic input cases are discussed. The effects of modeling errors and modal truncation are also examined with a numerical example.

4.2 Load Vectors for Damage Localization

Consider a system that can be treated as linear in the pre and post damage states, but which is otherwise arbitrary, having undamaged and damaged flexibility matrices at *m* sensor locations given by F_U and F_D respectively. To establish the theoretical foundation of the localization approach we consider first the ideal situation where the flexibility matrices are exact. Performance of the technique when these matrices reflect error in the identified modal parameters and truncation of the modal space is examined in a later section. Assume there are a number of load vectors, defined in sensor coordinates, which produce identical deformations at the sensors in the undamaged and the damaged states. If all the linearly independent vectors that satisfy this requirement are collected in a matrix *L* it is evident that one can write

$$(F_D - F_U)L = DF \cdot L = 0 \tag{4.1}$$

The relationship in eq.4.1 may be satisfied in two ways, either *DF = 0*, or *DF* is rank deficient and *L* is a basis for the null space. The first possibility implies that there is either no damage or that the damage is confined to a region of the structure where the stresses are zero for any loading in sensor coordinates. In practice, of course, one never computes *DF* as identically zero so the real issue is to distinguish *DF* matrices that derive from damage from those that are purely the byproduct of inevitable fluctuations. While the issue is important for low levels of damage we restrict our attention in the remainder of this chapter to the case where there is damage and the associated $DF \neq 0$. From a singular value decomposition (SVD) one gets

$$DF = [U]\begin{bmatrix} s_r & 0 \\ 0 & 0 \end{bmatrix}\begin{bmatrix} \tilde{V}^T \\ L^T \end{bmatrix} \tag{4.2}$$

where $U \in \Re^{m \times m}$ contains bases for the column space and the left null space, $s_r \in \Re^{r \times r}$ is diagonal and contains the non-zero singular values, $\tilde{V} \in \Re^{m \times r}$ is a basis for the row space and $L \in \Re^{m \times (m-r)}$ is a basis for the null space. The property of the vectors in *L* that is relevant for damage localization is the fact that these vectors, when treated as loads on the system, lead to stress fields that are zero over the damaged elements. The basic idea, therefore, is that the intersection of the null stress regions corresponding to the load distributions defined by the null

space of *DF* can be used to localize the damage. The column vectors in *L* are designated here as damage locating vectors or DLVs.

Depending on the number and location of the sensors, the intersection of the null stress regions may or may not contain elements that are not damaged in addition to the damaged ones. Elements that are undamaged but which can not be discriminated from the damaged ones by changes in flexibility (for a given set of sensors) are denoted as inseparable. While it is always possible to specify a sensor arrangement that eliminates the possibility of inseparable elements for ideal conditions, when the modal information is approximate and incomplete it is necessary to operate with finite thresholds and perfect spatial discrimination (at the element level) can not be guaranteed. A discussion on the question of inseparability is helpful for clarifying some features of the DLV technique and, for this reason, the matter is taken up in a later section.

4.3 Theoretical Formulation

Consider a load vector defined in sensor coordinates acting on a system. If this vector leads to zero stresses in certain elements, and the properties of these elements change while the loads remain constant, the state of stress and strain in the system will not vary. It is evident, therefore, that a sufficient condition for a load vector to be in the null space of *DF* is that, when acting on the undamaged system, it leads to zero stresses over the region where the damage is located. It is not immediately apparent, however, given that the displacements at the unmeasured coordinates are undetermined, whether or not the zero stress condition is necessary for a vector to be in the span of *L*. The derivation that follows clarifies this matter.

Consider a linear structure that has been discretized using *n DOF*. For notational convenience we partition the vector of DOF as $y = [y_a \; y_b]^T$ with a = 1,2 ,3 … m and $b = m+1, m+2 \ldots n$, where m is the number of loaded coordinates (sensors locations). The total potential for the system, Φ, is given by

$$\Phi_{(y_a\, y_b)} = U_{(y_a\, y_b)} - W_{(y_a)} \tag{4.3}$$

where U is the strain energy function and W is the potential of the loads. Assume now that the displacements at the loaded points for the equilibrium condition are known and are treated as constants. An inspection of eq.4.3 shows that for this condition the potential of the loads is a constant and Φ and U are reduced to functions of y_b. Invoking the principle of stationary potential energy one gets

$$\delta \Phi_{(y_b)} = \delta U_{(y_b)} = 0 \tag{4.4}$$

which shows that strain energy is stationary at equilibrium (with y_a = cst) and for any variation from the equilibrium configuration, the change in the strain energy, δU is zero. Furthermore, recognizing that for stable equilibrium the total potential is a minimum, one concludes (by inspection of eq.4.3), that $U_{(y_b)}$ is also a minimum. For the purpose of the subsequent analysis it is convenient to summarize the previous results in a form that can be recognized as the theorem of minimum strain energy, namely:

> *Of all the admissible strain distributions that yield the correct displacement at the loaded coordinates, the strain field that satisfies equilibrium minimizes the strain energy.*

Consider now a finite dimensional linear structure for which the flexibility has been synthesized before and after damage. The incremental flexibility has been computed and a certain null space L has been identified. We designate an arbitrary column vector from this null space as DLV_i. As Figure 4.1 illustrates, the domain of the structure can be subdivided into an undamaged portion Ω_U and a number of regions where the stiffness properties have changed as a result of damage, which we collectively designate as Ω_D.

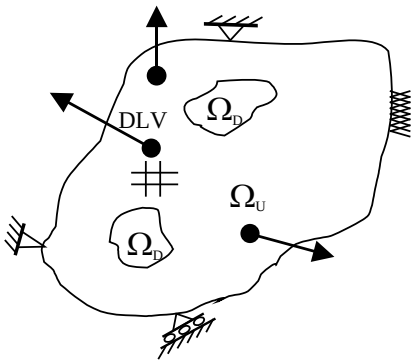

Figure 4.1 Schematic illustration of damaged and undamaged domains

The strain energy for the undamaged and the damaged states are given by

$$U_U = \frac{1}{2}\left[\int_{\Omega_U} \varepsilon_u^T E_u \varepsilon_u \, dV + \int_{\Omega_D} \varepsilon_u^T E_u \varepsilon_u \, dV \right] = DLV_i^T y_a = q \tag{4.5}$$

$$U_D = \frac{1}{2}\left[\int_{\Omega_U} \varepsilon_d^T E_u \varepsilon_d \, dV + \int_{\Omega_D} \varepsilon_d^T E_d \varepsilon_d \, dV \right] = DLV_i^T y_a = q \tag{4.6}$$

where ε stands for the strain tensor, E is the strain to stress mapping matrix and the subscripts *u* and *d* stand for undamaged and damaged states. Note that while ε is a function of position, we have opted to skip the subscripts *x,y,z* to keep the notation uncluttered. Needless to say, the material stiffness matrix, E, may also depend on the *x,y,z* coordinates.

The next step is to obtain an expression that is either equal to, or is larger than U_D and we do this by invoking the minimum strain energy theorem. What is needed is simply to replace ε_d in eq.4.6 with any strain field that is geometrically admissible and leads to the correct deformation at the sensor locations. A member of the set of admissible functions is the undamaged strain field ε_u. Substituting this strain field into eq.4.6 and expressing *q* by means of eq.4.5 one gets

$$\int_{\Omega_U} \varepsilon_u^T E_u \varepsilon_u \, dV + \int_{\Omega_D} \varepsilon_u^T E_d \varepsilon_u \, dV \geq \int_{\Omega_U} \varepsilon_u^T E_u \varepsilon_u \, dV + \int_{\Omega_D} \varepsilon_u^T E_u \varepsilon_u \, dV \tag{4.7}$$

or;

$$\int_{\Omega_D} \varepsilon_u^T E_d \varepsilon_u \, dV \geq \int_{\Omega_D} \varepsilon_u^T E_u \varepsilon_u \, dV \tag{4.8}$$

The stiffness over the damaged region can be expressed in terms of the undamaged stiffness as

$$E_d = \alpha_{(x,y,z)} E_u \tag{4.9}$$

where α is a scalar, and, since damage only reduces the stiffness, $0 \leq \alpha < 1$. Substituting eq.4.9 into eq.4.8 one gets

$$\int_{\Omega_D} \alpha_{x,y,z}\, \varepsilon_u^T E_u \varepsilon_u \, dV \geq \int_{\Omega_D} \varepsilon_u^T E_u \varepsilon_u \, dV \tag{4.10}$$

which, given the fact that E_u is positive definite, can be satisfied only if the undamaged strain field (and as a consequence the stress field) is identically zero over the damaged region - thus completing the proof.

The fact that the proof depends on the premise that the changes from the undamaged to the damaged state are all stiffness reductions is worth restating. At first glance the requirement appears to have no practical significance, since damage always leads to reductions in stiffness. It is conceivable, however, that in addition to damage the changes between the two states may also include closing of previously open gaps or the consolidation of soil under supports which can increase the stiffness at some locations. When increases and reductions in stiffness take place simultaneously the damage bypass property of the stress fields can not be guaranteed. For the purpose of all subsequent discussion we assume that the damage scenario is defined by reductions in stiffness only.

Illustration of the DLV Technique

The basic steps of damage localization using the DLV technique are illustrated using the simple system shown in Figure 4.2(a).

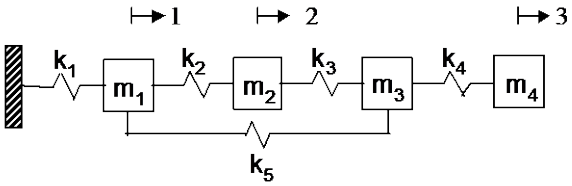

	k1	k2	k3	k4	k5
Before Damage	1	1	1	1	1
After Damage	1	0.5	1	1	1

Figure 4.2(a) System considered

For the output sensors provided at coordinates 1, 2 and 3 the flexibility matrices at the undamaged and damaged states can be assembled as follows:

$$F_U = \begin{bmatrix} 1 & 1 & 1 \\ 1 & 5/3 & 4/3 \\ 1 & 4/3 & 8/3 \end{bmatrix} \qquad F_D = \begin{bmatrix} 1 & 1 & 1 \\ 1 & 2 & 1.5 \\ 1 & 1.5 & 2.75 \end{bmatrix}$$

The change in flexibility is then calculated as

$$DF = F_D - F_U = \begin{bmatrix} 0 & 0 & 0 \\ 0 & 1/3 & 1/6 \\ 0 & 1/6 & 1/12 \end{bmatrix}$$

which leads to the nullspace given by

$$N(DF) = \begin{bmatrix} 1 & 0 \\ 0 & -0.5 \\ 0 & 1 \end{bmatrix}$$

Treating these vectors as loads on the system

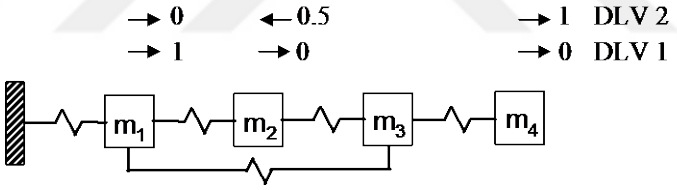

Figure 4.2(b) Damage locating vectors

leads to the following stress fields

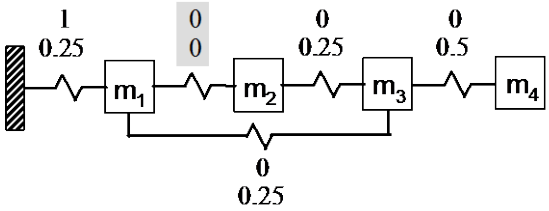

Figure 4.2(c) Stress distributions corresponding to DLV 1 and 2

Note that the intersection of the null stress regions corresponding to the two DLVs localizes the damaged member.

4.4 Relationship between damage and the dimension of null space of DF

It was shown in the preceding section that if a load vector leads to identical displacements at the sensors then the stress field that it creates in the undamaged system is null over the damaged region. The next important issue is to establish the conditions for the existence of a null space in *DF*. To clarify the relation between the rank of *DF* and the extent of damage consider again a structure that has been discretized using *n* DOF and has *m* sensors. Since the system has been assumed linear, one can write

$$RV = z \tag{4.11}$$

where *R* is an appropriately defined stress influence coefficient matrix, *V* is a vector of loads at the sensor locations and *z* is a vector containing the independent internal forces in all the elements. Consider now the scenario where a number of elements, say *qe*, have been damaged and we wish to determine if there is a load vector *V* that will behave as a DLV, i.e., a vector that leads to zero stresses in all the damaged elements. To examine this question we assume (without loss in generality) that the damaged elements are listed first and write eq.4.11 in partitioned form as

$$\begin{bmatrix} r \\ \overline{R} \end{bmatrix} \{V\} = \begin{Bmatrix} 0 \\ \overline{z} \end{Bmatrix} \tag{4.12}$$

Since eq.4.12 can be satisfied exactly only if *r* is rank deficient we conclude that the requirement for *DF* to have a null space is that the number of independent rows in *r* be smaller than the number of sensors. We note at this juncture that the number of rows in *r* is not only a function of the number of damaged elements but also of the type of finite elements affected by the damage. In particular, if the number of deformation modes or, equivalently, the number of independent internal forces for a given element type is *nb* and there are *qe*-damaged elements, the number of rows in *r* is $\sum_{i=1}^{qe} nb_i$. In a truss, for example, *nb* = 1 and one concludes that the maximum number of damaged bars for which *DF* will have a null space (assuming these bars are independent for the sensor arrangement) is (*m*-1), where *m* is the number of sensors.

Combining the previous analysis with the information contained in the proof on the property of the DLV vectors one concludes that the subspaces $\mathsf{N}(r)$ and $\mathsf{N}(DF)$, where $\mathsf{N}(.)$ stands for null space, are identical. The distinction of practical significance, however, lies in the fact that while $\mathsf{N}(r)$ can only be computed when the damage is known and a model is formulated, $\mathsf{N}(DF)$, i.e., the DLVs, can be computed from flexibility matrices synthesized from the measured data without any knowledge about the damage and without reference to any mathematical model of the system.

Inseparable Elements

From the partitions in eq.4.12 one gets

$$V = \mathsf{N}(r)\beta \tag{4.13a}$$

and

$$\bar{z} = \bar{R}V \tag{4.13b}$$

where β is an arbitrary vector of appropriate size. Combining eqs.4.13a and 4.13b one obtains

$$\bar{z} = \bar{R}\mathsf{N}(r)\beta \tag{4.14}$$

where $\bar{z}$ is clearly the vector of stresses in the undamaged elements. An inspection of eq.4.14 shows that elements associated with any zero rows in the matrix $\bar{R}\mathsf{N}(r)$ will have null stresses when the DLVs are applied to the structure and can not, therefore, be separated from the damaged elements by inspection of the stress fields. More generally, any element where the associated rows in $\bar{R}\mathsf{N}(r)$ can be moved to *r* without changing the rank of *r* can not be separated from the truly damaged set and are, therefore, inseparable. One concludes, therefore, that under ideal conditions the DLV technique provides a set of potentially damaged elements that contains those that are truly damaged plus the inseparable ones. When working with imprecise and truncated modal data, however, finite thresholds become necessary and, as a consequence, the potentially damaged set is often larger than the theoretical minimum.

4.5 Implementation of the DLV Technique

4.5.1 The Normalized Stress Index (*nsi*)

To discriminate between large and small stresses it is convenient to reduce the independent internal stresses in every element to a single value that we denote as the characterizing stress, σ. The characterizing stress is taken to be positive and is defined in such a way that the strain energy stored in an element per unit characterizing dimension is proportional to the square of its value. The normalized stress index *nsi* is defined as the characterizing stress in a given element normalized by the largest characterizing stress over all the elements of its kind.

$$nsi_i = \frac{\sigma_i}{\sigma_i\big|_{\max}} \tag{4.15}$$

We note that the term stress is used here in a generalized sense to mean either an actual stress or a stress resultant. For a truss bar, for example, σ can be taken as the absolute value of the bar force. For a planar beam element there are two independent moments and, if the member is prismatic, σ can be taken as $\sqrt{(m_i^2 + m_j^2 + m_i m_j)}$ where m_i and m_j are the two end moments. We note, however, that since σ is used in the damage localization only in the form of the ratio in eq.4.15, one can usually depart from the requirement that σ^2 be strictly proportionality to strain energy without introducing undue error. In the case of beam elements, for example, a definition of σ as the average of the absolute value of the end moments has been found to work just as well as the expression given previously.

4.5.2 The DLV Vector Set

The selection of a threshold to separate significant singular values from those that can be considered as defining the null space is ubiquitous in system realization theory (Akaike 1968; Rissanen 1978). The information from this knowledge base, however, does not appear to be directly applicable to the selection of a set of DLVs because, as will be apparent from the derivation, the singular vectors that contain localization information often extent to singular values that need not be negligibly small. What is needed to select DLVs non-subjectively in a

noisy environment is to identify an index that can be computed without knowledge of the damage but which is correlated to the expected maximum value of *nsi* over the damaged domain. To arrive at this index consider the SVD of *DF* in the general case where there may or may or may not be any zero singular values, namely;

$$DF = U\, S\, V^T \tag{4.16}$$

where *U* and *V* are orthogonal, *S* is diagonal and contains the singular values and all three matrices $\in \Re^{m\,x\,m}$. Pre and post multiplying eq.4.16 by a vector from *V*, say V_i one gets;

$$V_i^T\, DF\, V_i = V_i^T\, F_D\, V_i - V_i^T\, F_U\, V_i = s_i \tag{4.17}$$

which shows that the singular values of *DF* can be interpreted as the difference in the external work done by the associated singular vector when treated as a load on the damaged and undamaged states of the system. Assume now that the characterizing stress resultants induced by V_i in the undamaged and the damaged states are sufficiently close to be taken as equal (the assumption, of course, being exactly satisfied if the system is statically determinate). Under this assumption the difference in work derives exclusively from changes in the strain energy in the damaged region and one can write

$$s_i = \sum_{\Omega_D} \alpha_j\, \sigma_j^2 \tag{4.18}$$

where the subscript *j* refers to the particular element in the damaged region and the α's are constants that depend on the extent of the damage on each element but not on *i*. Multiplying the vector V_i by a constant, c_i, such that largest σ over the *full domain* is equal to unity one gets

$$c_i^2\, s_i = \sum_{\Omega_D} \alpha_j\, nsi_j^2 \tag{4.19}$$

which can also be written as

$$c_i^2 \, s_i = nsi_m^2\Big|_i \, \xi_i \sum_{\Omega_D} \alpha_j \tag{4.20}$$

where nsi_m is the largest nsi in the damaged region and $0 < \xi_i \leq 1$. Assume now that the vector that leads to the largest value of eq.4.20 is that where $i=q$. Normalizing eq.4.20 with respect to its value for $i = q$, recognizing that the Σ term cancels out and taking a square root on both sides one gets, after some trivial rearranging

$$nsi_m\Big|_i = \rho_i \, svn_i \tag{4.21}$$

where;

$$svn_i = \sqrt{\frac{s_i \, c_i^2}{s_q \, c_q^2}} \tag{4.22}$$

$$\rho_i = nsi_m\Big|_q \sqrt{\frac{\xi_q}{\xi_i}} \tag{4.23}$$

Eq.4.21 shows that the problem of estimating the largest *nsi* over the damaged region is reduced to that of selecting ρ (since the *svn* index can be computed without knowledge of the damage). While an upper bound for ρ can not be ascertained, we do know that $nsi_m\Big|_q \leq 1$ and there does not appear to be any reason why the term in the square root of eq.4.23 would have an expected value that differs from one. It is reasonable, therefore, to assume that estimates of nsi_m based on $\rho = 1$ will prove conservative most of the time. Eliminating for notational simplicity the subscript i from nsi_m and taking $\rho = 1$ one gets

$$nsi_m = svn_i \tag{4.24}$$

By choosing a value for nsi_m that is not to be exceeded one obtains a cut on *svn* and therefore a set of vectors that qualify as DLVs. If the flexibility matrices are very accurate and the modeling error in the stress computations is small one expects optimum performance at very low values of nsi_m. In practice, of course, one does not have this information and a cutoff that allows for a

robust operation is appropriate. A value of 0.2 has been found to operate well for a wide range of conditions and is recommended. In summary, the DLV vectors may be taken as those that satisfy

$$svn \leq 0.20 \tag{4.25}$$

The flowchart given in Figure 4.3 illustrates the steps of the methodology to select DLVs discussed in this subsection. In closing we note that the conservatism implicit in the ρ = 1 selection is not uniform. Specifically, inspection of eqs.4.20, 4.21and 4.23 shows that the variance of ρ increases with the number, the relative size and the extent of the damage in the elements. In the next section we combine the information from multiple DLVs in a way that introduces additional robustness into the technique.

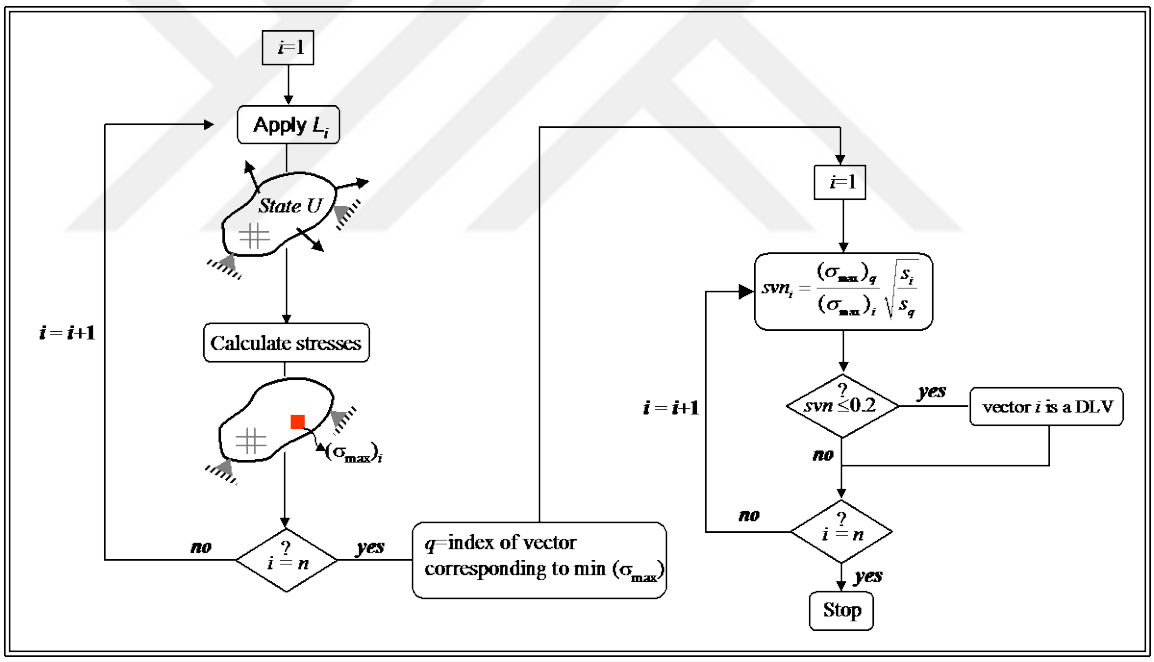

Figure 4.3 Selection of DLVs

4.5.3 Selection of the Set of Potentially Damaged Elements

The procedure is straightforward and can be succinctly described as follows: the potentially damaged set can be taken as those elements having *WSI* <=1, where;

$$WSI = \frac{\sum_{i=1}^{ndlv} \frac{\{nsi\}_i}{\overline{svn_i}}}{ndlv} \tag{4.26a}$$

where,

$$\overline{svn_i} = \max(svn_i, 0.015) \tag{4.26b}$$

In eq.4.26 a *ndlv* is the number of DLV vectors and $\{\text{nsi}\}_i$ is the vector of *nsi* values for the ith DLV. Note that *WSI* is a weighted average of the *nsi* values for each of the DLV vectors, with the weights being the reciprocal of the *svn* indices. The limit of 0.015 is introduced to prevent excessively large weights when *svn* is very small. Justification for taking the potentially damaged elements as those having *WSI*<=1 follows from an inspection of eq.4.24.

A few closing comments are appropriate. We note that the potentially damaged set has not been defined using the intersection of the sets for each of the individual DLVs. The reason for this decision can be appreciated by noting that, in an intersection based approach, truly damaged elements are missed whenever the actual ρ for any DLV happens to be greater than the value used to make eq.4.21 quantitatively useful. Because ρ displays significant variability, the likelihood of missing a damaged element in an intersection approach increases with the number of DLV vectors and this is clearly an undesirable feature. The robustness introduced by the average of eq.4.26 is significant when there are multiple DLVs and extensive results show that this is realized with very little penalty on the size of the identified set. It is realized that elements where the numerator of eq.4.26 is large enough in *any DLV* (say >2.5) can be eliminated from the potentially damaged set independently of their final *WSI* index. A provision along these lines, however, proved to be an unnecessary refinement and was not included for simplicity. We note, finally, that because of the nature of the computations the *WSI* cut of 1.0 should not be treated as a rigid boundary so in a case, for example, where *WSI* ={0.3 0.7 1.1 2.3 …} one should take the set of potentially damaged elements as the first 3. The fact that the DLV provides a ranking of the elements for the potentially damaged set is, of course, a very useful feature.

4.6 Compatibility of the Scalar Multiplier for the Stochastic Input Case

For the stochastic input case, the system matrices, including the flexibility, that differ from the true ones by a single undetermined multiplier can be obtained under certain conditions as

discussed in chapter 3. This procedure however, does not ensure that the scalar missing from the flexibility will be the same in the undamaged and damaged states. Yet, it is evident that for damage localization it is necessary to ensure that the missing constants are equal so that the null space is preserved. In fact, one can only hope for nearly equal when the basis is not complete because the matrices contain approximation beyond that associated with the modal truncation.

For assuring compatible scalars for the two states of the system: prior to and after damage using the mass matrix appears to be a possible option since damage is usually associated with changes in the stiffness and the mass remains unchanged. Hence, one way to attain a reasonable compatibility is to re-scale the results in such a way that some norm of the inverse of the mass is the same in the two states. This selection is very suitable for cases where one has all the modes, if the modal basis is incomplete however, then the method would be approximate since the contribution of the available modes in the undamaged and damaged states are not equivalent. By examining the type of structure that the method is applied to, one can intuitively decide on the best norm for the mass matrix. Consider, for example, the structure described in the next section and lets look at two different norms that can be used: 1) the trace of M^{-1}, 2) the coefficient in the main diagonal of M^{-1}corresponding to the roof. Table 4.1 displays how these two norms vary for the undamaged case and the damaged case of fractured connections on the first and second floors, as the modal basis vary. These results indicate that although the roof coefficient converges much faster than the trace, the trace is also quite accurate especially if the modal truncation is not very severe. In this work we use trace as the norm, further research on this issue, however, is recommended.

Table 4.1 Comparison of two different norms for the example

No. of modes	Trace of M^{-1}		M^{-1} at the roof	
	Undamaged	Damaged	Undamaged	Damaged
8	1.25E-02	1.25E-02	2.50E-03	2.50E-03
7	1.12E-02	1.12E-02	2.49E-03	2.49E-03
6	9.63E-03	9.64E-03	2.44E-03	2.44E-03
5	8.03E-03	7.96E-03	2.32E-03	2.31E-03
4	7.24E-03	7.14E-03	2.10E-03	2.07E-03

An alternative re-scaling which was also explored in this study to ensure that the null space of the change in flexibility is unaffected is described next. Assume that the scaled undamaged and damaged flexibility matrices are $\bar{F}_U$ and $\bar{F}_D$, we have

$$\bar{F}_U = \alpha F_U \tag{4.27}$$

$$\bar{F}_D = \beta F_D \tag{4.28}$$

where α and β are arbitrary constants. Assume now that *L* is a vector in the null space of the true change in flexibility, it follows then that $F_U L = F_D L = d$ and one can write

$$\bar{F}_U L = \alpha\ d \tag{4.29}$$

$$\bar{F}_D L = \beta d \tag{4.30}$$

Solving for *L* in eq.4.29 and substituting the result in eq.4.30 one gets

$$\bar{F}_U^{-1} \bar{F}_D d = \frac{\beta}{\alpha} d \tag{4.31}$$

From where its evident that the desired β/α ratio is a real eigenvalue of the matrix on the left side of eq.4.31. In the case where the matrices are exact the correct β/α ratio appears as a repeated eigenvalue with multiplicity equal to the dimension of the null space of the $\bar{F}_U^{-1} \bar{F}_D$ matrix and this is often sufficient to determine it uniquely. In practice, however, the matrices are never exact and the selection of the correct β/α is not always evident. One approach that has been found useful is to first normalize the matrices $\bar{F}_U$ and $\bar{F}_D$ in such a way that the β/α ratio is necessarily less than 1. This would be the case, for example, if the flexibility proportional matrices were normalized to equal trace because the true value of the trace in the damaged flexibility is larger. Doing this one can then discard the β/α ratios that are complex or greater than 1. Unfortunately, in many cases the solution is still not unique after this is done and one has to look for further means to discriminate. The scaling methods using the trace and the eigenvalue approach discussed previously are examined and the sensitivity of the flexibility proportional matrices to approximations resulting from modeling errors, measurement noise and modal truncation is investigated with a numerical example in the next section.

4.7 Numerical Example

An eight-story frame, which has lumped masses of 400 kg at each floor, is depicted in Figure 4.4. The moment of inertia of the columns and the beams are taken to be 1.97×10^6 mm^4 and be 2.44×10^6 mm^4, respectively. Damping is modeled as classical with 1% in each of the modes of the system. The structure is subjected to an unmeasured white noise excitation at the roof and output acceleration signals are measured at six of the eight DOF. The flexibility of the beam-column connections is taken to be uniform throughout the frame and the values are selected such that the flexibility coefficient at the roof is 40% larger than the case with the rigid connections. Damage is simulated as four fractured connections, two in the first floor and two in the second floor. The shifts in the frequencies are also tabulated in the figure. The mass and the modal damping ratios are assumed to remain unchanged after damage.

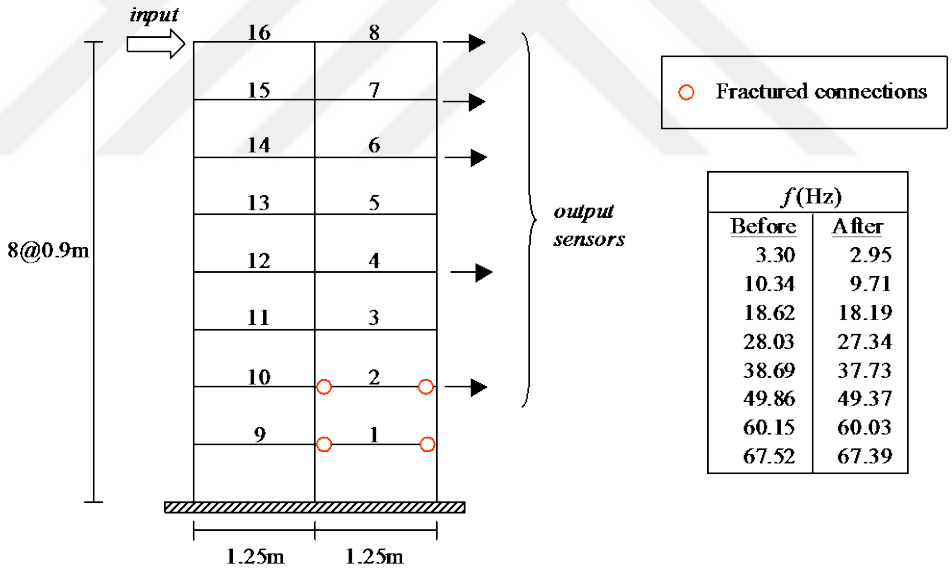

f (Hz)	
Before	After
3.30	2.95
10.34	9.71
18.62	18.19
28.03	27.34
38.69	37.73
49.86	49.37
60.15	60.03
67.52	67.39

Figure 4.4 Eight story frame used to illustrate technique presented

Modeling Errors

The first issue to be examined is the effect of modeling errors on damage localization when the flexibility proportional matrices are made compatible using the norm and eigenvalue approaches. The term 'modeling errors' in this study refers to discrepancies between the model that is used to generate the data and the one that is used to locate the damage. The errors in the modeling of the semi-rigid connections or the flexibility of the foundation rather than the variability in the value

of certain parameters such as the modulus of elasticity or moment of inertia of the members are the major sources of modeling problems encountered in practice. This example therefore examines this issue at the localization stage by generating the data using a model that has flexible connections and carrying out the localization task with a static model that has rigid connections. To isolate the effect of modeling errors from the errors due to modal truncation and measurement noise, the system realization is obtained analytically. Following the approach discussed in chapter 3 for the stochastic input case, the flexibility proportional matrices and the inverse of the mass matrices are synthesized prior to and after the damage. Note that since the modal basis is complete in this case and there is no measurement noise, the approach leads to the exact mass matrix at sensor locations. Re-scaling using the trace of the inverse of the mass matrix or using the eigenvalues of eq.4.31 (which in this case is exactly 1), therefore leads to the exact flexibility matrices.

Performing a SVD of the change in flexibility and applying the *DLV* approach one finds that there are 3 *DLV*s. The *svn* index and the *WSI* values calculated using the characterizing stress as defined in section 4.4.1 are shown in Table 4.2 and the truly damaged members are highlighted. It can be seen that the damage is clearly localized and the first and second floor beams are listed as potentially damaged. As expected, members 9 and 10 also appear in the potentially damaged list of members since they are inseparable. This example clearly illustrates that the technique is not sensitive to the modeling errors because it operates with the stresses induced by the DLV's, and these vectors are correct since they are obtained strictly from the data.

Measurement Noise

The effect of measurement noise is the next issue considered with this example. In this case, noise with an RMS of 5% of the value in the 2nd floor signal is added to all the output sensors. System realization is carried out using a subspace algorithm and the flexibility proportional matrices are synthesized for the undamaged and damaged cases. Now, we look at the two different scaling methods explained previously. First, we carry out the scaling using a normalization to an equal trace. DLV approach is applied under the presence of modeling errors as described previously and the *svn* values and the *WSI* index given in Table 4.3 are obtained. By inspecting these results one can see that the damaged members together with the inseparable counterparts, are correctly identified in the list of potentially damaged elements.

Table 4.2 Damage Localization with the two scaling methods in the presence of modeling errors

Using the trace			*Using eq.*4.31		
svn	*Member*	*WSI*	*svn*	*Member*	*WSI*
1.00	1	0.05	1.00	1	0.05
0.30	9	0.05	0.30	9	0.05
3.62×10^{-4}	2	0.43	3.62×10^{-4}	2	0.43
8.93×10^{-5}	10	0.43	8.93×10^{-5}	10	0.43
9.60×10^{-5}	3	1.53	9.60×10^{-5}	3	1.53
	11	1.53		11	1.53
	4	23.41		4	23.41
	12	23.41		12	23.41
	14	31.93		14	31.93
	6	31.93		6	31.93
	13	41.87		13	41.87
	5	41.87		5	41.87
	16	45.41		16	45.41
	8	45.41		8	45.41
	15	48.79		15	48.79
	7	48.79		7	48.79

* truly damaged bars are shaded in the table

Table 4.3 Damage Localization with the two scaling methods in the presence of measurement noise

Using the trace			*Using eq.*4.31		
svn	*Member*	*WSI*	*svn*	*Member*	*WSI*
1.00	1	0.27	1	1	0.46
0.27	9	0.27	0.28	9	0.46
0.19	2	0.59	0.23	2	0.92
0.16	10	0.59	0.16	10	0.92
0.07	11	1.48	6.43×10^{-8}	3	2.57
	3	1.48		11	2.57
	4	2.69		6	5.47
	12	2.69		14	5.47
	6	3.62		4	10.95
	14	3.62		12	10.95
	13	4.77		13	16.25
	5	4.77		5	16.25
	16	5.34		16	32.07
	8	5.34		8	32.07
	15	6.42		15	33.82
	7	6.42		7	33.82

* truly damaged bars are shaded in the table

Next, we look at the solution of the eigenvalue problem of eq.4.31 with the flexibility proportional matrices normalized to equal trace. The eigenvalues are calculated to be $\beta/\alpha = \begin{bmatrix} 1.454 & 1.055 & 0.977 & 1.018 & 0.997 \end{bmatrix}$. After discarding the values larger than 1 there are two possible solutions. Assuming that the upper floors are undamaged the constant that fits the expectation is 0.997. Multiplying $\bar{F}_U$ by this constant (or dividing $\bar{F}_D$ which is equivalent) one gets matrices with compatible missing scalars. Performing a SVD of the change in flexibility and applying the DLV approach one finds two DLVs in this case. The *svn* values and *WSI* coefficients for this case are also displayed in Table 4.3.

By examining these values it is evident that although the scalar multiplier obtained using eq.4.31 forces a perfect nullspace (*svn*=6.43×10^{-8}), the WSI values obtained for the damaged members are higher than those obtained using the trace. Although the undamaged members also have higher WSI values, the results obtained with this example is not conclusive enough to claim that any one of the methods is a better choice for scaling.

Modal Truncation

Finally, we examine the issue of modal truncation. In this case noise with an RMS of 2% of the value in the 2nd floor signal is added to all the output sensors and the system realization is carried out using the first 6 of the identified modes. The noise level is lowered to 2% since the idea is to have accurate but truncated modes. Note that since the modal basis is incomplete, the approach to extract the flexibility matrices is no longer exact. Figure 4.5 displays the ratio of the flexibility matrix synthesized with the truncated set of modes to the exact flexibility matrix. In this figure, the index corresponds to the location in the matrix counting from the main diagonal downward.

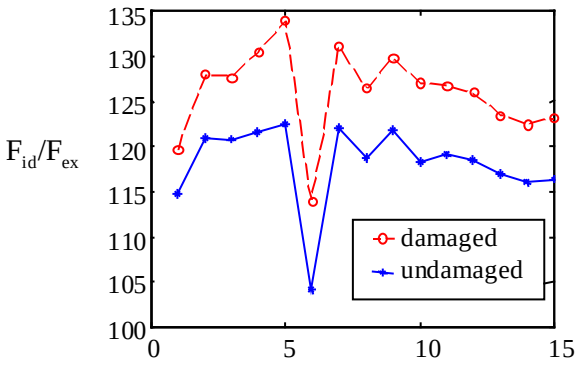

Figure 4.5 Ratio of identified to the exact flexibility matrix

The DLV procedure is carried out first by using the trace as the re-scaling factor. Table 4.4 displays the *svn* values and the *WSI* index obtained in this case. As can be seen from these results, although members 1 and 2 are included in the set of potentially damaged members, in this case the selected set is not exclusively the damaged members and the inseparables; but includes several others primarily due to the effects of modal truncation. Alternatively, with the eigenvalues obtained using eq.4.31 ($\beta/\alpha = [2.492 \quad 1.553 \quad 1.115 \quad 0.994 \quad 1.206]$) the only possible alternative for the scaling factor is 0.994. Multiplying the undamaged flexibility with this constant and performing the DLV approach leads to the results shown in Table 4.4. As can be seen, both methods lead to comparable results in terms of its success in localizing the damage. Among all the possible complications, modal truncation, as expected, leads to the most adverse effect in terms of localizing the damage. The set of potentially damaged members is the largest when the modal space is truncated.

Table 4.4 Effect of Modal Truncation

Using the trace			*Using eq.*4.31		
svn	*Member*	*WSI*	*svn*	*Member*	*WSI*
1.00	4	0.02	1.00	7	0.02
0.72	12	0.02	0.74	15	0.02
0.76	7	0.15	0.77	12	0.06
0.56	15	0.15	0.53	4	0.06
0.11	2	0.21	1.22×10^{-7}	2	0.21
	10	0.21		10	0.21
	1	0.59		1	0.55
	9	0.59		9	0.55
	11	0.96		11	0.92
	3	0.96		3	0.92
	5	1.08		5	1.21
	13	1.08		13	1.21
	16	1.58		16	1.49
	8	1.58		8	1.49
	14	1.77		14	1.89
	6	1.77		6	1.89

4.8 Concluding Remarks

A damage localization technique that applies to systems that can be treated as linear in the pre- and post-damage states is presented. The approach is based on computing a set of vectors, *DLV*s that have the property of inducing stress fields whose magnitude is zero in the damaged elements. The *DLV*s are associated with sensor coordinates and are computed systematically as the nullspace of the change in the measured flexibility. The approach does not depend on the type of the structure and can be applied to single and multiple damage scenarios. Model dependence is small since knowledge about the system is restricted to that needed for a static analysis at the undamaged state. The experience derived from numerical experiments has thus far supported the robustness of the technique in the presence of noise, modal truncation and limited sensor information. Yet, further examination using experimentally measured data is required to gain an understanding of its true capabilities.

CHAPTER 5

Quantification of Damage

5.1 Introduction

Research in the area of fault/damage detection has shown that localizing the damage is the most exacting task of the structural health monitoring (SHM) problem. It is worth noting that in many applications establishing the location of damage may be sufficient since with the guidance of this information, visual inspections can be used to further characterize the damage. Nevertheless, extracting the degree of damage from the measured data without recourse to visual inspections is germane since it is a natural progression in the information that can be provided by a SHM system. This chapter therefore, continues to further investigate the SHM problem with the ultimate goal of determining the degree of damage.

The Damage Locating Vector (*DLV*) approach has been described in the previous chapter as a systematic way for interrogating changes in flexibility matrices with respect to the localization of the damage. This chapter attempts to use the flexibility at the damaged state to estimate the severity of the damage taking advantage of the guidance provided by the localization information. Figure 5.1 illustrates the components of the flexibility-based damage identification strategy. As depicted in this figure, once the flexibility matrices are synthesized from the vibration data at the pre and post damage states, the DLV approach is used to localize the damage and restrict the free parameter space. A model update on the improved reference model using these parameters then leads to the estimation of the extent of damage.

Since the quantification task relies on model update methodologies to determine the changes in the parameters of a structural model this chapter starts with a brief introduction on finite element model updating. Our goal here is not to go into a detailed model update discussion but to give an

overall perspective on the capabilities and difficulties of a model based SHM approach that may provide further information in characterizing the damage. More specifically, the first approach introduced in this chapter is a flexibility-based quantification approach that extends the use of flexibility information beyond the localization stage by fitting a model of the structure to the damaged flexibility using the restricted set of free parameters identified as potentially damaged. The discussion on quantification of the severity of damage using flexibility is followed by illustration of the performance of the technique using two examples. The second method is a general update strategy that uses identified modal parameters to update the finite element model of the structure that can be applied to cases in which the flexibility based approach is not applicable. As noted before the flexibility-based procedure can not be applied when the number of available sensors is less than $\sqrt{2N}$, where N is the number of identified modes unless information not contained in the measured data is used. Numerical examples demonstrating the techniques conclude the chapter.

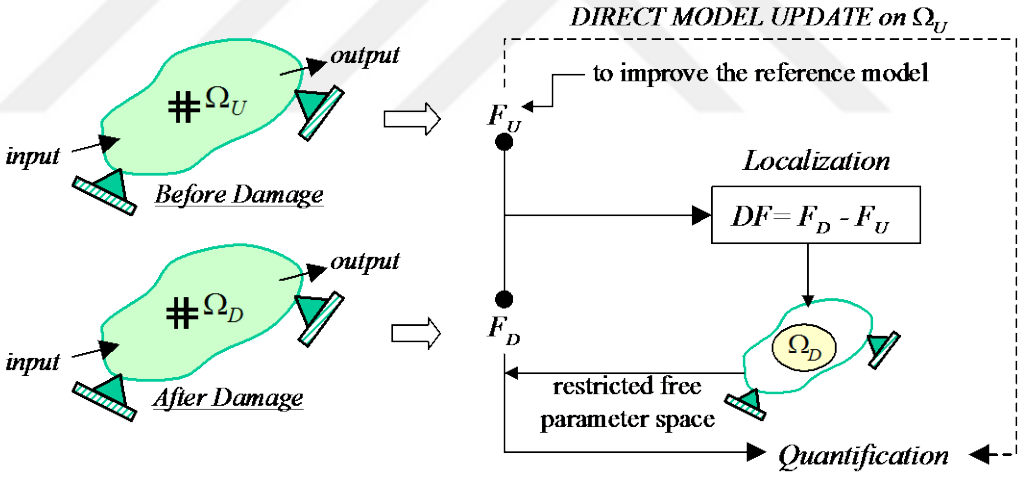

Figure 5.1 Flexibility-based damage identification strategy

5.2 Finite Element Model Updating

Assessment of the severity of the damage typically relies on structural model updating methodologies to solve the inverse problem of determining the parameters of the damaged structure. Finite element model updating is the process by which the parameters of a model are

adjusted to increase the correlation between the measured response of a structure and the predictions from the model. The work on the model updating field has various levels of ambition that can be summarized as (Ewins, 1990):

(a) a model which reproduces exactly all the measured modal properties,
(b) a model which reproduces all the measured FRF properties,
(c) a model which is capable of reproducing all of the measured FRFs and modal properties,
(d) a model which, in addition to the above requirements, exhibits the correct connectivity,
(e) a model which possess all of the correct mass, stiffness and damping elements.

It is evident that each of these criteria becomes increasingly more difficult to achieve, and damage identification problem requires a model that is the most ambitious and demanding of all. That is why SHM remains a technically challenging problem, and no global technique has been well established.

Model updating is essentially an optimization process that minimizes an objective function based on the discrepancies between experimental data and finite element model prediction. Optimization problems, which are the minimization or maximization of a real-valued function of a number of real variables subject to a number of constraints, can be written as

$$\min_{x \in \Re^n} f(x) \qquad \text{subject to} \begin{cases} c_i(x) = 0, \ i \in \mathsf{E} \\ c_i(x) \geq 0, \ i \in \mathsf{I} \end{cases} \tag{5.1}$$

where x is the set of free parameters, f and c_i are scalar-valued functions of the variables x and I and E are sets of indices.

Although we attempt to find the global minimum of the objective function with respect to the updating parameters, optimization algorithms, in general, can only find a local solution, a point at which the objective function is smaller than all other feasible points in the vicinity. They do not always find the best of all such minima, that is, the global minimum but locate the closest one based on the starting point of the search. Global solutions, therefore are difficult to identify and locate if the function is non-convex (has multiple local minima). If the function is convex on the other hand, unconstrained optimization algorithms are guaranteed to converge to the global

minimum of the objective function. Unfortunately however, even when the objective function is convex, the problem may be highly ill conditioned and very sensitive to errors in the model. Regularization techniques are commonly mentioned in the literature for improving the condition of the solution. The basic idea of regularization is to add constraints based on apriori knowledge so the global minimum becomes well-defined. Nevertheless, in a damage identification problem this is often difficult to do.

An important aspect of finite element model updating is the choice of updating parameters. The parameters that are candidates for updating are typically selected with guidance from a priori knowledge on what aspects of the model are most uncertain when experimental data is used to improve a mathematical model. In the damage identification problem, however, uncertainty or sensitivity can not be used as criteria to arrive at a set of free parameters. Damage localization is, therefore, critical as guidance for selecting the free parameter space for the optimization process.

Assuming the parameterization of the problem is adequate, quantifying the damage correctly is still an issue due to errors deriving from the model. If the model is not exact in the undamaged state then the estimated parameters will absorb as much of the modeling error as possible. Even though one attains a solution through optimization, it may have significant error in the sense that it is not close to the true model. To illustrate this point, assume for simplicity that the model update leads to a linear least square problem of the form;

$$[A]\{\theta\} = \{b\} \tag{5.2}$$

where θ is the vector of free parameters.

Partitioning the above equation so that the subscripts 1 and 2 indicate partitions associated with the unknown (free) and "known parameters", one can write

$$[A_1 \quad A_2]\begin{Bmatrix}\theta_1\\ \theta_2\end{Bmatrix} = \{b\} \tag{5.3}$$

which leads to the solution for θ_1 in terms of θ_2 as:

$$\theta_1 = A_1^t(b_1 - A_2\theta_2) \tag{5.4a}$$

where ^{t} indicates pseudo-inverse operation and we have used " " for the known parameters to point out that these are those parameters for which we do not anticipate large changes (not damaged), we do not, however, know them precisely.

Due to the inaccuracies in the analytical model of the structure, however, the above equation can be modified as

$$\theta_1 = A_1^t b - A_1^t A_2 (\theta_{2tr} + \varepsilon) \tag{5.4b}$$

from where it can be seen that the error in θ_1 deriving from the modeling errors is $-A_1^t A_2 \varepsilon$. The error in θ_1 parameters, therefore, depends not on the magnitude of ε itself but on the magnitude of its projection on $A_1^t A_2$. In other words, if the outcome of the singular value decomposition of $A_1^t A_2$ is such that the vector ε is parallel to the right side singular vectors corresponding to large singular values, then the error will have a large effect on θ_1 parameters. If, on the other hand, ε is parallel to the vectors corresponding to small singular values then its effect will be small.

An accurate base-line model of the structure at the undamaged state, therefore, is essential for the success of the update approach to quantify the damage. Errors in the model of the undamaged structure are, however, inevitable and for this reason considerable difficulties are generally encountered when one attempts to quantify the damage in practice. The discussion presented in this chapter does not focus on the question of improving analytical models. It is assumed that the analytical model of the structure at the undamaged state is validated using the experimental data obtained before damage. The updated FEM prior to damage is therefore a 'good' representation of the undamaged structure and is capable of predicting the observed behavior of the system. A rigorous and comprehensive guide to FEM updating field can be found in the book by Friswell and Motthershed (1995).

5.3 Estimation of the Extent of Damage

Consider a discrete structure for which an arbitrary number of coordinates are defined. Assume, for simplicity, that the stiffness of the various elements is characterized by scalar quantities such as *EI*, *EA* or *GJ* if the element is a beam, a truss bar or a member subjected to torsion. The reciprocals of these stiffness terms are element flexibilities and we designate them in general as b_j, where the subscript identifies an element number. An arbitrary coefficient of the flexibility matrix can then be written as

$$f_{i,j} = z^T b \tag{5.5}$$

where z is a vector of influence coefficients and b is the vector of element flexibilities. Placing all the coefficients of the upper triangular portion of the flexibility matrix in a vector one can write

$$Z\, b = \hat{f} + \varepsilon \tag{5.6}$$

where the matrix Z contains the influence vectors z^T, $\hat{f}$ is the estimate of the damaged flexibility and ε is a vector of residuals which exists due to the fact that there is modeling error in the computation of Z and truncation and approximation in the measured flexibility. Ordering eq.5.6 so that the flexibility of the potentially damaged elements appears first and introducing the subscripts 1 and 2 to indicate partitions associated with potentially damaged and undamaged elements one can write

$$\begin{bmatrix} Z_1 & Z_2 \end{bmatrix} \begin{Bmatrix} b_1 \\ b_2 \end{Bmatrix} = \hat{f} + \varepsilon \tag{5.7}$$

or,

$$Z_1 b_1 = \Delta\hat{f} + \varepsilon \tag{5.8}$$

where the first term on the right side of eq.5.7, $\hat{f}$, is the total estimated flexibility minus the contribution that derives from the undamaged portion of the system. Minimizing $\varepsilon^T \varepsilon$ one gets

$$b_1 = (Z_1^T Z_1)^{-1} Z_1 \Delta\hat{f} + \mathrm{N}\ \ (Z_1^T Z_1)\gamma \tag{5.9}$$

where γ is a vector of appropriate dimension and $\mathsf{N}(\cdot)$ indicates null space. If there is a null space in $Z_1^T Z_1$, the parameters in b_1 can not be computed uniquely. For cases in which $Z_1^T Z_1$ is rank deficient by *j*, one needs *j* pieces of information to solve for γ. However, even without any additional information, in some cases it is still possible to further localize the damage and reduce the potentially damaged sets identified by the *DLV*s and even obtain reasonably accurate estimates of damage. For instance, any row of $\mathsf{N}(Z_1^T Z_1)$ that is zero, is a member in b_1 that can be computed independently of the rank deficiency. In the following section we will use some examples to demonstrate these issues. We conclude this section by noting that, with the exception of statically determinate systems, eq.5.9 needs to be solved using iterations because *Z* is dependent on b_1.

5.4 Performance of the Flexibility-Based Approach

5.4.1 Example 1 – Static Data with Measurement Noise and Modeling Error

The selected structure is a planar truss made up of 15 bars as shown in Figure 5.2. All bars are made up of steel (*E*=200 GPa) and the undamaged areas of the bars are randomly selected from a uniform distribution that ranges between [11.4 cm^2-14 cm^2]. The system is indeterminate both internally and externally. It is subjected to extensional static forces in both directions at the free joints of the lower chord and the horizontal and vertical translations of joints 2, 3 and 4 are measured. Sensor noise is contemplated as 2% random uniform noise at the six output sensors. Modeling error is simulated by computing the stresses from the identified *DLV* vectors using a model where the bar areas are assumed to be 12.7 cm^2. The two damage scenarios that are examined are as follows:

1. Damage Pattern 1 (DP 1): Bar 2-3 has its area reduced by 25% and the areas of bar 3-4 and bar 4-5 are reduced by 50%

2. Damage Pattern 2 (DP 2): Bar 2-6 loses 25% and bar 4-8 loses 20% of its area.

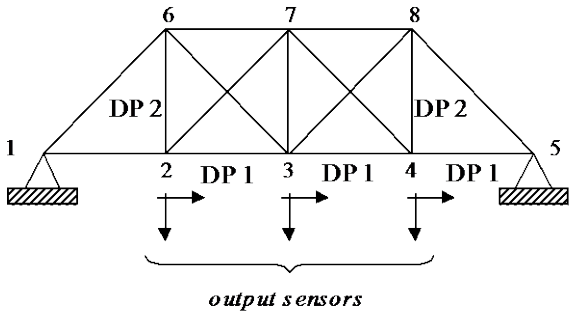

Figure 5.3 Structure utilized in Examples 1 and 2

It was shown in chapter 4 that elements with zero rows in the matrix $\overline{R}\mathrm{N}(r)$ will have null stresses when the *DLV*s are applied to the structure. These members therefore, can not be separated from the damaged elements by inspection of the stress fields and are termed as inseparable. On this basis under ideal conditions one expects the *DLV* technique to provide a set of potentially damaged members that contains the truly damaged members plus the inseparable ones. To gain some insight to the effect of imprecise data, one can calculate $\overline{R}\mathrm{N}(r)$ for a given damage pattern and obtain the theoretical minimum for the potentially damaged set. These can then be compared to the potentially damaged set identified by the technique to see the effect of imprecision and truncation of the data. Matrices in eqs.5.10a and 10b display the $\overline{R}\mathrm{N}(r)$ damage patterns 1 and 2 of this problem, respectively. Note that rows of this matrix that are blank correspond to the members that are truly damaged.

	Bar								
	1-2	>	3.05E-16	1.32E-16	1.67E-16	0.74	0.13	0.26	0.51
	2-3	>				0.24	0.02	0.25	0.47
DP1	3-4	>				0.24	0.13	0.24	0.46
	4-5	>				0.26	0.01	0.75	0.52
	6-7	>	0.10	0.69	0.49	0.03	0.42	0.03	0.11
	7-8	>	0.40	0.48	0.58	0.03	0.44	0.03	0.01
	2-6	>	0.34	0.51	0.52				
DP2	3-7	>	0.24	0.28	0.12	0.04	0.38	0.04	0.04
	4-8	>	0.34	0.03	0.73				
	3-6	>	0.30	0.26	0.08	0.03	0.35	0.03	0.09
	4-7	>	0.10	0.35	0.15	0.02	0.23	0.02	0.13
	5-8	>	0.54	0.42	0.94	0.03	0.36	0.03	0.01
	1-6	>	0.12	0.89	0.73	0.03	0.35	0.03	0.09
	2-7	>	0.40	9.65E-16	1.08E-15	0.02	0.25	0.03	0.07
	3-8	>	0.12	0.38	0.03	0.03	0.36	0.03	0.01

(5.10a,b)

As a consequence, it is evident that under ideal conditions the *DLV* approach will provide a set that includes an additional member, bar 1-2, together with the truly damaged members of 2-3, 3-4 and 4-5 for damage pattern 1 (DP1). For damage pattern 2 (DP2) however, it should lead to a set that is exclusively the damaged members with perfect data.

Table 5.1 Results of the localization approach

Damage Pattern 1			Damage Pattern 2		
Svn	*Bar*	*WSI*	*Svn*	*Bar*	*WSI*
1.00	3-4	0.07	0.87	2-6	0.03
0.96	4-5	0.08	1.00	4-8	0.08
0.45	2-3	0.14	0.28	1-6	0.32
0.29	1-2	0.29	0.32	3-6	0.35
0.16	3-6	0.65	0.25	6-7	0.40
0.11	3-7	0.80	0.08	4-7	0.85
⇓	3-8	0.86	⇓	3-7	1.04
2 DLVs	2-7	1.04	1 DLV	3-8	1.79
	4-7	2.04		5-8	1.89
	7-8	3.63		2-7	2.16
	4-8	3.66		7-8	2.21
	6-7	3.81		2-3	6.42
	2-6	4.04		3-4	7.56
	5-8	5.31		4-5	10.64
	1-6	5.70		1-2	11.77

*truly damaged bars are shaded in the table

Applying the technique to the data described previously, one obtains the localization information displayed in Table 5.1. Note that the truly damaged bars for each damage pattern are shaded in the table. For damage pattern 1, in addition to the members that are expected to be in the set, one has 5 additional members due to the imprecision in the data. Note that, although the *WSI* threshold for the potentially damaged member is taken as 1, one can include bar 2-7 (*WSI*=1.04) in the potentially damaged set, and let the quantification procedure to further localize the damage if the bar is in fact undamaged. Similarly for damage pattern 2, the set is larger than the theoretical minimum and we have 5 additional bars included in the set of potentially damaged elements. Next, we attempt to quantify the damage using the flexibility matrices obtained at the damaged state coupled with the localization information collected in the previous step. Applying

the procedure described in the previous section to the damage patterns, one concludes the following:

1. For the first damage case, $Z_1^T Z_1$ is full rank and hence the parameters in b_1, i.e. the areas of members in the set of potentially damaged members can be computed uniquely. As can be seen in Table 5.2, the damaged areas for bars 2-3, 3-4, 4-5 are correctly calculated and bars 1-2, 3-6, 3-8 and 2-7 that appear in the set of potentially damaged members are correctly determined as undamaged. Bar 3-7, which is in fact undamaged, is calculated to have a 5.6% change in its area.

Table 5.2 Quantification results for damage pattern 1

Bar	Area (cm^2)	
	Identified	Exact
3-4	6.12	6.15
4-5	6.17	6.17
2-3	9.25	9.27
1-2	12.73	12.73
3-6	12.60	12.32
3-7	11.81	12.52
3-8	12.75	12.12
2-7	13.13	12.85

2. In damage case 2, $Z_1^T Z_1$ is observed to be rank deficient by 1 and the correction $\mathrm{N}\ (Z_1^T Z_1)\gamma$ is calculated as:

Table 5.3 Null space of $Z_1^T Z_1$ for damage pattern 2

Bar	$\mathrm{N}\ (Z_1^T Z_1)\,\gamma$
2-6	0.34
4-8	2.12E-16
1-6	-0.35
3-6	-0.35
6-7	0.80
4-7	-8.54E-16
3-7	8.70E-17

Due to the rank deficiency encountered in this case one needs to provide additional information for one of the potentially damaged bars in the identified set to completely identify the areas for

these members. Note that this information needs to be provided from one of the bars that does not have a zero in the nullspace. Regardless of the correctness of the information however, it is possible to quantify the areas of bars 4-8, 4-7 and 3-7 since they are independent of the rank deficiency. The results obtained for these members are displayed in Table 5.4. Needless to say, if none of the rows of in the nullspace is zero and one has no further none of the areas after damage are known correctly, then the quantification procedure described here can not provide any further localization information than that provided by the DLV technique.

Table 5.4 Quantification results for damage pattern 2

Bar	Area (cm^2)	
	Identified	Exact
2-6		
4-8	10.01	9.68
1-6		
3-6		
6-7	11.81	12.60
4-7	12.12	12.37
3-7		

With this example we presented the two possible scenarios for which further localization and quantification can be made to the potentially damaged set using the damaged flexibility matrix obtained from static measurements. In the following example we study the same system using vibration data. Noise in the input and output signals, modeling error and modal truncation are investigated as possible sources of error.

5.4.2 Example 2 – Dynamic Data with Measurement Noise

We consider again the truss of Figure 5.2, but in this case with dynamic data. Six sensors located at each joint at the lower chord records the acceleration in both horizontal and vertical directions of joints 2, 3 and 4. The input motion is random white noise applied in the vertical directions at joints 3 and 4. Sensor noise is contemplated in the excitation and the computed response. The output and the input noise are prescribed to have RMS equal to 5% of the response measured at the sensor at joint 2 and of the excitation level, respectively. Modeling error is simulated as described in the previous example. Damping matrix is calculated assuming 2% constant modal damping both for the undamaged state and the damage cases defined in the previous example.

The identified 10 modes out of a possible 12 are displayed in Table 5.5 and the percent error in the identified flexibility matrices are depicted in Figure 5.3. As can be seen from the WSI indices presented, the damaged members in both cases are included within the sets. For damage pattern 1, the identified set as potentially damaged with one additional bar is full rank and hence the damaged areas can be calculated as shown in Table 5.6. Bar 1-2 is correctly identified as undamaged, the extent of damage for bars 3-4 and 4-5 are very accurately quantified. Bar 2-3 is identified within 11% error, which is relatively high compared to the other members. For damage pattern 2, the set is rank deficient, yet the approach still serves as a further means of localizing the damage.

Table 5.5 Modal properties

Mode	No Damage			Damage 1			Damage 2		
	Exact	*Identified*		*Exact*	*Identified*		*Exact*	*Identified*	
	f(Hz)	*f*(Hz)	ξ(%)	*f*(Hz)	*f*(Hz)	ξ(%)	*f*(Hz)	*f*(Hz)	ξ(%)
1	1.3079	1.3070	2.03	1.3068	1.3070	2.01	1.2914	1.2920	2.02
2	2.3084	2.3050	2.20	2.1351	2.1440	3.50	2.2791	2.2790	2.23
3	2.6026	2.6020	1.99	2.4660	2.4660	2.04	2.5928	2.5930	2.00
4	4.4314	4.4320	2.01	4.1906	4.1910	1.99	4.3816	4.3820	2.01
5	4.9847	4.9840	2.02	4.7429	4.7440	2.00	4.9787	4.9780	2.01
6	5.3217	5.3260	2.79	5.1349	5.1330	2.03	5.2469	5.2430	2.30
7	5.9478	5.9460	1.96	5.8141	5.8130	2.00	5.6569	5.6570	2.01
8	6.4104	6.4110	2.00	5.9770	5.9780	2.03	5.8915	5.8920	1.99
9	6.6386	6.6400	1.98	6.3733	6.3740	2.02	6.6020	6.6030	1.99
10	7.6792	7.6810	2.01	7.2522	7.2550	2.01	7.5675	7.5680	1.99

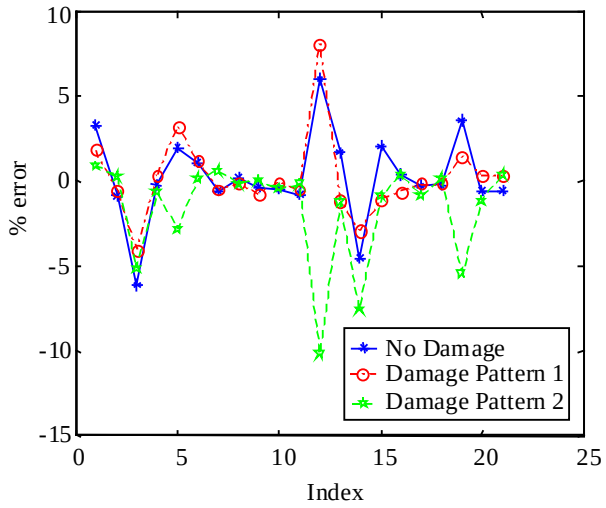

Figure 5.3 Percent error in the identified flexibility matrices

As illustrated by these examples, after a portion of the domain where the damage is localized is identified by the *DLV* approach, it may still be possible to further localize and in some cases quantify the damage using only the flexibility information at the damaged state. For some others, however, the quantification technique is not capable of characterizing the damage completely due to of rank deficiency problem caused by the inseparable elements in the set. Next section presents a model update strategy that may be employed for cases where the flexibility-based approach is not applicable due to limited sensors or the quantification technique described in the previous section does not provide further information for the set of bars identified as potentially damaged.

Table 5.6 Results of the localization procedure

Damage Pattern 1					Damage Pattern 2					
svn	Bar	WSI	ID	Exact	svn	Bar	WSI	N $(Z_1^T Z_1)$	ID	Exact
0.95	2-3	0.18	10.31	9.27	0.48	7-8	0.07	-0.80		
1.00	3-4	0.28	6.17	6.15	1.00	5-8	0.37	0.35		
0.52	4-5	0.42	6.07	6.17	0.67	2-6	0.48	1.57E-16	9.22	9.83
0.20	1-2	0.86	12.78	12.73	0.28	3-8	0.49	0.35		
0.13	4-7	2.20			0.25	2-7	0.51	1.93E-16	12.83	12.85
0.11	7-8	2.30			0.11	4-8	0.68	-0.34		
⇓	3-6	2.43			⇓	2-7	0.84	-4.76E-16	10.54	12.29
3 DLVs	3-8	2.43			1 DLV	3-7	0.90	-4.45E-16	12.24	12.52
	2-7	2.81				6-7	1.36			
	6-7	3.03				1-6	1.44			
	3-7	3.04				4-7	1.63			
	5-8	3.07				2-3	2.66			
	4-8	3.12				3-4	3.49			
	2-6	5.36				4-5	7.97			
	1-6	5.88				1-2	8.80			

*truly damaged bars are shaded in the table

5.5 Model Update Strategy

When the input is not measured and the matrix $Y \in \Re^{m^2 \times 2N}$ given in eq.3-72 is not a tall matrix (i.e. $m^2 < 2N$, where *m* is the number of available sensors and *N* is the number of identified modes), the flexibility-based strategy can not be applied since the rank deficiency is a spurious byproduct of the restricted number of sensors. Conceivably one could discard some modes to arrive at a tall *Y* but then failure of the technique is likely due to excessive error on the

assumption that the inverse of the mass is diagonal. To examine cases that cannot be considered by the flexibility-based approach, a model update strategy can be implemented. The reader is referred to the text by Friswell and Mottershed (1995) for a comprehensive discussion on the model updating techniques. In the particular version that is used here, however, the cost function is taken as the sum of the square of the differences between identified undamped eigenvalues λ_m and estimates of these eigenvalues, λ_e, obtained from a Rayleigh quotient, namely;

$$J = \sum_{i=1}^{n\,\mathrm{mod}\,es} (\lambda_{m,i} - \lambda_{e,i})^2 \tag{5.11}$$

where;

$$\lambda_{e,i} = \frac{\Phi_i^T K(\theta) \Phi_i}{\Phi_i^T M \Phi_i} \tag{5.12}$$

and θ are the free parameters. Since the modes are not necessarily available at all coordinates an expansion technique is invoked. Specifically, assume the mode shapes are partitioned as $\Phi = \begin{Bmatrix} \phi_m \\ \phi_u \end{Bmatrix}$, where ϕ_m is the measured partitioned and ϕ_u the unmeasured one. In each mode, for any given set of parameters θ the unmeasured partition can be estimated by minimizing the norm of the vector ε computed from the eigenvalue equation.

$$\varepsilon(\phi_u) = K(\theta) \begin{Bmatrix} \phi_m \\ \phi_u \end{Bmatrix} - \lambda_m M \begin{Bmatrix} \phi_m \\ \phi_u \end{Bmatrix} \tag{5.13}$$

which is a linear least square problem having the explicit solution ;

$$\phi_u = -(K_u - \lambda_m M_u)^{\mathrm{t}} (K_m - \lambda_m M_m) \phi_m \tag{5.14}$$

where $^{\mathrm{t}}$ is the pseudo inverse.

K_m and M_m in eq.5.14 are the columns of the stiffness and mass matrices corresponding to the measured coordinates whereas K_u and M_u are those corresponding to the unmeasured coordinates. As is evident from the previous equations, the model update approach presented here is developed under the premise that the identified modes are real. The numerical examples presented next demonstrate the performance of this strategy. Factors such as measurement noise and modeling errors are also incorporated in these examples to test the robustness of the technique.

5.6 Performance of the Model-Update Approach

5.6.1 Numerical Example 1

The performance of the model-update approach in the presence of measurement noise is illustrated with this example. Modeling errors and modal truncation are not contemplated in this example.

Consider a 6-story shear building that is subjected to some unmeasured random white noise excitation at the roof. The structure, at its undamaged state, has a uniform stiffness distribution of as shown in Figure 5.4. The mass distribution for the finite element model is also shown in this figure. A total of three sensors recording the acceleration response are placed at floors 2, 4 and 6. The output noise is prescribed to have a root-mean-square (RMS) equal to 5% of the RMS of the response measured on the sensor located on the second floor. Damping matrix is calculated assuming 2% constant modal damping. Damage is simulated by a 25% reduction in the stiffness of the 2nd floor. Modal identification for the structure at the damaged state is carried out using a subspace identification algorithm and the frequencies and mode shapes are obtained as shown in Figure 5.5.

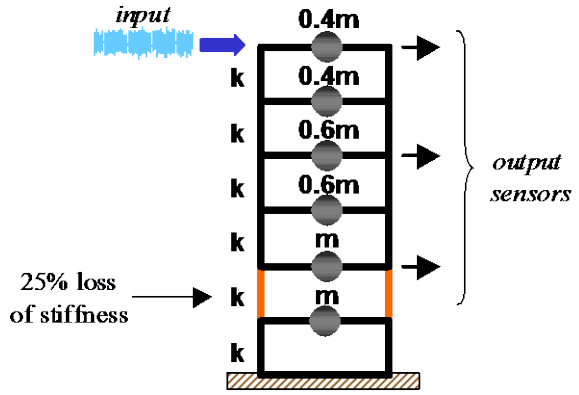

f (Hz)	
Before	After
2.37	2.25
6.09	6.07
9.94	9.62
12.35	11.69
15.74	15.66
19.46	19.46

Figure 5.4 System considered for illustration of model update strategy

Note that in this case, we have 3 sensors and 6 modes and the matrix Y is not tall. The flexibility-based approach therefore, is not valid and a model update strategy needs to be employed without a localization information. The stiffness of the columns in each floor is included in the free parameter space and the model update strategy outlined in the previous section is followed. Table 5.7 displays the updated floor stiffnesses obtained with this parameterization. Note that since the model of the undamaged structure is essentially exact, quantification is carried out very successfully and the second floor is identified to suffer a 25% damage. The effect of measurement noise reflects itself with slight errors in the updated stiffness values of other floors.

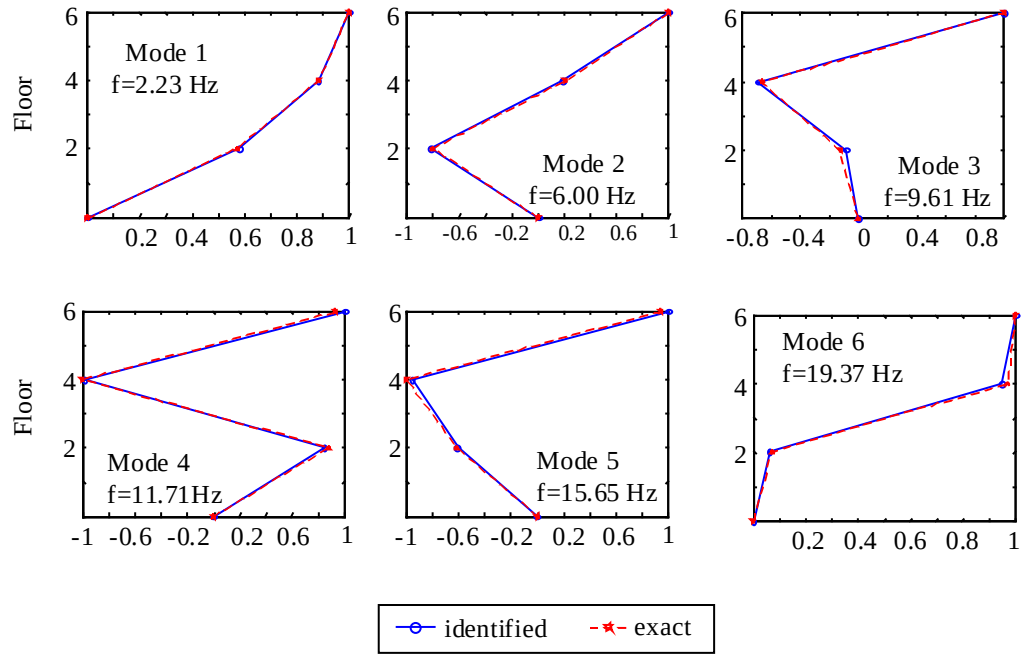

Figure 5.5 Comparison of identified and exact mode shapes after damage

Table 5.7 Results of the model-update approach

Floor	$K_{identified}$	$\%\Delta_{identified}$	$\%\Delta_{exact}$
1	1960.0	2.0	0
2	1493.7	25.3	25
3	2000.0	0.0	0
4	2000.0	0.0	0
5	1978.5	1.1	0
6	1950.9	2.4	0

5.6.2 Numerical Example 2

To further investigate the effects of modeling errors on the performance of the technique, consider again the 6-story frame of the previous example but with flexible beam-column connections. The assumed mass distribution at the translational degrees-of-freedom is the same as the previous example shown in Figure 5.5. The true mass of the structure on the other hand, is this assumed distribution times a random scalar that vary between [0.9-1.1] The spatial distribution of the output sensors and the prescribed output noise are taken to be the same as the previous example. The structure is excited by an unmeasured white noise excitation at the roof and damping is modeled as classical with 2% in each of the modes of the system. The flexibility of the connections is selected such that the flexibility coefficient at the roof is 40% larger than the case with the rigid connections. In addition to the uncertainty in the mass of the structure, modeling error is also prescribed to the flexibility of the connections by multiplying the assigned values by a random scalar that is uniformly distributed between [0.8 and 1.2]. Damage is simulated by a 25% loss in the inertia of the columns of the second floor. Table 5.8 presents the exact modal properties for the real structure and the analytical model.

Table 5.8 Comparison of the modal properties

	f (Hz)		
Mode	System-exact		Model
	Before Damage	After Damage	Undamaged
1	2.44	2.39	2.43
2	7.40	7.14	7.33
3	14.19	13.98	14.00
4	24.31	23.96	23.72
5	33.63	33.19	32.52
6	44.19	44.71	43.90

Based on the comparison of the undamaged frequencies for the structure under examination and the finite element model, we proceed by accepting that we have a 'good' representation of the undamaged system. Defining the free parameter space as the inertia of the columns in each floor and following the model update strategy outlined previously, the following results shown in Table 5.9 are obtained for the change in the moment of inertia of columns:

Table 5.10 Model Update Results

Floor	% Reduction
1	0.0
2	37.7
3	0.0
4	19.6
5	3.9
6	10.7

Although the truly damaged floor, floor 2, is identified to undergo the largest change, modeling errors appear to compromise the effectiveness of the updating method by spreading the identified damage over a number of parameters. According to these results, floors 4 and 6 in addition to floor 2 appear to be potentially damaged.

It should be noted that the examples included here focus on relatively simple structures with a relatively small free parameter space and we further reduced the space by considering the free parameter space being composed of only the column stiffnesses. Even with these simplifications a direct modal update has not been entirely successful. These difficulties would be compounded in realistic structures pointing to the importance of the localization stage.

5.7 Concluding Remarks

Damage quantification is essentially an optimization problem that is based on modification of a set of parameters representing the elemental stiffnesses to reproduce the measured data as closely as possible. An important aspect of model update based techniques is the choice of the updating parameters. The damage locating vector technique introduced in the previous chapter helps to reduce the set of candidate parameters for updating by localizing the damage. A flexibility-based update approach applied subsequently may provide further localization and quantification

information in some cases as shown in this chapter. For cases in which the flexibility matrix at the damaged state yields no additional information or when the flexibility-based approach is simply not applicable, an update strategy that utilizes the measured modal properties can be attempted. Unlike the localization stage, however, an accurate base-line model is critical to obtain good estimates of the updating parameters. Errors in the undamaged model may result in false localization and erroneous updates of the parameters.

CHAPTER 6

Analytical Studies on the IASC-ASCE Benchmark Structure

6.1 Introduction

There have been numerous studies that focus on applying SHM techniques to different structures. Despite the substantial body of research however, the progress in the transfer of acquired knowledge and expertise from research to practical applications has not been entirely satisfactory. One reason for this is that various studies apply different methods to different structures, which makes it difficult for researchers to compare the performance of these methods and to understand their advantages and disadvantages. To address this issue, the US SHM task group decided to prepare a benchmark problem, where participants apply a number of monitoring techniques to a common structure with common objectives. Keeping in mind that credible SHM technology must be shown to work with real data a benchmark problem for which a physical model was available, was selected (Ventura et.al., 1997).

The objective of this chapter is to describe the first phase of the IASC-ASCE benchmark problem and present the results obtained for the simulation cases using the damage identification strategy developed in the previous chapters. The chapter starts by description of the selected four story, two-by-two bay steel frame, the simulation cases and the analytical data generation models. The identification strategy employed by NU team is then summarized and illustrated step-by-step with a selected case. The results of the application for the other cases are also presented (Bernal and Gunes, 2002). The chapter concludes with a brief discussion on the performance of the proposed approach.

6.2 Benchmark Structure

The structure selected for the first benchmark problem is a 4 story 2-bay by 2-bay steel braced frame scale-model structure depicted in Figure 6.1(a) (Black and Ventura, 1998). The structure has a 2.5×2.5 m plan, stands 3.6 m. tall and is located at the Earthquake Engineering Research Laboratory a the University of British Columbia (UBC). All members are hot rolled grade 300W steel (nominal yield stress of 300 MPa). The sections chosen are S75×11 for the beams and B100×9 that are specially designed light sections for the columns of 1/3 scale model. The frame is braced with equal angle braces L25×25×3 in a chevron configuration as shown in Figure 6.1(b). The properties of these members are displayed in Table 6.1. There are four added weights on each floor. The weights are depicted in Figure 6.2. Note that at the roof there are either four 400kg weights or three 400kg and one 550 kg to create some asymmetry.

Table 6.1 Properties of Structural Members

Property	*Units*	*Columns*	*Beams*	*Braces*
Section type		B100×9	B100×9	L25×25×3
Cross-sectional area, A	mm^2	1.133×10^3	1.43×10^3	0.141×10^3
Moment of inertia, I_x	mm^4	1.97×10^6	1.22×10^6	0
Moment of inertia, I_y	mm^4	0.664×10^6	0.249×10^6	0
St. Venant torsion constant, J	mm^4	8.01×10^9	38.2×10^9	0
Young's Modulus, E	MPa	2×10^5	2×10^5	2×10^5
Mass per unit length, ρ	kg/mm	8.89×10^{-3}	11.0×10^{-3}	11.0×10^{-3}

Two finite element models based on this structure were developed to generate the simulated data for the phase 1 of the analytical work (Johnson et. al., 2000). The first is a 12 DOF shear building model that constrains all motion except two horizontal translations and one rotation per floor (translation in the x- and y- directions and rotation θ about the center column). The natural frequencies and the story stiffnesses for the 12 DOF model at the undamaged and damaged states are given in Tables B1 and B2 in Appendix B. The second is a 120 DOF model that is obtained by allowing 6 DOF at each joint (except for the foundation, which is assumed rigid) and imposing the constraint that the floor slabs are rigid in their own planes. The remaining out-of-plane degrees-of-freedom (vertical motions, pitching and rolling) are active. The columns and beams are modeled as Euler-Bernoulli beams in both finite element models and the braces have no bending stiffness. It is worth noting here that by having two models with different degrees of refinement, the inevitable error in the model that one faces in actual cases can be simulated.

Specifically, data could be generated using the 120 DOF model and the analyst is forced to use a 12 DOF model to fit the data, if in fact a model is needed. The effect of the modeling error in this case may have different consequences depending on the damage detection technique being used. For localizing the damage using the *DLV* technique, model dependence is typically small since the *DLV*s are computed strictly from the data and only the undamaged statical properties enter into computations.

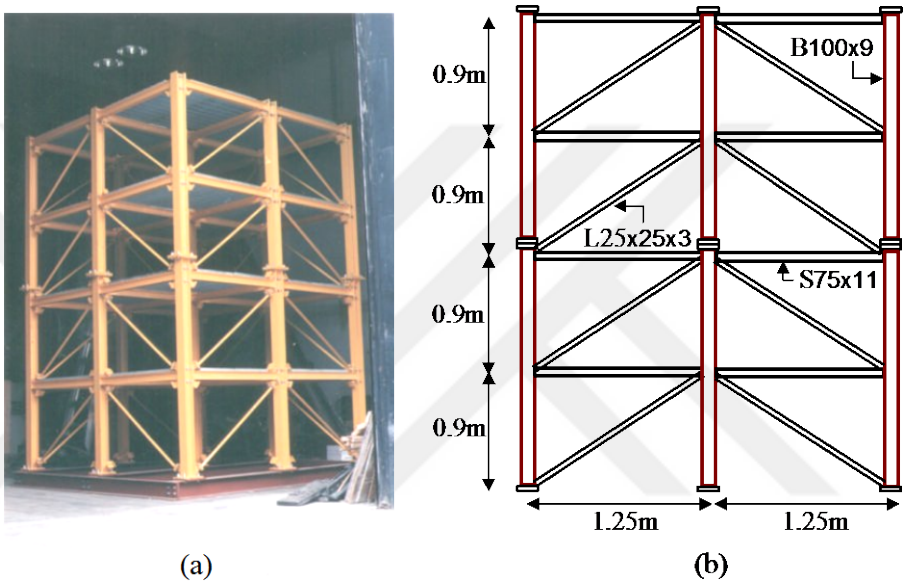

Figure 6.1 (a) Photo of steel-frame, (b) Schematic diagram of frame

Table B1 displays the first 12 natural frequencies for the undamaged and damaged cases for the 120 DOF model. Both models are assumed classically damped with 1% in each one of the modes. A diagram of the analytical model is shown in Figure 6.2(a). A total of sixteen accelerometers, two in *x*- and two in *y*-directions are placed in each floor as shown in Figure 6.2(b). Sensor noise is prescribed to be Gaussian with RMS 10% of the RMS of the roof acceleration. The sampling rate for the data for all simulation cases is taken to be 250 Hz (dt=0.004 sec) and a the total number of time points is 10000 (duration=40 sec). The MATLAB® programs generating the data can be found on the Task Group web site: wuscel.cive.wustl.edu/asce.shm/.

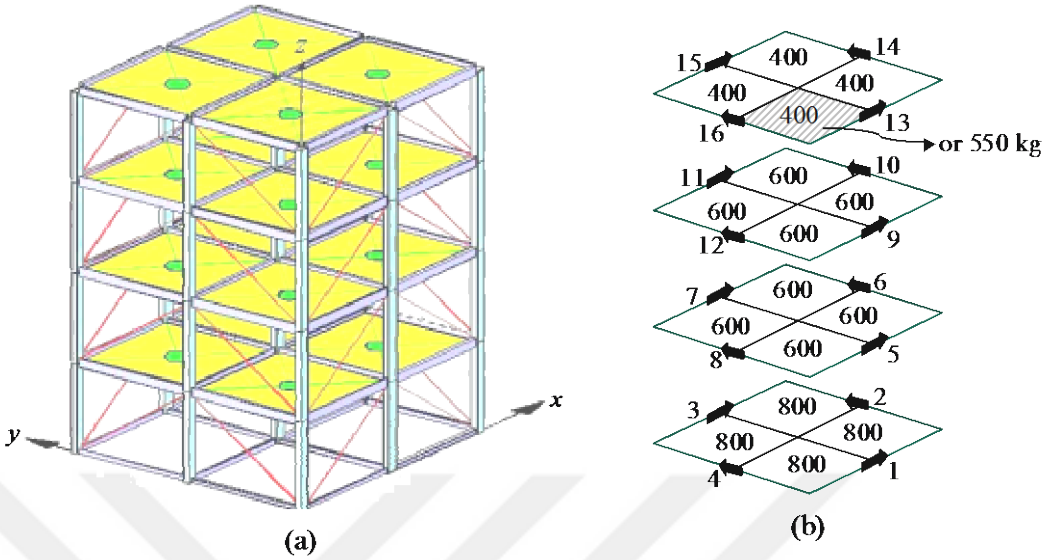

Figure 6.2 (a) Diagram of analytical model (b) Location of sensors and distribution of floor masses

Table 6.2 Simulation Cases 1-3 for the Benchmark Structure (1-D)

	Case 1	**Case 2**	**Case 3**
Data Generation Model	12 DOF	120 DOF	12 DOF
ID Model	12 DOF shear building		
Sensors	4 on each floor		
Mass Distribution	Symmetric (4×400 kg on roof)		
Excitation	Ambient		Shaker
Input Information	Known Unknown		Unknown
Damage Patterns	Removal of: *i*. all braces in 1st floor *ii*. all braces in 1st and 3rd floors		

The simulation cases considered in the first phase of the analytical work are summarized in Table 6.2 and Table 6.3. The first three cases depicted in Table 6.2 are one-dimensional analysis in the weak (*y*) direction. The excitations are applied one per floor in this direction and are modeled as Gaussian white noise in cases 1 and 2. The only difference between the two simulation cases is the introduction of 120 DOF data generation model with case 2. Starting with case 3, ambient excitation is replaced with shaker on the roof. The shaker is assumed to have a line of action that passes through the geometric center of the roof at a 45^{o} angle as shown in Figure 6.3. Note that

although the structure is excited in two directions in case 3, only the weak direction is to be analyzed. Damage is introduced by removal of certain braces as shown in the above table.

Subsequent cases summarized in Table 6.3 increase complexity and add additional realism to the simulations. Cases 4-6 introduce asymmetry by replacing one of the 400 kg floor slabs on the roof with a 550 kg slab as shown in Figure 6.2(b). Modeling error, which is eliminated in case 4, is brought back into the picture in case 5. Finally, with case 6 additional complications are introduced by limiting the sensor information (50% reduction in the number of sensors) and considering a partial damage pattern (reduction in the brace area instead of a removal of the entire brace).

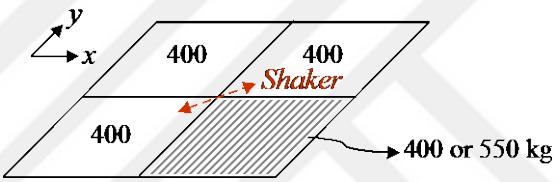

Figure 6.3 Location and orientation of the shaker at the roof

Table 6.3 Simulation Cases 4-6 (3-D) for the Benchmark Structure

	Case 4	**Case 5**	**Case 6**
Data Generation Model	12 DOF	120 DOF	
ID Model	12 DOF		
Mass Distribution	Asymmetric (three 400kg, one 550 kg on roof)		
Excitation	Shaker		
Sensors	4 on each floor		2nd & 4th floors only
Input Information	Unknown		
Damage Patterns	(*i*) all braces in 1st floor (*ii*) all braces in 1st and 3rd floors (*iii*) removal of 1 brace on the 1st floor (*iv*) removal of 1 brace on the 1st and 3rd floors, (*v*) 1/3 reduction in the area of 1 brace on the 1st floor		

6.3 Damage Identification Strategy

Figure 6.4 depicts the steps of the damage identification technique employed here for simulation cases 1-6.

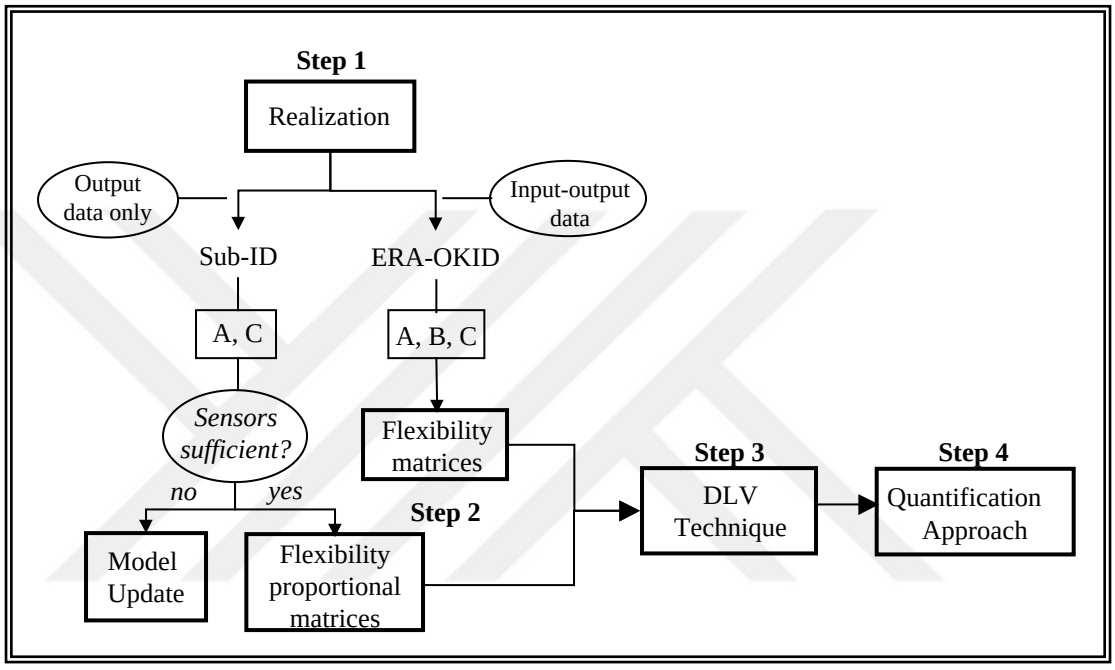

Figure 6.4 Flowchart for the damage identification strategy used in this study

The strategy applies independently of the number of available sensors, or identified modes, when the input is measured. The only theoretical restriction in this case is that there be, at least, one co-located input-output coordinate. For the case of output only data, however, exact results are obtained only when the modal basis is complete and a lower bound on the number of output sensors (for a given set of modes) applies. Note that using the term 'complete basis' shows that we carry this discussion (for simplicity) as if there is an 'exact' finite dimensional representation for the system. A model update strategy, described in chapter 5, can be carried out to examine cases of stochastic input where the number of sensors was insufficient to extract the required flexibility proportional matrices.

6.4 Illustration of the Technique

In this section the application of the methodology described in the previous section is put together step-by-step for one of the cases considered in the benchmark study. In particular, we consider case 3 with damage pattern (*ii*), which involves damage in all the diagonals of the first and third floors with the input treated as unknown. A brief description of this case can be found in Table 6.2.

Step 1: *System Realization*

The system realization is carried out using a subspace algorithm (Van Overschee and Moor, 1996), system order is selected as 8 from an examination of the singular values in Figure 6.5. The system matrices A_c (in continuous time), and C are obtained as follows:

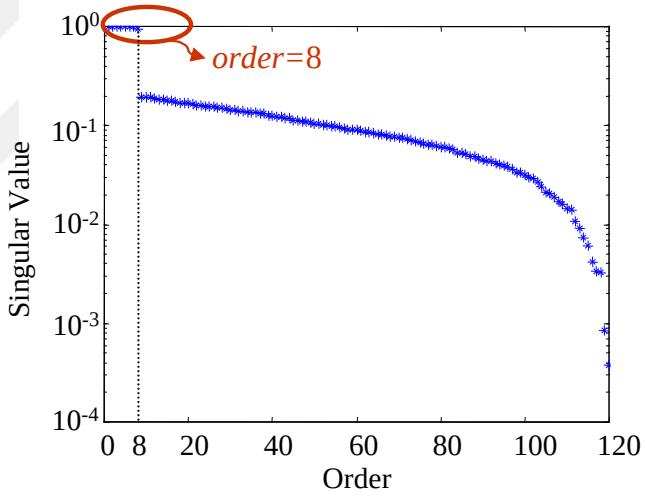

Figure 6.5 Singular value plot for the system order

$$A_c = \begin{bmatrix} -0.37 & 240.03 & 13.25 & 12.89 & 6.40 & -15.15 & -2.84 & 1.34 \\ -244.37 & -4.79 & -19.91 & 11.48 & -12.38 & -20.57 & 1.10 & 2.34 \\ -12.71 & 22.46 & -0.17 & -157.78 & -10.39 & 17.86 & 1.72 & -2.40 \\ -15.85 & -18.58 & 159.50 & -2.58 & -26.61 & -42.27 & -0.70 & 1.99 \\ -6.22 & 15.50 & 10.09 & 28.80 & 0.26 & 291.57 & 2.21 & -0.80 \\ 20.63 & 31.79 & -21.05 & 50.65 & -295.66 & -6.52 & -3.99 & -4.88 \\ 2.26 & -2.45 & -1.31 & -0.39 & -1.99 & 5.62 & -0.04 & 58.44 \\ -3.56 & -7.92 & 3.60 & -5.83 & 2.80 & 11.47 & -59.54 & -1.18 \end{bmatrix} \quad (6.1a)$$

$$C=10^{-4}\begin{bmatrix} 3.46 & -0.20 & 4.29 & -0.10 & 1.31 & -0.17 & 0.88 & -0.06 \\ -3.90 & 0.75 & 2.29 & 1.05 & -3.49 & 0.50 & 1.63 & -0.15 \\ -2.70 & -1.07 & -1.34 & -0.87 & 3.79 & 0.21 & 2.31 & -0.17 \\ 5.10 & 0.84 & -3.57 & 0.15 & -2.57 & -0.66 & 2.43 & -0.38 \end{bmatrix} \quad (6.1b)$$

Step 2: *Extraction of Flexibility Proportional Matrices*

The first task is to extract arbitrarily scaled complex mode shapes Ψ_m at the sensor coordinates using eq.3-13. For this case the result at the undamaged state is:

$$\Psi_m=\begin{bmatrix} \text{-10.84+15.23i} & \text{-10.66-1.47i} & \text{1.58-4.30i} & \text{-0.08-1.02i} \\ \text{-19.96+27.75i} & \text{-7.35-1.02i} & \text{-1.58+4.30i} & \text{0.21+2.68i} \\ \text{-26.21+36.60i} & \text{3.35+0.47i} & \text{-1.09+2.99i} & \text{-0.25-3.15i} \\ \text{-28.99+40.53i} & \text{10.67+1.48i} & \text{1.91-5.22i} & \text{0.18+2.21i} \end{bmatrix} \quad (6.2)$$

The next step is to obtain the normalization constants from eq.3-72. This requires that one assemble $\overline{H}$ using eqs. 3-68 and 3-69 and $\overline{S}$ using eqs.3-70 and 3-71. The result is:

$$\overline{H}=\begin{bmatrix} 6.77 & -19.68 & -9.27 & -2.48 & -21.29 & 5.97 & 8.21 & 0.10 \\ 8.98 & 8.98 & -6.45 & 2.91 & -28.02 & -2.75 & 5.70 & -0.30 \\ 16.16 & 6.19 & 6.45 & -7.66 & -51.33 & -1.90 & -5.68 & 0.63 \\ 9.96 & 28.58 & 11.27 & -2.04 & -31.01 & -8.69 & -9.97 & 0.37 \\ 17.91 & 19.69 & -11.26 & 5.37 & -56.80 & -6.00 & 9.94 & -0.79 \\ 23.76 & -8.99 & -7.84 & -6.30 & -74.76 & 2.77 & 6.90 & 2.41 \end{bmatrix} \quad (6.3)$$

$$\overline{S}=\begin{bmatrix} 0.196 & -0.052 & 0.034 & -0.001 & 0.066 & -0.179 & 0.039 & 0.003 \\ 0.359 & -0.036 & -0.033 & 0.001 & 0.118 & -0.123 & -0.039 & -0.008 \\ 0.657 & -0.025 & 0.033 & -0.003 & 0.213 & -0.085 & 0.039 & 0.022 \\ 0.472 & 0.017 & -0.023 & -0.001 & 0.157 & 0.056 & -0.027 & 0.010 \\ 0.865 & 0.012 & 0.023 & 0.004 & 0.282 & 0.039 & 0.027 & -0.025 \\ 1.139 & -0.005 & 0.016 & -0.004 & 0.374 & -0.018 & 0.019 & 0.030 \\ 0.523 & 0.052 & 0.041 & 0.001 & 0.174 & 0.179 & 0.047 & -0.007 \\ 0.957 & 0.036 & -0.041 & -0.003 & 0.313 & 0.123 & -0.047 & 0.018 \\ 1.260 & -0.017 & -0.028 & 0.003 & 0.415 & -0.056 & -0.033 & -0.021 \\ 1.395 & -0.053 & 0.049 & -0.002 & 0.460 & -0.179 & 0.057 & 0.015 \end{bmatrix} \quad (6.4)$$

Combining $\overline{\overline{H}}$ and $\overline{S}$ one obtains the matrix *Y*. Obtaining the singular value decomposition of *Y* and treating the last right side singular vector as the nullspace β one readily gets the complex constants, d_g from eq.3-67 as:

$$d_g = \begin{bmatrix} 0.0292 - 0.0885i \\ -0.2226 + 0.0525i \\ 0.3064 - 0.2142i \\ 0.8914 - 0.0685i \end{bmatrix} \tag{6.5}$$

The inverse of the mass and the stiffness matrix (flexibility) to within a constant can then be calculated from eqs.3-42 and 3-43 as;

$$F_U = 10^{-6}\alpha \begin{bmatrix} 9.18 & 9.16 & 9.14 & 9.19 \\ 9.16 & 18.37 & 18.39 & 18.46 \\ 9.14 & 18.39 & 27.64 & 27.75 \\ 9.19 & 18.46 & 27.75 & 37.10 \end{bmatrix} \qquad M^{-1} = \alpha \begin{bmatrix} 0.18 & 0.00 & 0.00 & 0.00 \\ 0.00 & 0.24 & 0.00 & 0.00 \\ 0.00 & 0.00 & 0.24 & 0.00 \\ 0.00 & 0.00 & 0.00 & 0.35 \end{bmatrix}$$

(6.6a, b)

Following the same steps outlined previously the system matrices extracted for the structure in the damaged state are;

$$F_D = 10^{-6}\alpha \begin{bmatrix} 31.78 & 31.72 & 31.74 & 32.00 \\ 31.72 & 40.81 & 40.86 & 41.20 \\ 31.74 & 40.86 & 72.69 & 73.19 \\ 32.00 & 41.20 & 73.19 & 82.98 \end{bmatrix} \qquad M^{-1} = \alpha \begin{bmatrix} 0.18 & 0.00 & 0.00 & 0.00 \\ 0.00 & 0.24 & 0.00 & 0.00 \\ 0.00 & 0.00 & 0.24 & 0.00 \\ 0.00 & 0.00 & 0.00 & 0.35 \end{bmatrix}$$

(6.7a, b)

where we note that M^{-1} has been normalized to unit trace to attain compatibility of the missing scalar.

Step 3: *Damage Localization: DLV Approach*

The singular value decomposition of *DF* ($DF = U\,S\,V^T$) gives

$$DF = \begin{bmatrix} -0.37 & 0.60 & 0.65 & 0.27 \\ -0.37 & 0.60 & -0.66 & -0.27 \\ -0.60 & -0.37 & -0.27 & 0.66 \\ -0.61 & -0.37 & 0.27 & -0.65 \end{bmatrix} \begin{bmatrix} 1.19E\text{-}04 & 0 & 0 & 0 \\ 0 & 1.72E\text{-}05 & 0 & 0 \\ 0 & 0 & 5.68E\text{-}08 & 0 \\ 0 & 0 & 0 & 3.52E\text{-}08 \end{bmatrix} \begin{bmatrix} 0.37 & 0.37 & 0.60 & 0.61 \\ -0.60 & -0.60 & 0.37 & 0.37 \\ 0.65 & -0.66 & -0.27 & 0.27 \\ -0.27 & 0.27 & -0.66 & 0.65 \end{bmatrix} \tag{6.8}$$

The characterizing stress (σ_i) can be taken as the story shears. Treating the columns in *V* as loads at each floor one gets the following results:

$$\sigma = \begin{array}{c} \begin{array}{cccc} \text{sv \#1} & \text{sv \#2} & \text{sv \#3} & \text{sv \#4} \end{array} \\ \begin{bmatrix} 1.945 & 0.464 & 0.005 & 0.006 \\ 1.574 & 0.139 & 0.658 & 0.264 \\ 1.205 & 0.741 & 0.002 & 0.005 \\ 0.605 & 0.371 & 0.268 & 0.651 \end{bmatrix} \end{array} \begin{array}{c} \text{Floor} \\ \leftarrow 1 \\ \leftarrow 2 \\ \leftarrow 3 \\ \leftarrow 4 \end{array} \tag{6.9}$$

The *svn* index is computed from eq.4-21 and 4-22. From eq.4-25 one concludes that the last 2 columns of *V* can be treated as DLVs. For these selected vectors, *the WSI* can be calculated as;

$$svn = \begin{bmatrix} 0.99 \\ 1.00 \\ 0.06 \\ 0.05 \end{bmatrix} \qquad WSI = \begin{bmatrix} 0.15 \\ 11.67 \\ 0.10 \\ 12.88 \end{bmatrix} \begin{array}{l} < 1 \quad \text{Floor 1} \\ \\ < 1 \quad \text{Floor 3} \\ \\ \end{array} \tag{6.10}$$

from where it is evident that the damage is in levels 1 and 3.

Step 4: *Quantification of Damage*

The undetermined scalar α is of no significance since the reductions in stiffness can be computed in percent without reference to specific values. Taking an arbitrary value for the mass of the first floor, the nominal flexibilities can then be computed. Fitting a shear building model to this flexibility, the story stiffnesses can be estimated at the undamaged state. Following the same procedure for the damaged state, yet allowing only the stiffness of the first and third floors to change in this case percent damage (%D) can be computed as tabulated below:

Table 6.4 Results of Quantification for Case 3 –DP (ii)

	Percent Damage	
Floor	*Identified*	*Exact*
1	71.3	71.0
2	-	
3	71.2	71.0
4	-	

6.5 Summary of the Results for the Benchmark Structure

System Realization

For the 1-D cases, the output information used in this study is the accelerations measured along the *y*-direction at one location per floor (sensor #3) as shown in Figure 6.6. For the 3-D cases, the sensor information collected at three locations per floor (sensors 1, 2 and 3) are transformed into the geometric center of the floor using the transformation matrix shown in the figure.

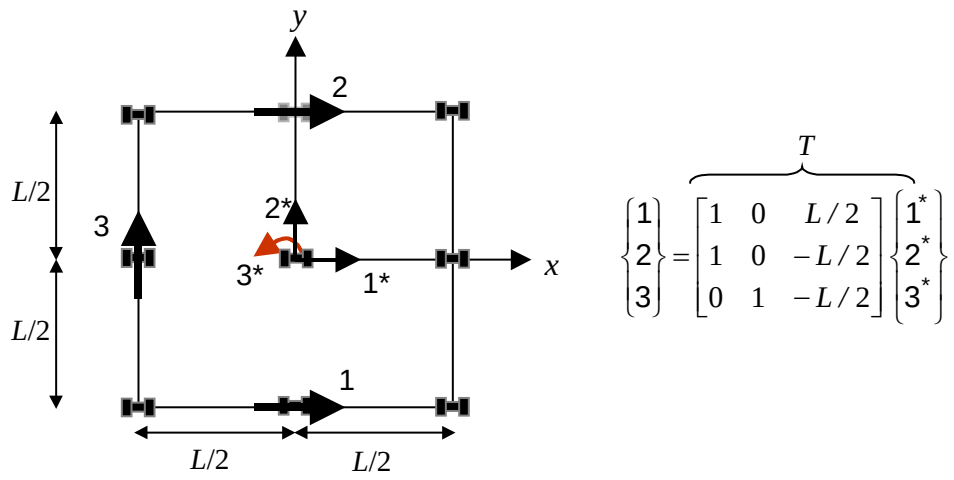

Figure 6.6 Sensors utilized as output measurements

System realization is carried out using the ERA-OKID algorithm for the known input cases and using a subspace identification approach (Sub-ID) for the unknown input cases. The identified frequencies and the damping ratios are presented in Table 6.5 and Table 6.6. Note that the slight asymmetry introduced by the additional mass at the roof for the 3-D cases is not sufficient to excite the torsional modes of the structure at the undamaged state with a shaker oriented at a 45^o

angle at the center column of the roof. Therefore, acceleration measurements corresponding to the rotational degree-of-freedom of the floor are not utilized.

No difficulties were encountered in the modal identification with the translational degrees-of-freedom defining the sensor locations. Four translational modes for the 1-D cases (cases 1-3) and eight modes for the 3-D cases (cases 4-6) are identified. As expected, however, the accuracy proved higher in the known input cases than the unknown input cases.

Damage Localization

In extracting the flexibility matrices with known input cases no apriori knowledge with regard to the mass matrix has been assumed. For the unknown input cases however, mass matrix is assumed to be diagonal to extract the flexibility proportional matrices. For the 1-D cases in which the mass-distribution is exactly symmetric this assumption is fully realized. Yet, for the 3-D cases this is not exactly true due to the asymmetry at the roof. Nevertheless, since this asymmetry is small, the method to extract the flexibility proportional matrices can still be assumed to hold approximately. This slight asymmetry, however, creates another problem since it does not lead to a significant coupling between the two directions for the structure at the undamaged state. The two directions behave independently yielding to two vectors in the null-space for the normalization constants. Hence, additional information is needed to reduce the null-space to 1 and to obtain the flexibility matrices within a scalar multiplier. As an additional apriori information, therefore we imposed the requirement that the mass of the first floor in both directions is identical.

The localization results using the DLV approach are shown in Table 6.7 and Table 6.8. Note that story shears are used as the characterizing stress in localizing the damage and damage localization is performed successfully for cases 1-5. In case 6, the flexibility-based approach can not be applied due to limitation imposed by the number of sensors. We recall that to extract the flexibility proportional matrices one needs to satisfy the requirement that $m \geq \sqrt{2N}$ where N is the number of identified modes and m is the number of available sensors. Thus, in theory, for N=8 the minimum number of sensors needed is 4 which appears to be satisfied for case 6. However, since the two directions do not have significant coupling then one has 2 sensors and 4 modes in each direction. In this case, the number of available sensors is not sufficient to solve for the normalization constants for the identified number of modes and the flexibility-based approach has to be abandoned unless we call on some additional information.

Table 6.5(a) Identified Natural Frequencies and Damping Ratios for Known Input Cases

CASE 1 (12 DOF)						
	No Damage		Damage (*i*)		Damage (*ii*)	
Mode	ξ(%)	*f*(Hz)	ξ (%)	*f*(Hz)	*f*(Hz)	ξ (%)
1	1.03	9.41	1.11	6.24	1.12	5.82
2	1.01	25.54	1.01	21.53	1.01	14.89
3	1.00	38.67	1.00	37.38	1.01	36.06
4	1.00	48.01	1.00	47.83	1.00	41.35
CASE 2 (120 DOF)						
	No Damage		Damage (*i*)		Damage (*ii*)	
Mode	ξ(%)	*f*(Hz)	ξ (%)	*f*(Hz)	ξ (%)	*f*(Hz)
1	1.03	8.59	1.08	5.47	1.11	4.96
2	1.00	23.45	1.01	19.32	1.01	12.34
3	1.00	36.82	1.00	35.29	1.00	34.79
4	1.00	46.98	1.00	46.73	1.00	38.75

Table 6.5(b) Identified Natural Frequencies and Damping Ratios for 1-D Cases with Unknown Input

CASE 1 (12 DOF)						
	No Damage		Damage (*i*)		Damage (*ii*)	
Mode	ξ(%)	*f*(Hz)	ξ (%)	*f*(Hz)	*f*(Hz)	ξ (%)
1	1.05	9.42	0.99	6.24	1.13	5.80
2	1.15	25.54	0.81	21.55	0.76	14.89
3	1.00	38.67	0.96	37.38	1.13	36.08
4	1.00	47.89	0.94	47.71	1.00	41.41
CASE 2 (120 DOF)						
	No Damage		Damage (*i*)		Damage (*ii*)	
Mode	ξ(%)	*f*(Hz)	ξ (%)	*f*(Hz)	ξ (%)	*f*(Hz)
1	1.25	8.61	0.83	5.47	0.98	4.98
2	0.83	23.47	0.87	19.29	0.87	12.35
3	0.98	36.86	1.09	35.23	0.99	34.74
4	0.81	46.94	0.82	46.73	0.99	38.78
CASE 3 (12 DOF)						
	No Damage		Damage (*i*)		Damage (*ii*)	
Mode	ξ(%)	*f*(Hz)	ξ (%)	*f*(Hz)	ξ (%)	*f*(Hz)
1	1.23	9.41	0.97	6.23	1.08	5.79
2	1.02	25.53	0.85	21.52	0.94	14.91
3	0.94	38.66	0.88	37.44	1.19	36.14
4	0.97	48.09	0.86	47.34	1.02	41.33

Table 6.6 Identified Natural Frequencies and Damping Ratios for 3-D Cases

CASE 4 (12 DOF)										
	No Damage		Damage (*i*)		Damage (*ii*)		Damage (*iii*)		Damage (*iv*)	
Mode	ξ(%)	*f*(Hz)	ξ (%)	*f*(Hz)	ξ(%)	*f*(Hz)	ξ(%)	*f*(Hz)	ξ(%)	*f*(Hz)
1	1.23	9.29	1.25	6.8	1.28	5.75	1.19	8.79	1.10	8.79
2	1.02	11.64	1.03	9.80	1.13	9.39	1.06	11.64	0.97	11.50
3	0.96	25.28	0.95	21.27	1.09	14.78	1.03	24.37	1.02	24.37
4	1.27	31.66	0.95	28.59	0.88	24.70	1.07	31.65	1.05	30.82
5	0.89	38.25	0.94	36.87	1.23	35.98	1.27	37.77	0.98	37.75
6	1.22	47.79	1.03	46.81	0.92	40.60	1.16	47.71	1.11	47.69
7	1.17	47.95	0.95	47.54	1.10	46.46	0.95	47.93	0.96	47.95
8	1.12	59.81	1.14	59.93	0.85	53.68	1.02	59.81	0.98	58.18
CASE 5 (120 DOF)										
	No Damage		Damage (*i*)		Damage (*ii*)		Damage (*iii*)		Damage (*iv*)	
Mode	ξ(%)	*f*(Hz)	ξ (%)	*f*(Hz)	ξ(%)	*f*(Hz)	ξ(%)	*f*(Hz)	ξ(%)	*f*(Hz)
1	1.15	8.47	1.18	5.42	1.38	4.91	1.11	8.00	1.11	7.99
2	1.08	9.05	1.09	7.29	1.08	6.59	1.05	9.05	1.06	8.81
3	1.10	23.19	1.07	19.06	1.08	12.26	1.03	22.25	0.99	22.22
4	0.86	25.63	1.02	22.47	1.03	17.65	0.88	25.63	0.85	24.72
5	0.89	36.44	1.13	34.94	0.95	34.62	1.03	35.80	1.10	35.77
6	1.07	41.85	0.87	40.23	1.01	38.17	0.98	41.83	1.04	41.71
7	0.89	46.78	0.92	46.50	1.12	40.12	1.11	46.69	1.14	46.68
8	0.90	56.55	1.13	56.15	1.02	49.20	1.09	56.54	0.93	54.67

CASE 6 (120 DOF)												
No Damage		Damage (*i*)		Damage (*ii*)		Damage (*iii*)		Damage (*iv*)		Damage (*v*)	
ξ(%)	*f*(Hz)	ξ (%)	*f*(Hz)	ξ(%)	*f*(Hz)	ξ(%)	*f*(Hz)	ξ(%)	*f*(Hz)	ξ(%)	*f*(Hz)
0.93	8.48	1.32	5.42	1.60	4.91	1.22	7.99	1.14	7.98	1.19	8.34
1.12	9.06	1.10	7.29	1.14	6.59	1.05	9.05	1.07	8.79	1.06	9.05
1.01	23.18	1.05	19.06	1.19	12.26	1.05	22.25	1.04	22.24	1.03	22.90
0.99	25.64	1.01	22.47	1.02	17.65	0.96	25.63	0.87	24.75	0.88	25.63
1.15	36.50	1.08	34.94	1.05	34.62	1.04	35.80	1.13	35.75	1.14	36.25
1.05	41.85	1.13	40.23	1.02	38.17	0.98	41.84	1.08	41.72	1.11	41.84
1.15	46.77	0.94	46.50	1.11	40.12	1.04	46.68	1.20	46.67	0.88	46.74
1.14	56.42	1.12	56.15	1.06	49.20	1.01	56.54	0.92	54.60	1.04	56.54

Table 6.7 WSI Indices for Cases 1-3

CASE 1

Known Input				*Unknown Input*			
Damage (*i*)		Damage (*ii*)		Damage (*i*)		Damage (*ii*)	
Floor	WSI	Floor	WSI	Floor	WSI	Floor	WSI
1	0.13	1	0.13	1	0.10	1	0.13
2	21.66	2	12.51	2	11.30	2	12.12
3	25.50	3	0.11	3	15.60	3	0.09
4	9.44	4	13.34	4	7.34	4	22.67

CASE 2

Known Input				*Unknown Input*			
Damage (*i*)		Damage (*ii*)		Damage (*i*)		Damage (*ii*)	
Floor	WSI	Floor	WSI	Floor	WSI	Floor	WSI
1	0.89	1	1.23	1	0.93	1	1.89
2	16.21	2	24.39	2	16.67	2	34.19
3	12.33	3	1.29	3	15.74	3	2.21
4	25.48	4	24.13	4	25.60	4	37.88

CASE 3

Unknown Input-Shaker			
Damage (*i*)		Damage (*ii*)	
Floor	WSI	Floor	WSI
1	0.11	1	0.15
2	7.55	2	11.67
3	7.64	3	0.10
4	6.88	4	12.88

Table 6.8 WSI Indices for Cases 4-5

CASE 4				
Floor	*WSI*			
	Damage (*i*)	Damage(*ii*)	Damage (*iii*)	Damage (*iv*)
1-x	0.17	0.09	7.13	3.65
2-x	2.77	6.58	7.18	7.15
3-x	6.82	0.08	6.69	0.17
4-x	5.56	5.68	6.44	10.07
1-y	0.08	0.02	0.51	0.58
2-y	6.82	7.37	1.09	1.18
3-y	5.53	0.04	1.47	1.80
4-y	6.09	6.20	1.41	1.23
CASE 5				
Floor	*WSI*			
	Damage (*i*)	Damage(*ii*)	Damage (*iii*)	Damage (*iv*)
1-x	0.34	0.73	6.67	1.19
2-x	3.13	5.11	2.81	1.45
3-x	3.71	0.13	2.53	0.78
4-x	4.29	6.18	1.73	1.02
1-y	0.36	0.51	0.59	0.97
2-y	8.81	7.60	3.70	5.32
3-y	9.03	0.53	3.09	5.96
4-y	8.32	9.24	4.70	3.90

Quantification

For the structure at the undamaged state, the stiffness of all floors were assumed unknown and a shear building model was fit to the undamaged flexibility. For quantifying the damage however, the localization information for cases 1-5 was used to define the free parameters and only the stiffness of these floors were allowed to change in fitting the shear building model to the damaged flexibility. Damage is characterized as percent change in the story stiffness for the complete system. The exact values for the 12 DOF model are displayed in Table B2. In cases 1 and 4 there is no modeling error because the data used in the identification was generated using a shear building model. The results of the quantification are in this case virtually exact. In cases 2 and 5 there is modeling error in the sense that the data was generated using a model that has 120 DOF while the model update of the last stage is carried out assuming a shear building model. The accuracy in the computed reduction in interstory stiffness can not in this case be compared to an

exact result since there is no exact inter-story stiffness (i.e, the ratio of shear to drift is dependent on the lateral load distribution). Nevertheless, the 'exact' values provided in Appendix B (Table B3) are based on a uniform load distribution as a means of providing guidance for the expected values. It is interesting to note, however, that the procedure correctly identifies the inter-story stiffness of the first floor, which has a full rotational restraint at the base, as substantially larger than the value of the other stories. Comparison of the identified percent damage values for cases 1-5 presented in Table 6.9 and Table 6.10 with the exact ones prove to be accurate for the extensive damage patterns. The error in the quantification is less than 4% for the data generated by the 12 DOF model and less than 10% for the data generated by the 120 DOF model. When the damage is not extensive (DP (*iii*)-DP(*v*)) however, the error in the quantified results proves to be higher (less than 20% for the 12 DOF model, and 28% for the 120 DOF model).

Table 6.9 Identified floor stiffnesses, Ki [MN/m] and the percent reductions, %D in the weak direction (1-D Cases)

CASE 1										
	Known Input					*Unknown Input*				
	No Damage	Damage (*i*)		Damage (*ii*)		No Damage	Damage (*i*)		Damage (*ii*)	
Floor	K_i	K_i	%*D*	K_i	%*D*	K_i	K_i	%*D*	K_i	%*D*
1	67.50	19.55	71.0	19.54	71.0	67.86	19.67	71.0	19.55	71.2
2	68.50	-	0.0	-	0.0	67.05	-	0.0	-	0.0
3	70.27	-	0.0	19.83	71.8	70.08	-	0.0	19.54	72.1
4	73.07	-	0.0	-	0.0	68.32	-	0.0	-	0.0
CASE 2										
	Known Input					*Unknown Input*				
	No Damage	Damage (*i*)		Damage (*ii*)		No Damage	Damage (*i*)		Damage (*ii*)	
Floor	K_i	K_i	%*D*	K_i	%*D*	K_i	K_i	%*D*	K_i	%*D*
1	56.60	11.94	78.9	12.27	78.3	57.01	11.85	79.2	11.90	79.1
2	49.40	-	0.0	-	0.0	47.66	-	0.0	-	0.0
3	48.27	-	0.0	7.91	83.6	48.17	-	0.0	7.52	84.4
4	48.98	-	0.0	-	0.0	45.92	-	0.0	-	0.0

CASE 3					
	Unknown Input				
	No Damage	Damage (*i*)		Damage (*ii*)	
Floor	K_i	K_i	%*D*	K_i	%*D*
1	68.61	19.53	71.5	19.47	71.6
2	67.68	-	0.0	-	0.0
3	66.49	-	0.0	19.07	71.3
4	66.41	-	0.0	-	0.0

Table 6.10 Identified floor stiffnesses, Ki [MN/m] and the percent reductions, %D, for cases 4 and 5

CASE 4									
	No Damage	Damage (*i*)		Damage (*ii*)		Damage (*iii*)		Damage (*iv*)	
Floor	K_i	K_i	%*D*	K_i	%*D*	K_i	%*D*	K_i	%*D*
1-*x*	108.37	58.44	46.1	58.67	45.9	-	0.0	-	0.0
2-*x*	105.67	-	0.0	-	0.0	-	0.0	-	0.0
3-*x*	111.16	-	0.0	58.77	47.1	-	0.0	95.88	13.7
4-*x*	98.94	-	0.0	-	0.0	-	0.0	-	0.0
1-*y*	67.39	19.25	71.4	19.42	71.2	55.32	17.9	52.80	21.6
2-*y*	68.52	-	0.0	-	0.0	-	0.0	-	0.0
3-*y*	67.43	-	0.0	18.69	72.3	-	0.0	-	0.0
4-*y*	68.96	-	0.0	-	0.0	-	0.0	-	0.0
CASE 5									
	No Damage	Damage (*i*)		Damage (*ii*)		Damage (*iii*)		Damage (*iv*)	
Floor	K_i	K_i	%*D*	K_i	%*D*	K_i	%*D*	K_i	%*D*
1-*x*	79.14	33.36	57.8	29.50	61.7	-	0.0	-	0.0
2-*x*	58.25	-	0.0	-	0.0	-	0.0	-	0.0
3-*x*	57.40	-	0.0	17.85	68.9	-	0.0	45.86	20.1
4-*x*	54.05	-	0.0	-	0.0	-	0.0	-	0.0
1-*y*	62.23	14.63	76.5	15.32	75.4	48.50	22.1	48.61	21.9
2-*y*	56.23	-	0.0	-	0.0	-	0.0	-	0.0
3-*y*	51.88	-	0.0	11.62	77.6	-	0.0	-	0.0
4-*y*	49.72	-	0.0	-	0.0	-	0.0	-	0.0

Table 6.11 Identified floor stiffnesses, Ki [MN/m] and the percent reductions, %D, for case 6 using direct model update approach

CASE 6											
	No Damage	Damage (*i*)		Damage (*ii*)		Damage (*iii*)		Damage (*iv*)		Damage (*v*)	
Floor	K_i	K_i	%*D*	K_i	%*D*	K_i	%*D*	K_i	%*D*	K_i	%*D*
1-*x*	65.6	26.0	60.4	24.1	63.3	66.8	-1.8	65.4	0.3	61.7	5.9
2-*x*	70.3	79.0	-12.4	69.5	1.1	66.6	5.3	68.8	2.2	79.1	-12.5
3-*x*	48.2	48.2	0.0	14.5	69.9	48.3	-0.3	38.9	19.3	48.8	-1.2
4-*x*	62.4	61.2	1.9	60.2	3.5	59.0	5.4	62.2	0.3	63.9	-2.5
1-*y*	54.5	12.3	77.4	11.7	78.5	42.8	21.4	42.5	22.0	50.6	7.1
2-*y*	61.2	62.3	-1.8	63.6	-3.9	59.7	2.5	59.5	2.8	61.2	0.1
3-*y*	46.9	45.8	2.3	8.1	82.8	46.7	0.4	46.6	0.7	46.1	1.7
4-*y*	53.7	51.3	4.5	50.6	5.8	53.2	0.9	53.1	1.1	53.3	0.7

For case 6, the model update approach discussed in the previous chapter was performed without prior localization. As shown in Table 6.11, although the percent damage estimates are not as

successful as before, reasonable estimates can still be obtained in this case especially for the extensive damage patterns. For damage pattern (*v*), however, the computed changes do not clearly localize the truly damaged floor (1-*y*). Although a 7.1% change is identified for this floor in the *y*-direction, the results also show a 5.9% change in the *x*-direction (false positive). In addition, positive changes as much as 12.5% are identified for some of the floor stiffnesses. Although a constrained optimization routine is implemented to circumvent this problem and improve the quality of the quantification, initial trials were not successful and an exhaustive exploration of the algorithm can not be carried out due to limitations with time.

6.6 Concluding Remarks

This chapter illustrates the performance of the proposed flexibility-based technique to locate and quantify linear damage in the case of the ASCE SHM task group benchmark structure. The approach operates by compressing the time histories into flexibility matrices synthesized at the sensor locations and uses these matrices as targets for identifying the location and severity of the damage.

The analytical simulations of the benchmark problem have included most of the complications that are encountered in actual applications, i.e., noise in the measurements of input and output signals, multiple damaged members, modal truncation and modeling error. As illustrated by the results the technique proved to be accurate when there are sufficient sensors. Unfortunately, for the limited sensor case, the number of available sensors was not sufficient to extract the flexibility proportional matrices to demonstrate the performance of the technique with incomplete sensor information. The complexity of realistic field conditions is, of course, never fully captured by simulations so experimental validations of damage identification techniques are essential.

CHAPTER 7

Summary and Conclusions

7.1 Summary

A flexibility-based methodology for locating and quantifying damage using the measured vibration response has been developed in this thesis. The results obtained in chapter 6 for a series of analytical simulation cases for the ASCE SHM benchmark structure suggest that the technique is robust, general, and scalable.

The methodology developed in this study is composed of the following modules:

1) Computation of a state-space realization from the measured signals.
2) Extraction of flexibility matrices from the matrices of the realization (to within a scalar multiplier when the input is stochastic).
3) Computation of the change in flexibility from the undamaged to the damaged state (or a matrix that differs from it by a scalar multiplier).
4) Reduction of the subset of potentially damaged elements by examination of the change in flexibility.
5) Use of the damage flexibility to quantify the damage.

Chapter 2 provides the mathematical framework for the first module of the proposed strategy. Extraction of flexibility or flexibility proportional matrices is discussed in chapter 3. Mapping the measured changes in the flexibility to the location of the physical damage in the structure is addressed in chapter 4 and a rigorous approach that removes heuristics of the traditional flexibility-based methods known as the DLV approach has been developed. Finally, the last

module of the strategy, estimation of the severity of damage is explored in chapter 5. The method examined here attempts to match the flexibility at the damaged state in a least square sense to quantify the damage using the restricted free parameter space provided by the DLV approach for updating.

7.2 Conclusions and Observations

The basic findings of this study can be summarized as follows:

1. State-space realizations are robust but the order of the system is not always easy to select when measurement noise is significant.

2. Identification of damage for symmetric structures with unsymmetric damage patterns can create problems in 'before and after' type investigations since modes that are not characterized at the undamaged state may appear in the damaged case.

3. Traditionally, methods to extract flexibility matrices focus on computation of mass normalized undamped modes and frequencies from the identified complex modes. There is no need or advantage, however, in searching for the undamped modes to assemble the flexibility. It is possible to operate in a more general setting by using directly the identified complex modes. When the input information is available, the only limitation of the method presented here is that it requires, at least, one collocated sensor actuator pair. Analytical simulations with realistic levels of noise incorporating complications such as incomplete sensor information and modal truncation suggest that the approach presented in chapter 3 is robust and has no difficulties to assemble flexibility matrix under realistic conditions. Without a doubt, the results are completely dependent on the accuracy of the realization since one can not get an accurate estimate of the flexibility if the identified modes are not accurate.

4. Although in the case of stochastic input one can not assemble the flexibility matrices it is possible to obtain approximations to within a scalar using only the output measurements, provided that the mass matrix can be assumed diagonal at the available coordinates. When all the modes are available, the method is exact, however if only a truncated modal space is

available then the approach becomes approximate since one equates a modally truncated approximation to a 'converged physical quantity'. (The off-diagonals of the mass matrix is zero when the modal basis is complete.)

5. The Damage Locating Vector technique presented here as a means of localizing the damage identifies load distributions where the static response of the structure is *the same* in the undamaged and the damaged systems. Implicit in the perspective of the approach is the fact that the DLV technique does not actually search for damaged elements but rather identifies undamaged elements as those that have significant stresses when the structure is loaded with the DLVs. The issue of what elements are inseparable for a given sensor set has been solved theoretically. In practice the set is typically larger than the theoretical minimum due to factors such as measurement noise and modal truncation.

6. The application of techniques that operate with the assumption of a single damage location, or apriori knowledge of probable damage locations are limited to systems where such knowledge is available. The DLV technique makes none of these assumptions. As long as there are sufficient number sensors that will allow the change in flexibility to have a null space, the method performs equally well with single or multiple damage locations.

7. Since DLVs are computed systematically in a structure-type independent fashion and strictly from the measured data, model dependence in localization using DLVs is typically small. Indeed the DLVs are unaffected by modeling errors and error in the localization derives exclusively from evaluating the effects of these loads on the structure. The model used to compute these effects require only the undamaged topology for statically determinate structures and plus the relative values of the stiffness characteristics for indeterminate systems.

8. The DLV technique operates with all the available sensors without recourse to DOF expansion strategies. The problems associated with implementation of these techniques and the inevitable modeling errors introduced in the process are therefore eliminated.

9. In localizing the damage using the DLV approach, uncertainties associated with inertial and damping characteristics are decoupled from the search for stiffness related damage since only a static model is needed to apply the DLVs.

10. Unlike the localization, quantification of damage is highly model dependent. The success of the approach is closely linked to the accuracy of the baseline model and the size of the free parameter space. While consistent with the modal data, the physical parameters obtained at this stage may be unrelated to actual values in the damaged state. Although this task is performed successfully for a series of cases in the benchmark study, it should be noted that the modeling errors introduced were small.

11. The analytical simulations of the benchmark problem have included most of the complications that are encountered in actual applications, i.e., noise in the measurements of input and output signals, multiple damaged members, modal truncation and modeling error. The technique developed here proved to be accurate within the complications captured by analytical simulations. The methodology, however, still waits for experimental validation.

7.3 Future Work

The issues that require further studies regarding the damage identification methodology developed in this thesis can be summarized as follows:

1. The method presented here looks for damage as changes introduced to the structure following a severe loading event for which structural damage is suspected. It does not, however, address the problem of distinguishing when changes in system characteristics are a reflection of damage and when they are a consequence of inevitable differences associated with measurements taken at different times. In order to detect the gradual deterioration of the structure, such as that due to fatigue and corrosion, more research in this direction is needed.

2. For the stochastic input case, further investigation is needed to find the best norm that ensures the flexibility matrices obtained to within a scalar is compatible between the undamaged and damaged states.

3. The ambient excitations considered in this study are modeled as white noise, which is an assumption that needs to be satisfied to apply the system identification algorithms. The

applicability of these identification techniques for cases in which the input excitations are not so rich in frequency needs to be explored. Formulation of realistic stochastic models for ambient excitation sources needs to be studied to help bridge the gap between the simulations and reality.

4. More thorough testing of the strengths and limitations of the technique is needed. The method must be tested on more complex structures to explore the effects of modeling errors due to boundary conditions, uncertainty in mass distribution, non-classical modes and non-linearities.

5. As for any damage characterization technology, experimental support is essential for the validation of the approach and for a final assessment on robustness.

6. Finally if the technique is found to perform robustly with experimental data, a software needs to be developed for implementation of the procedure in an automated fashion.

REFERENCES

Akaike, H. (1968). "Information theory and an extension of the maximum likelihood principle," *Second International Symposium on Information Theory*, B. N. Petrov, F. Caski, eds., Akademiai Kiado, Budapest, pp.267-281.

Aktan A., E., Lee, K. L., Chuntavan, C. and Aksel, T. (1994). "Modal testing for structural identification and condition assessment of constructed facilities," *Proceedings of the 12th International Modal Analysis Conference*, pp.462-468.

Alvin, K. F. and Park, K. C. (1994). "Second-order structural system identification procedure via state-space-based system identification," *AIAA Journal*, vol.22, no.2, pp.397-406.

Balmes, E. (1997). "New results on the identification of normal modes from experimental complex modes," *Mechanical Systems and Signal Processing*, vol.11, no.2, pp.229-243.

Beck, J. and Bernal, D. (2001). "A Benchmark Problem for Structural Health Monitoring", *Experimental Techniques*, vol.25, no.3, pp.49-53.

Bernal, D. and Gunes, B (2000). "An examination of instantaneous frequency as a damage detection tool", *14th Engineering Mechanics Conference*, Austin, TX.

Bernal, D. and Gunes, B. (2000). "Extraction of system matrices from state-space realizations", *14th Engineering Mechanics Conference*, Austin, TX.

Bernal, D. (2002). "Load vectors for damage localization", *Journal of Engineering Mechanics*, ASCE, to appear in the January issue.

Bernal, D. and Gunes, B. (2002). "A flexibility based approach for the localization and quantification of damage: A benchmark application," to appear in the *Journal of Engineering Mechanics*.

Bernal, D. and Gunes, B. (2002). "Damage localization in output-only systems: A flexibility based approach," to appear in the *Proceedings of the 20th International Modal Analysis Conference*, February 4-7, 2002.

Black, C. J. and Ventura, C. E. (1998). "Blind Test on Damage Detection of a Steel Frame Structure." *Proceedings of the 16th International Modal Analysis Conference*, pp. 623-629, Santa Barbara, California, February 2-5, 1998.

Cawley, P. and Adams, R. D. (1979). "The locations of defects in structures from measurements of natural frequencies," *Journal of Strain Analysis*, vol.14, no.2, pp.49-57.

Chance, J., Tomlinson, G. R., and Worden, K. (1994). "A simplified approach to the numerical and experimental modeling of the dynamics of a cracked beam," *Proceedings of the 12th International Modal Analysis Conference*, pp.778-785.

Chen, J. C., ed. (1996). *Proceedings of the Second International Workshop on Structural Control: Next Generation of Intelligent Structures*, December 18-21, Hong Kong University of Science and Technology.

Conturisi, T., Messina, A. and Williams, E. J. (1997). "Multiple damage evaluation using natural frequency changes", *Proceedings of the 15th International Modal Analysis Conference*, pp.658-664.

Doebling, S.C, Farrar, C.R., Prime, M.B. and Schevitz, D.W. (1996). Damage identification and health monitoring of structural and mechanical systems from changes in their vibration characteristics: A literature review, Los Alamos National Laboratory, Los Alamos, New Mexico.

Doebling, S. W., Hemez, F. M., Peterson, L. D., and Farhat, C. (1997). "Improved damage location accuracy using strain energy-based mode selection criteria," *AIAA Journal*, vol.35, no.4, pp.693-699.

Doebling, S. W., Farrar, C. R., and Prime, M. B. (1998). "A summary review of vibration-based damage identification methods," *The Shock and Vibration Digest*, vol.30, no.2, pp.91-105.

Doherty, J. E., (1987). "Non destructive evaluation," *Handbook on Experimental Mechanics*, A. S. Kobayashi, ed., Society for Experimental Mechanics.

Ewins, D. J. (1990). "Modal testing as an aid to vibration analysis," *23rd Conference on Mechanical Engineering*, pp.1-15, May, 1990.

Farrar, C. R., Doebling, S. W., Cornwell, P. J., and Straser, E. G. (1997). "Variability of modal parameters measured on the Alamosa Canyon Bridge," *Proceedings of the 15th International Modal Analysis Conference*, Orlando, FL., pp.257-263.

Fox, C. H. J. (1992) "The location of defects in structures: A comparison of the use of natural frequency and mode shape data," *Proceedings of the 10th International Modal Analysis Conference*, pp.522-528.

Friswell, M. I., Penney, J.E.T, Wilson, D.A.L. (1994). "Using vibration data and statistical measures to locate damage in structures", *The International Journal of Analytical and Experimental Modal Analysis*, vol.9,no.4, pp.239-254.

Friswell, M.I. and Motthershed, J.E. (1995). *Finite Element Updating in Structural Dynamics, Kluwer Academic Publishers*, Boston, MA.

Hemez, F. M. (1993). "Theoretical and experimental correlation between finite element models and modal tests in the context of large flexible space structures," *Ph.D. dissertation*, University of Colorado, Boulder.

Ibrahim, S. R. (1983). "Computation of normal modes from identified complex modes," *AIAA Journal*, vo.21, pp.446-451.

Ibrahim, S. R. and Fullekrug, U. (1990). "Investigation into exact normalization of incomplete complex modes by decomposition transformation," *Proceedings of 8th International Modal Analysis Conference*, pp.205-212.

Ibrahim, S. R. and Sestieri, A. (1995). "Existence and normalization of complex modes in post experimental use in modal analysis," *Proceedings of the 13th International Modal Analysis Conference*, pp.483-489.

Johnson, E, A., Lam, H. F., Katafygiotis, L.S. and Beck, J. L. (2000). "A Benchmark Problem for Structural Health Monitoring and Damage Detection", *14th ASCE Engineering Mechanics Conference*, Austin, Texas, May 21-24 2000.

Juang, J., (1994). *Applied System Identification*, Prentice-Hall, Englewood Cliffs, New Jersey.

Kaouk, M. (1993). "Finite element model adjustment and damage detection using measured test data," *Ph.D. dissertation*, University of Florida, Gainsville.

Kenley, R. M., and Dodds, C. J. (1980). "West sole WE Platform: Detection of damage by structural response measurements", *Proceedings of 12th Annual Offshore Technology Conference*, pp.111-118.

Kim, H.M., Bartkowicz, T.J., Smith, S.W., and Zimmerman, D.C. (1995). "Structural health monitoring of large structures," *Proceedings of the 49th Meeting of the Society for Machinery Failure Prevention Technology*, pp.403-412.

Kim, J. H., Jeon, H.-S., and Lee, C.-W. (1992). "Application of the modal assurance criteria for detecting and locating structural faults," *Proceedings of the 49th Meeting of the Society for Machinery Failure Prevention Technology*, pp.403-412.

Ko, J. M., Wong, C. W., and Lam, H. F. (1994). "Damage detection in steel framed structures by vibration measurements approach," *Proceedings of the 12th International Modal Analysis Conference*, pp. 280-286.

Law, S. S., Shi, Z. Y., and Zhang, L. M. (1998). "Structural damage detection from incomplete and noisy modal data," *Journal of Engineering Mechanics*, vol. 124, no.11, pp.1280-1288.

Lim, T. W. (1994). "Structural damage detection of a planar truss structure using a constrained eigenstructure assignment," *Proceedings of the 35th AIAA/ASME/ASCE/ AHS/ASC Structures, Structural Dynamics and Materials Conference, AIAA*-94-1715-CP, pp.336-346.

Lim, T.W. and Kashangaki, T.A.L. (1994). "Structural damage detection of space truss structure using best achievable eigenvectors," *AIAA Journal*, vol.32, no.5, pp.1059-1057.

Lim, T.W. (1995). "Structural damage detection using constrained eigenstructure assignment," *Journal of Guidance, Control and Dynamics*, vol.18, no.3, pp.411-418.

Meneghetti, U. and Maggiore, A. (1994). "Crack detection by sensitivity analysis", *Proceedings of the 12th International Modal Analysis Conference*, pp.1292-1298.

Osegueda, R.A, Dsouza, P. D., and Qiang, Y. (1992). "Damage evaluation of offshore structures using resonant frequency shifts," *Serviceability of Petroleum, Process and Power Equipment*, ASME PVP 239/MPC 33, pp.31-37.

Pandey, A. K., Biswas, M, and Samman, M. M. (1991). "Damage detection in curvature mode shapes," *Journal of Sound and Vibration*, vol.145, no.2, pp.321-332.

Pandey A. K, and Biswas, M. (1994). "Damage detection in structures using changes in flexibility," *Journal of Sound and Vibration*, vol. 169, no. 1, pp.3-17.

Pandey A. K, and Biswas, M. (1995). "Damage diagnosis of truss structures by estimation of flexibility change," *Modal Analysis: The International Journal of Analytical and Experimental Modal Analysis*, vol.10, no.2, pp.104-117.

Penney, J.E.T, Wilson, D.A.L., and Friswell, M. I. (1993). "Damage location in structures using vibration data", *Proceedings of the 11th Modal Analysis Conference*, pp.861-867.

Peterson, L. D., Doebling, S. W., and Alvin, K. F. (1995). "Experimental determination of local structural stiffness by disassembly of measured flexibility matrices," *Proceedings of the 36th AIAA/ASME/ASCE/AHS/ASC Structures, Structural Dynamics, and Materials Conference*, AIAA-95-1090-CP, pp.2756-2766.

Phan, M. Q., Horta, L. G., Juang, J.-N., and Longman, R. W. (1992). "Identification of linear systems by an asymptotically stable observer", *NASA Technical Report*, TP-3164.

Ricles, J. M. (1991). "Nondestructive structural damage detection in flexible space structures using vibration characterization," *NASA Report*, CR-185670.

Rissanen, J. (1978). "Modeling by shortest data description," *Automatica*, vol.14, pp.465-471.

Rytter, A. (1993). "Vibration based inspection of civil engineering structures," *Ph.D. Dissertation*, Aalborg University, Denmark.

Salawu, O. S. and Williams, C. (1994). "Damage location using vibration mode shapes," *Proceedings of the 12th International Modal Analysis Conference*, pp. 933-939.

Salawu, O. S. (1997). "Detection of structural damage through changes in frequency: A review," *Engineering Structures*, vol.19, no.9, pp.718-723.

Sanayei, M. and Onipede, O. (1991). "Damage assessment of structures using static test data," *AIAA Journal*, vol.29, no.7, pp.1174-1179.

Silva, J. M. M. and Gomes, A. J. M. A (1994) "Crack identification of simple structural elements through the use of natural frequency variations: The inverse problem," *Proceedings of the 12th International Modal Analysis Conference*, pp.1728-1735.

Smith, S. W. and Beattie, C. A (1991). "Model correlation and damage location for large space truss structures: Secant method development and evaluation," *NASA Report*, NASA-CR-188102.

Stubbs, N., Kim, J.-T., and Topole, K. (1992). "An efficient and robust algorithm for damage localization in offshore platforms," *Proceedings of the ASCE 10th Structures Congress*, pp.543-546.

Stubbs, N. and Kim, J.-T. (1996). "Damage localization in structures without baseline parameters," *AIAA Journal*, vol.34, no.8, pp.1644-1649.

Van Overschee, P. and Moor, B.L.R. (1996). *Subspace Identification for Linear Systems*, Kluwer Academic Publishers, Boston.

Ventura, C. E., Prion, H. G. L., Black, C., Rezai, K., and Latendresse, V. (1997). "Modal properties of a steel frame used for seismic evaluation studies," *Proceedings of the 15the International Modal Analysis Conference*, pp. 1885-1891.

West, W. M. (1984). "Illustration of the use of modal assurance criterion to detect structural changes in an orbiter test specimen," *Proceedings if the Air Force Conference on Aircraft Structural Integrity*, pp.1-6.

Wylie, C. R. and Barrett, L.C. (1982). *Advanced Engineering Mathematics*, Mc.Graw-Hill, New York.

Yang, C.-D., and Yeh, F.-B. (1990). "Identification, reduction and refinement of model parameters by the eigensystem realization algorithm," *Journal of Guidance, Control and Dynamics*, vol.13, no.6, pp.1051-1059.

Zhang, Q. and Lallemant, G. L. (1987). "Comparison of normal eigenmodes calculation method based on identified complex modes," *Journal of Spacecraft and Rockets*, vol.24, no.1, pp.69-73.

Zimmerman, D. C. and Kaouk, M. (1992). "Eigenstructure assignment approach for structural damage detection," *AIAA Journal*, vol.30, no.7, pp.1848-1855.

APPENDIX A

Matlab Programs

```
% ********************************************* MICKI.m ***************************************************
%*********************************************************************************************************
% DESCRIPTION
%
%This function extracts partitions of the inverse of the mass and stiffness matrices. The modal
%contribution to the damping matrix can also be extracted under special circumstances as
%discussed in Chapter 3. For stochastic systems the matrices are computed to within one
%undetermined scalar (the output is normalized so that trace(MI)=1 and KI is consistent. Further
%work on normalization may be appropriate.

%FEATURES:
%The solution for M^-1 and K^-1 is theoretically exact for the number of identified %modes when
%the input is measured. In the stochastic case the results are approximate unless the modal
%basis is complete and the partition of the inverse of the mass matrix is diagonal for the
%measured coordinates.
%
% INPUT:
%A,B,C - matrices of the realization in continuous time.
%
% im -  matrix with two columns and as many rows as there are colocated inputs. The first column
%has the positions in the list of outputs that corresponds to colocated inputs and the second
%column the corresponding position in the input vector.
%Example im =[ 2 4; 3 1]; indicates that the second output is associated with the 4th input while
%the third output corresponds to the first input.
%
% p = 0,1 or 2 to indicate if the realization is for displacement, velocity or acceleration.
%
%reord = vector to reorganize the output - in the unadjusted form the order of the dof in the
%results corresponds to the order of the output sensors followed by the input sensors where the
%colocated sensors are excluded from the input list. The reorder version is useful for comparing
%results with those from a model. The reord vector must have pre = (#out+#inp-#colocated)
%entries and must contain all the integers from 1 to pre. A valid entry in a case with 4 outputs, 3
%inputs and 2 colocated sensors could be reord=[5 1 2 3 4];

% OUTPUT - Modal contributions to:
% MI - Inverse of the mass matrix at the coordinates
% KI - Inverse of the stiffness (Flexibility) at the coordinates
% CD - Damping matrix at the coordinates
%*********************************************************************************************************
```

```
function [MI,CD,KI,fi,tfids,lam,aai]=micki(A,B,C,im,p,reord);

% Check if the run is Stochastic or Deterministic
x=isempty(B);
if x==1;
  flag1=1;
% Stochastic Matrix Extraction
else
  flag1=0;
  % Deterministic Matrix Extraction
end;

if nargin<6;
  reord=[];
else
  end;
 reorcheck=isempty(reord);

  if flag1==0;
disp('This is a Determininstic Run');
% Part 1 - Check Consistency of the Input
[rb,r]=size(B);
[m,cc]=size(C);
[ra,ca]=size(A);
v=max(im);
pp=[0 1 2];
v1=intersect(pp,p);
x1=isempty(v1);
ci=im(:,2);
co=im(:,1);
pre=m+r-length(co);
if ra~=ca;
  disp('A matrix not square');
  break
elseif rb~=ra;
  disp('inconsistency between the rows of B and the dimension of A');
elseif cc~=ra;
  disp('inconsistency in the number of columns in C');
elseif v(1)>m
  disp('reference to an output number larger than the total number in im');
  break
%elseif v(2)>r
%   disp('reference to an input number lager than the total number of inputs');
elseif x1==1;
  disp('p must be either 0 1 or 2');
  break;
else
  end;
if reorcheck~=1;
if pre-length(reord)~=0;
  disp('error in the specification of the reorder vector')
  disp('reorder discarded - output is in the standard form');
  reord=[];
end;
end;
```

```
% Part 2 - Compute the part of B that is colocated
Bcc=B(:,ci);

% Part 3 - Compute the eigenvalues and eigenvectors of A
[aa,bb]=eig(A);

% Part 4 - Sort the eigenvectors according to the 'undamped natural frequency'.
[w,zai]=ceig(diag(bb));
[ws,Y]=sort(w);
aas=aa(:,Y);
bb=diag(bb);
bbs=bb(Y);
kk=0;
for j=1:2:ra;
   kk=kk+1;
   fi(:,kk)=aas(:,j);
   lam(kk)=bbs(j);
end;
lam=lam.'

% Part 5 - Reorganize the spectral matrix in standard form
fe=[fi conj(fi)];

% ********************** MAIN SECTION FOR DETERMINISTIC CASE ******************************
%*************************************************************************************************************
% Open a loop from 1 to the number of identified modes
dof=round(0.5*ra);
aai=inv(fe)
tfids=[];
for kk=1:dof;

%Part 6 - Compute the mode in displacement velocity form at the sensors (displacement
%partition).
fid(:,kk)=C*fi(:,kk)*lam(kk)^-p;

%Part 7 - Compute the normalization constant (if there is redundant information select the
%largest modal amplitude.
[dum,I]=max(abs(fid(co,kk)));
num=lam(kk)^-1*aai(kk,:)*Bcc;
den=fid(co,kk);
al2(kk)=num(I)/den(I);

%Part 8 - Compute the normalized mode
fids=fid(:,kk)*sqrt(al2(kk))

%Part 9 - Compute the modal amplitudes at the coordinates where there are only inputs -
%use the largest amplitude of the denominator.
R=1:r;
pin=setxor(R,ci);
Fmrp=C*fi(:,kk)*aai(kk,:)*lam(kk)^-(p+1)*B(:,pin);
[dum,I]=max(abs(fids));
nume=Fmrp(I,:);
den=fids;
e=nume/den(I);
e=e(:)
```

```
% Part 10 - Pad the mode to get the complete set
fids=[fids;e];
tfids=[tfids fids];

% Part 11 - Compute the contributions to MI and KI
MIp{kk}=2*real(fids*fids.'*lam(kk)^2);
KIp{kk}=-2*real(fids*fids.');
end;

% Part 12 - Get the total MI and KI;
for j=1:dof;
  if j==1;
    KI=KIp{j};
    MI=MIp{j};
  else
    KI=KI+KIp{j};
    MI=MI+MIp{j};
  end;
end;

% Part 13 - Compute the damping
rak=rank(MI);
if rak<(m+r-length(ci));
  disp('MI is rank deficient - C can not be computed without discarding some coordinates');
  CD=[];
  break;
end;
ker=2*real(tfids*diag(lam.^3)*tfids.');
M=inv(MI);
CD=-M*ker*M;

% Part 14 - Reorder if desired
v=isempty(reord);
if v==0;
  TT=zeros(length(reord));
  for j=1:length(reord);
  TT(reord(j),j)=1;
  end;
  MI=TT'*MI*TT;
  KI=TT'*KI*TT;
  CD=TT'*CD*TT;
else;
end;

else;
disp('This is a Stochastic Run');

% ************************************** STOCHASTIC SECTION ***********************************
%*************************************************************************************************
% Part 1b - Check Consistency of the Input
[m,cc]=size(C);
[ra,ca]=size(A);
pp=[0 1 2];
v1=intersect(pp,p);
x1=isempty(v1);
pre=m;
```

```
if ra~=ca;
  disp('A matrix not square');
  break
elseif cc~=ra;
  disp('inconsistency in the number of columns in C');
elseif x1==1;
  disp('p must be either 0 1 or 2');
  break;
else;
end;

if reorcheck~=1;
if pre-length(reord)~=0;
  disp('error in the specification of the reorder vector')
  disp('reorder discarded - output is in the standard form');
  reord=[];
end;
end;

% Part 3b - Compute the eigenvalues and eigenvectors of A
[aa,bb]=eig(A);

% Part 4b - Sort the eigenvectors according to the 'undamped natural frequency'.
[w,zai]=ceig(diag(bb));
[ws,Y]=sort(w);
aas=aa(:,Y);
bb=diag(bb);
bbs=bb(Y);
kk=0;
for j=1:2:ra;
  kk=kk+1;
  fi(:,kk)=aas(:,j);
  lam(kk)=bbs(j);
end;
lam=lam.';

%Part 5b - Reorganize the spectral matrix in standard form
fe=[fi conj(fi)];
% Open a loop from 1 to the number of identified modes
dof=round(0.5*ra);
aai=inv(fe);
E1=[];
E2=[];
S1=[];
S2=[];
for kk=1:dof;

%Part 6b - Compute the mode in displacement velocity form at the sensors (displacement
%partition).
fid(:,kk)=C*fi(:,kk)*lam(kk)^-p;

% Part 7b - Form the matrices E1 and E2
z=12345*ones(m);
z=tril(z);
RI=fid(:,kk)*[fid(:,kk)].'*lam(kk)^2;
RIr=real(RI);
```

```
RIi=imag(RI);

RIr=triu(RIr,1)+z;
RIr=RIr(:);
s=find(RIr~=12345);
RIrb=RIr(s);

RIi=triu(RIi,1)+z;
RIi=RIi(:);
s=find(RIi~=12345);
RIib=RIi(s);

E1=[E1 RIrb];
E2=[E2 RIib];
```

% Part 7c - Form the matrices S1 and S2

```
z=12345*ones(m);
z=tril(z,-1);
RI=fid(:,kk)*[fid(:,kk)].'*lam(kk);
RIr=real(RI);
RIi=imag(RI);

RIr=triu(RIr)+z;
RIr=RIr(:);
s=find(RIr~=12345);
RIrb=RIr(s);

RIi=triu(RIi)+z;
RIi=RIi(:);
s=find(RIi~=12345);
RIib=RIi(s);

S1=[S1 RIrb];
S2=[S2 RIib];
end;
```

% Part 8b - Form Y and solve for the constants

```
E=[E1 -E2];
S=[S1 -S2];
Y=[E;S];

% Approach based on the "null space of Y" - direct extension of exact.
 [dum,cy]=size(Y);
 cee=round(0.5*cy);
 [q1,s,q2t]=svd(Y);
 diag(s)
 be=q2t(:,end);
 ber=be(1:cee,:);
 bei=be(cee+1:end,:);
 be2=ber+bei*i
```

% Part 9b - Compute the normalized modes

```
fids=fid*sqrt(diag(be2));
```

% Part 10b - Matrices to within a scalar

```
KI=-real(fids*fids.');
```

```
MI=real(fids*diag(lam.^2)*fids.');

% Part 11b - Compute the damping
rak=rank(MI);
if rak<m;
   disp('MI is rank deficient - C can not be computed without discarding some coordinates');
   CD=[];
   break;
end;
ker=real(fids*diag(lam.^3)*fids.');
M=inv(MI);
CD=-M*ker*M;

% Part 11c - Normalize to equal trace;
scale=1/trace(MI);
MI=MI*scale;
KI=KI*scale;
CD=CD/scale;


% Part 12b - Reorder if desired
v=isempty(reord);
if v==0;
   TT=zeros(length(reord));
   for j=1:length(reord);
   TT(reord(j),j)=1;
   end;
   MI=TT'*MI*TT;
   KI=TT'*KI*TT;
   CI=TT'*CI*TT;
else;
end;
end;
```

```
% ****************************************** POSTP1.m ***************************************************
%*********************************************************************************************************
% DESCRIPTION
% This function implements the DLV approach lumped spring-mass systems. The characterizing
% stress for this file is taken to be the story shears.

% INPUT
% FU=Identified flexibility at the undamaged state
% FD=Identified flexibility at the damaged state

% OUTPUT
% wsi = weighted stress index
%*********************************************************************************************************
function [R,wsi]=postp1(FU,FD)

DF=FD-FU;
[q1,s,q2t]=svd(DF);
V=abs(flipud(cumsum(flipud(q2t))));

% Selection criteria
sdf=diag(s);
cdf=1./[max(V)]';
crit=sdf.*cdf.^2;
svn=sqrt(crit/max(crit))

I=find(svn<=0.2)
%
if isempty(I)
disp('Warning! None of the svn values is < 0.2')
break;
end;

% Compute nsi for each vector and normalize it by the cut for that vector
r9=zeros(length(svn),1);
r9(I)=1;
mbf=max(abs(V));
NSI5=[abs(V)*diag(1./mbf)];
nsic=max(0.015,1.0*svn);
scale=diag(1./nsic);
wsi=NSI5*scale*r9/length(I);
[pp,qq]=sort(wsi);
R=[qq pp]
```

```
%********************************************** QUANTIFY.m ***********************************************
%*********************************************************************************************************
%DESCRIPTION
%This function quantifies the damage using the localization information together with the
%identified flexibility matrix at the damaged state. This particular version is written for truss-type
%structures.
%
%INPUT
%eai(matrix)    = Each row lists E,A,I the length (l) and the angle fi (measured in degress
%counterclockwise from the local bar axis), as many rows as bars in the structure.
%kc (matrix)    = Each row has the three coefficients of the localflexural stiffness (typically 4 4 2).
%lm (matrix)    = Each row indicates the relationship between the local DOF in the bar and the
%global DOF in the structure. For example, if the first row for lm is [0 0 0 1 2 4] it means that the
%first node is not associated with DOF (a fixed support) and that at node 2 the x,y and z
%displacements correspond to the structural DOF 1 2 and 4. This matrix has 6 columns and as
%many rows as bars in the structure.
%fd             = flexibility matrix at the damaged state
%sensor         = a vector of dofs for which an output sensor is available
%dm             = potentially damaged members identified by the DLV approach
%
%OUTPUT
%areas          = updated areas for the potentially damaged bars
%*********************************************************************************************************
function[areas]=quantify(eai,kc,lm,fd,sensor,dm);
ml=zeros(length(eai),6);
maxiter=10;
flag=0;
whcount=0;
user=1;
cnt1=0;
cnt2=1;
eai_p=eai;
Results=[];
betas=[];
%
%end of input
%*****************************************************************************************
[r,c]=size(fd);
ii=0;
for i=1:c
  for j=i:r
    ii=ii+1;
    flexd(ii,1)=fd(i,j);
  end
end
fd=flexd;

%ii=0;
%for i=1:c
%  for j=i:r
%    ii=ii+1;
%    fdex(ii,1)=FDex(i,j);
%  end
%end

nelem=size(eai,1);
```

```
nd=length(dm);
nn=length(sensor);
initial=eai(:,2);

%Determine the no. of dof's of the system
[nb,qq]=size(lm);
dof=max(max(lm));

%Start the iterations
eai=eai_p;
for niter=1:maxiter  %since bar forces depend on the areas (indet case)
  col_d=[];
  for i=1:nn
    jl=zeros(dof,1);
          jl(sensor(i))=1;
          [res,delta]=plane(eai,kc,lm,ml,jl);
    F(:,i)=res(:,1);
  end

  cnt=0;
  for j=1:nn
    for i=j:nn
      cnt=cnt+1;
      col(:,cnt)=F(:,j).*F(:,i).*eai(:,4)./eai(:,1);
    end
  end
  %Select the presumably damaged members
  for i=1:nd
    col_d(i,:)=col(dm(i),:);
  end

  %Contribution of all UNdamaged members
  for i=1:nelem
    col_all(i,:)=col(i,:)./eai(i,2);
  end
  for i=1:nd
    col_all(dm(i),:)=0;
  end
  undam_cont=(sum(col_all))';
  dam_cont=col_d';
  cond(dam_cont)

  %Subtract the undamaged contribution from the total flex
  fbar=fd-undam_cont;
  R=rank(dam_cont);

  %Equation is b=1/Ad=x1+x2*beta
  x2=null(dam_cont)
  cond(dam_cont)
  %IF dam_cont is full rank, then one can obtain a least squares solution
  if R==nd
    %x=pinv(dam_cont)*fbar;
    alpha=1;
    diags=[1 10 18 25 31 36 40 43 45];
    W=diag(eye(45));
    W(diags)=alpha;
```

```
  W=diag(W);
  x=pinv(W*dam_cont)*(W*fbar);
  Ad=1./x;
  eai(dm,2)=Ad;
  fest=undam_cont+dam_cont*x;
  r=abs(fd-fest);
  err=sum((fd-fest).^2)
else
  if flag == 0
    disp(' There is rank deficiency')
    disp(' You need to fix some values in the solution')
    %calculate the degree of rank deficiency
    d=nd-R;
    disp(' The number of values you need is = '),disp(d),
    select=[];
    r=rref(dam_cont);
    for i=1:dm;s{i}=find(r(i,:)>=10^(-14));end;
    for i=1:dm;jj(i)=size(s{i},2);end;
    jjj=find(jj>1);
    disp('Here is the suggested grouping:')
    for i=1:length(jjj);
      group=dm(s{jjj})
    end;
    for i=1:d
      user=0;
        while user == 0
        disp(' Input the INDEX no. for the bar & the AREA you want to fix')
        addinfo(i,:)=input(' Enter in brackets ==> ');
        row(i)=addinfo(i,1);
        check=x2(row(i),:)
        dummy=[select;check];
        if rank(dummy) ~=i
          disp(' The info you provide is NOT independent')
          disp(' Please try again')
          user=0;
        else
          user=1;
          select=dummy;
        end
        end
    end
    b=1./addinfo(:,2);
    %UPDATE the areas with the provided info
    eai(row,2)=1./b;
    flag=1;
    %UPDATE the unknown list
    dm2=dm;dm_p=dm;dm_p(addinfo(:,1))=[];dm=dm_p
    nd=length(dm);
       end
 end

 areas=eai(dm,2)
end
```

```
% ********************************************** BENCH.m ***************************************************
%*************************************************************************************************************
% This is the static model of the benchmark structure used for localizing the damage

%Properties
E=2*10^11;
Icz=0.664*10^(-6);        % column (weak)
Icy=1.97*10^(-6);         % column (strong)
Ac=1.13*10^(-3);          % column area
Ib=1.22*10^(8);           % beam
Ab=1.43*10^(9) ;          % beam area
Abr=0.141*10^(-3);        % brace area
Ibr=0;
Lc=0.9;
Lb=1.25;
Lbr=sqrt(0.9^2+1.25^2);
fi1=atan(0.9/1.25)*180/pi;
fi2=180-fi1;

%Input the joints at the ends of each bar for each frame type
jc(1)={[0 1;1 2;2 3;3 4;0 5;5 6;6 7;7 8;0 9;9 10;10 11;11 12;1 5;2 6;3 7;4 8;5 9;
        6 10;7 11;8 12; 0 5;1 6;2 7;3 8;0 5;9 6;10 7;11 8]};
jc(2)=jc(1);
jc(3)=jc(1);
jc(4)=jc(1);
jc(5)={[0 1;1 2;2 3;3 4;0 5;5 6;6 7;7 8;0 9;9 10;10 11;11 12;1 5;2 6;3 7;4 8;5 9;6 10;7 11;8 12]};
jc(6)=jc(5);

% Input E,A,I,L and fi for each frame type
eai(1)={[E Ac Icy Lc 90; E Ac Icy Lc 90; E Ac Icy Lc 90; E Ac Icy Lc 90;
         E Ac Icy Lc 90; E Ac Icy Lc 90; E Ac Icy Lc 90; E Ac Icy Lc 90;
         E Ac Icy Lc 90; E Ac Icy Lc 90; E Ac Icy Lc 90; E Ac Icy Lc 90;          % columns
         E Ab Ib  Lb  0; E Ab Ib  Lb  0; E Ab Ib  Lb  0; E Ab Ib  Lb  0;
         E Ab Ib  Lb  0; E Ab Ib  Lb  0; E Ab Ib  Lb  0; E Ab Ib  Lb  0;          % beams
         E Abr Ibr Lbr fi1;E Abr Ibr Lbr fi1;E Abr Ibr Lbr fi1;E Abr Ibr Lbr fi1;
         E Abr Ibr Lbr fi2;E Abr Ibr Lbr fi2;E Abr Ibr Lbr fi2;E Abr Ibr Lbr fi2]};  % braces
eai(2)=eai(1);
eai(3)={[E Ac Icz Lc 90; E Ac Icz Lc 90; E Ac Icz Lc 90; E Ac Icz Lc 90;
         E Ac Icz Lc 90; E Ac Icz Lc 90; E Ac Icz Lc 90; E Ac Icz Lc 90;
         E Ac Icz Lc 90; E Ac Icz Lc 90; E Ac Icz Lc 90; E Ac Icz Lc 90;          % columns
         E Ab Ib  Lb  0; E Ab Ib  Lb  0; E Ab Ib  Lb  0; E Ab Ib  Lb  0;
         E Ab Ib  Lb  0; E Ab Ib  Lb  0; E Ab Ib  Lb  0; E Ab Ib  Lb  0;          % beams
         E Abr Ibr Lbr fi1;E Abr Ibr Lbr fi1;E Abr Ibr Lbr fi1;E Abr Ibr Lbr fi1;
         E Abr Ibr Lbr fi2;E Abr Ibr Lbr fi2;E Abr Ibr Lbr fi2;E Abr Ibr Lbr fi2]};  % braces
eai(4)=eai(2);
eai(5)={[E Ac Icy Lc 90; E Ac Icy Lc 90; E Ac Icy Lc 90; E Ac Icy Lc 90;
         E Ac Icy Lc 90; E Ac Icy Lc 90; E Ac Icy Lc 90; E Ac Icy Lc 90;
         E Ac Icy Lc 90; E Ac Icy Lc 90; E Ac Icy Lc 90; E Ac Icy Lc 90;          % columns
         E Ab Ib  Lb  0; E Ab Ib  Lb  0; E Ab Ib  Lb  0; E Ab Ib  Lb  0;
         E Ab Ib  Lb  0; E Ab Ib  Lb  0; E Ab Ib  Lb  0; E Ab Ib  Lb  0]};        % beams

eai(6)={[E Ac Icz Lc 90; E Ac Icz Lc 90; E Ac Icz Lc 90; E Ac Icz Lc 90;
         E Ac Icz Lc 90; E Ac Icz Lc 90; E Ac Icz Lc 90; E Ac Icz Lc 90;
         E Ac Icz Lc 90; E Ac Icz Lc 90; E Ac Icz Lc 90; E Ac Icz Lc 90;          % columns
         E Ab Ib  Lb  0; E Ab Ib  Lb  0; E Ab Ib  Lb  0; E Ab Ib  Lb  0;
         E Ab Ib  Lb  0; E Ab Ib  Lb  0; E Ab Ib  Lb  0; E Ab Ib  Lb  0]};        % beams
```

```
%Input local flexural stiffnesses for each frame type
kc(1)={[4 4 2;4 4 2;4 4 2;4 4 2;4 4 2;4 4 2;4 4 2;4 4 2;4 4 2;4 4 2;4 4 2;4 4 2;4 4 2; 4 4 2;4 4 2;4 4 2;4 4 2;4 4
2;4 4 2;4 4 2;4 4 2;4 4 2;4 4 2;4 4 2;4 4 2;4 4 2;4 4 2;4 4 2;4 4 2;4 4 2;4 4 2;4 4 2;4 4 2;4 4 2;4 4 2;4 4 2;4 4 2]};
kc(2)=kc(1);
kc(3)=kc(1);
kc(4)=kc(1);
kc(5)={[4 4 2;4 4 2;4 4 2;4 4 2;4 4 2;4 4 2;4 4 2;4 4 2;4 4 2;4 4 2;4 4 2;4 4 2;4 4 2;4 4 2;4 4 2;4 4 2;4 4 2;4 4 2;4 4
2;4 4 2;4 4 2;4 4 2;4 4 2;4 4 2]};
kc(6)=kc(5);

%Input the type and position of each frame in the floor plan
D=[0 -1.25 0 1;0 1.25 0 1;-1.25 0  90 3;1.25 0 90 4;0   0   0 5;0   0  90  6];
DF=FD-FU;
[q1,s,q2t]=svd(DF);
axx=[];

for i=1:8
  jl=zeros(12,1);
  jl(1:3:10)=q2t(1:2:8,i);
  jl(2:3:11)=q2t(2:2:8,i);
  [F,def,stiff]=capsld(jc,eai,kc,D,jl);
  V1=abs(flipud(cumsum(flipud(F{1}))));
  V2=abs(flipud(cumsum(flipud(F{2}))));
  V3=abs(flipud(cumsum(flipud(F{3}))));
  V4=abs(flipud(cumsum(flipud(F{4}))));
  ax=[V1+V2;V3+V4];
  axx=[axx ax];
  for jj=1:4
    V{jj}(:,i)=abs(flipud(cumsum(flipud(F{jj}))));
  end;
end;

% Selection criteria
sdf=diag(s);
cdf=1./[max(axx)]';
crit=sdf.*cdf.^2;
svn=sqrt(crit/max(crit));
I=find(svn<=0.2);

% Compute nsi for each vector and normalize it by the cut for that vector
r9=zeros(length(sdf),1);
r9(I)=1;
mbf=max(abs(axx));
NSI5=[abs(axx)*diag(1./mbf)];
nsic=max(0.015,1.0*svn);
scale=diag(1./nsic);
wsi=NSI5*scale*r9/length(I);

%Display shears
Framesx=[[1:4]' wsi(1:4)]
Framesy=[[1:4]' wsi(5:8)]
```

APPENDIX B

Exact Analytical Values

Table B1 Natural Frequencies (Hz)

12 DOF – Symmetric Mass			**12 DOF - Asymmetric Mass**				
No Damage	DP (*i*)	DP (*ii*)	No Damage	DP (*i*)	DP (*ii*)	DP (*iii*)	DP (*iv*)
9.41	6.24	5.82	9.29	6.18	5.76	8.79	8.79
11.79	9.91	9.51	11.64	9.80	9.39	11.64	11.50
16.38	11.73	11.01	16.19	11.63	10.90	15.80	15.68
25.55	21.53	14.89	25.27	21.27	14.78	24.37	24.36
32.01	28.92	24.91	31.66	28.59	24.70	31.66	30.82
38.66	37.37	28.41	38.26	36.87	28.22	37.77	37.76
44.64	38.28	36.06	44.20	37.93	35.97	43.61	42.91
48.01	47.34	41.35	47.75	46.81	40.60	47.68	47.68
48.44	47.83	46.79	47.97	47.54	46.46	47.96	47.96
60.15	59.99	54.34	59.81	59.63	53.68	59.81	58.18
67.48	65.31	63.64	66.90	64.67	63.44	66.58	66.56
83.62	83.31	72.61	83.23	82.89	71.58	83.18	81.76
120 DOF – Symmetric Mass			**120 DOF – Asymmetric Mass**				
No Damage	DP (*i*)	DP (*ii*)	No Damage	DP (*i*)	DP (*ii*)	DP (*iii*)	DP (*iv*)
8.59	5.47	4.96	8.47	5.42	4.90	7.99	7.99
9.18	7.37	6.68	9.05	7.28	6.59	9.05	8.81
14.58	9.69	8.70	14.40	9.61	8.60	14.01	13.85
23.45	19.31	12.34	23.19	19.06	12.26	22.25	22.22
25.95	22.77	17.79	25.63	22.47	17.65	25.63	24.72
36.81	34.18	21.56	36.44	33.73	21.44	35.81	35.78
40.65	35.29	34.79	40.21	34.94	34.62	39.68	38.84
42.21	40.66	38.75	41.85	40.23	38.17	41.84	41.71
46.98	46.73	40.62	46.77	46.50	40.13	46.68	46.68
56.74	56.38	49.47	56.55	56.17	49.20	56.55	54.67
62.96	60.43	59.98	62.42	59.82	59.58	62.04	62.04
81.05	80.53	68.57	80.75	80.20	67.85	80.67	79.07

Table B2 Exact Interstory stiffnesses [MN/m] and Percent Changes for the 12 DOF Model

12 DOF Model									
	No Damage	Damage (*i*)		Damage (*ii*)		Damage (*iii*)		Damage (*iv*)	
Floor	K_i	K_i	%*D*	K_i	%*D*	K_i	%*D*	K_i	%*D*
1-*x*	106.60	58.37	45.2	58.37	45.2	-	0.0	94.54	11.3
2-*x*	106.60	-	0.0	-	0.0	-	0.0	-	0.0
3-*x*	106.60	-	0.0	58.37	45.2	-	0.0	-	0.0
4-*x*	106.60	-	0.0	-	0.0	-	0.0	-	0.0
1-*y*	67.90	19.67	71.0	19.67	71.0	55.85	17.8	55.85	17.8
2-*y*	67.90	-	0.0	-	0.0	-	0.0	-	0.0
3-*y*	67.90	-	0.0	19.67	71.0	-	0.0	-	0.0
4-*y*	67.90	-	0.0	-	0.0	-	0.0	-	0.0

Table B3 'Exact'Interstory stiffnesses [MN/m] and Percent Changes for the 120 DOF Model used for comparison with the identified values

120 DOF Model											
	No Damage	Damage (*i*)		Damage (*ii*)		Damage (*iii*)		Damage (*iv*)		Damage (*v*)	
Floor	K_i	K_i	%*D*	K_i	%*D*	K_i	%*D*	K_i	%*D*	K_i	%*D*
1-*x*	77.75	33.75	56.6	34.07	56.2	-	0.0	-	0.0	-	0.0
2-*x*	57.51	-	0.0	-	0.0	-	0.0	-	0.0	-	0.0
3-*x*	54.34	-	0.0	20.49	62.3	-	0.0	45.74	15.8	-	0.0
4-*x*	46.03	-	0.0	-	0.0	-	0.0	-	0.0	-	0.0
1-*y*	61.76	14.95	75.8	14.95	75.8	49.78	19.4	49.78	19.4	57.77	6.5
2-*y*	53.75	-	0.0	-	0.0	-	0.0	-	0.0	-	0.0
3-*y*	50.75	-	0.0	11.39	77.6	-	0.0	-	0.0	-	0.0
4-*y*	44.38	-	0.0	-	0.0	-	0.0	-	0.0	-	0.0

APPENDIX C

Inversion of Modally Truncated Flexibility Matrices

It has been shown in Chapter 3 that from realization results one can extract the partitions of the inverse of the mass and inverse of the stiffness matrix for whatever modes are identified from the data. In some cases it may be of interest to invert the flexibility to obtain a condensed version of stiffness, *K* at the sensor coordinates. A difficulty arises, however, because although the flexibility itself may be quite accurate (residual from truncated modes is small), if the condition number of *F* is high then the estimated *K* may be far from the inverse of the true flexibility. Indeed, a classical result from matrix theory states that;

$$\frac{\left\|(S+\Delta S)^{-1}\right\|}{\left\|S^{-1}\right\|} \leq \kappa(S)\frac{\left\|\Delta S\right\|}{\left\|S\right\|} \qquad \text{(C.1)}$$

where ΔS is an infinitesimal perturbation and $\kappa(.)$ stands for condition number of (.). Although the result in eq.C.1 is only a bound that holds for infinitesimal perturbations, it does suggest that the accuracy of the inverse is likely to be much worse than that of the matrix itself, even for moderate condition numbers.

The possibility of reducing error from modal truncation when the flexibility is inverted is examined here. The idea explored uses the Cayley-Hamilton theorem to obtain a series expression for the inverse of the truncated flexibility and evaluates the condensed stiffness by truncating the series. The reason why the truncated version of the Cayley-Hamilton series was though likely to provide a better result than the complete series will be discussed later, in the context of the derivation. We begin by recalling the Cayley-Hamilton Theorem statement, namely;

$$\textit{If } S \in C^{n\times n} \textit{ and } p(\lambda) = \det(S-\lambda I) \textit{ then } p(S)=0$$

In simple terms, all matrices satisfy their characteristic polynomial.

Assume that $\hat{S}$ is a modally truncated version of an unknown flexibility matrix S, where the norm of the difference between S and $\hat{S}$ is small compared to the norm of S. Calling on the Cayley-Hamilton theorem one can write:

$$\sum_{i=1}^{n+1} \hat{\lambda}_i \hat{S}^{n+1-i} = 0 \qquad \text{(C.2)}$$

where the $\hat{\lambda}$s are the coefficients of the characteristic polynomial of $\hat{S}$ (which are related to the eigenvalues of the matrix $\hat{S}$ by well known relationships, see for example ref.??). For our purposes we separate the series in eq.C.1 into two terms, from 1 to r and the remainder, namely;

$$\sum_{i=1}^{r} \hat{\lambda}_i \hat{S}^{n+1-i} + \sum_{i=r+1}^{n+1} \hat{\lambda}_i \hat{S}^{n+1-i} = 0 \qquad \text{(C.3)}$$

assume now that the second summation is negligible (in accordance with some criterion which we leave undefined at this point). Multiplying eq.C.3 by $S^{-(n+2-r)}$ and performing some simple manipulations one gets;

$$\hat{S}_r^{-1} = -\frac{1}{\lambda_r}\left[\sum_{i=1}^{r-1} \lambda_i \hat{S}^{r-1-i}\right] \qquad \text{(C.4)}$$

where $\hat{S}_r^{-1}$ may be interpreted as the r term truncated estimate of the inverse of $\hat{S}$. The reason why this truncation may be a better estimate to S^{-1} than the full series derives from the fact that the difference between $\hat{\lambda}_i$ and λ_i and the difference between S^i and $\hat{S}^i$ increase with i. Having said that, recognizing that when S is exact any truncation reduces accuracy it is evident that eq.C.4 does not always lead to a better estimate of the condensed stiffness than a direct inversion. The questions are then: a) when is eq.C.4 a good candidate for improving the estimate of the condensed stiffness and b) how should the value or r be selected. We do not have, at this time, satisfactory answers for either one of these questions and are not certain whether or not there is in fact information to arrive at good decisions. Notwithstanding, it is of interesting to illustrate the kind of improvement that can be attained under some cases if the appropriate truncation can be selected.

Consider for this purpose the simple system shown in Figure C-1. Output sensors exist at masses 4, 6, 8, and 10. The stiffness and the mass distribution are as shown in the figure.

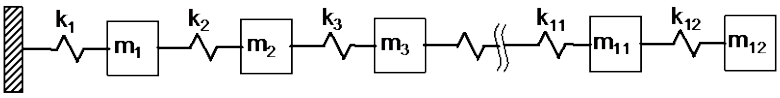

$k_1=k_2=k_3=k_4=2000, k_4=k_5=k_6=k_7=1000, k_8=k_9=k_{10}=k_{11}=k_{12}=3000$

$m_1=m_2=20, m_3=m_4=24, m_5=m_6=28, m_7=m_8=32, m_9=m_{10}=36, m_{11}=m_{12}=40$

Figure C-1 Simple spring-mass system

Figure C-2 shows the variation of the maximum percent error in the diagonal of the flexibility matrix at the sensor points with the number of modes used to assemble the flexibility. The maximum percent error in the condensed stiffness is then illustrated for two computations: a) based on the direct inversion (pseudo-inverse when matrix is rank deficient) and b) based on eq.C.4 with $r = 4$ (one truncated term). Note that even though the condition number of the flexibility is relatively low the error in the condensed stiffness can be as high as 160% when the direct inversion is used. In the truncated series approach (C-H), however, the maximum error never exceeded 35%. The choice of $r = 4$ in this example was done because it lead to the best results for the cases where the flexibility had less than 7 modes.

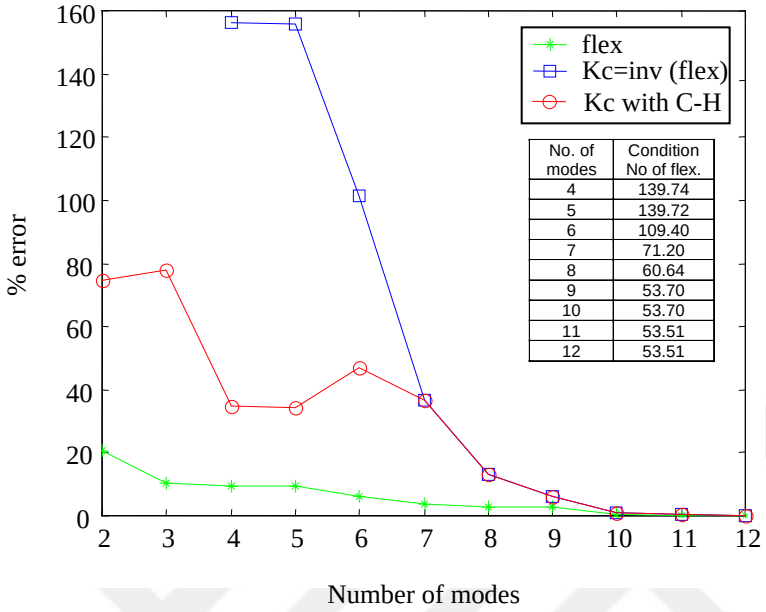

Figure C2 Maximum % error in the diagonal coefficients of the flexibility and the condensed stiffness matrices